Modelling Artificial Stimulation and Response in Peripheral Nerves Including Ephaptic Interactions

Miguel Capllonch Juan

A thesis presented for the degree of
Doctor of Philosophy

School of Computer Science and Electronic Engineering
University of Essex
September 2019

Acknowledgements

Many have accompanied me in this journey, and I would like to express my deepest gratitude to all of them. Firstly, I want to thank my supervisor, Dr Francisco Sepulveda, for introducing me to the topic and for his excellent guidance during this process. Your wisdom, team work, and professionalism have been invaluable to me. I highly appreciate your interest and dedication during all my process.

I would like to thank my colleagues in the BCI-NE group for taking me in when I arrived and being supportive peers and friends. Spending time and sharing ideas with you has been a bliss. The University of Essex is a great place to work, and the BCI-NE group has a unique atmosphere.

I want to dedicate special thanks to Dr Ana Matran, Dr Wulfrano Arturo Luna, and Jonathan Clark for their invaluable support and friendship along all these years, and for the technical, editorial, and logistical help they have provided me.

I wish to express my deepest love and gratitude to my beloved friends, Maria, Natanael, Aina, Ismael, Maria del Mar, Pere, and Jaume; to my parents, siblings, and extended family for their inmense support and love. You have all been understanding, kind, and patient along all these years. Also, to Andy Stedman, who took me in from the beginning and with whom I have shared great moments. Lastly, and most especially, my deepest heartfelt appreciation is to my partner Juana for her unconditional support and constant encouragement.

Abstract

This research aims to (1) extend our knowledge on the response of peripheral nerves to artificial stimulation for sensory feedback provision from neural interfaces, and (2) create a computational tool to facilitate this study. We were interested in studying how ephaptic coupling between myelinated fibers influences activity in nerve trunks under artificial stimulation and during action potential propagation. Ephaptic interaction simulations in nerve trunks were performed to quantify this influence. For this, we created peripheral nerve models containing electrodes for electrical stimulation and recording within a tool that can be further used in electrode design optimisation and neural activity research. The created model can use a self-contained or a hybrid field-neuron method. The self-contained method uses a resistor network that electrically couples all axons, tissues, electrodes, and surrounding medium, and is solved by the NEURON simulation environment. The resistor network uses weighted Voronoi tessellations in the Laguerre geometry to define the electrical connections between all nerve elements given any cross-sectional anatomy. The hybrid field-neuron approach also uses the resistor network to compute the fields, but uses them stimulate fiber in a separate simulation. The self-contained model was designed so that it could simulate artificial stimulation, neural activity with ephaptic coupling and electrode recordings simultaneously. Researchers often assume ephaptic coupling is weak among myelinated axons, and therefore, tend to ignore it. Simulations carried out in this work, however, show that ephaptic coupling increases axon recruitment during artificial stimulation. This effect should be taken into account in further research. On the other hand, ephaptic coupling during propagation in realistic bundles with large numbers of heterogeneous myelinated fibers is weaker, unstable, and more complex than what is known from previous studies on bundles of few homogeneous fibers. This research provides detailed results and insights on these aspects of peripheral neural activity.

Keywords: Peripheral nerves; myelinated axons; computational modelling; ephaptic coupling; electrical stimulation

Contents

List of Figures

List of Tables

List of Acronyms

AF Activating Function.

AP Action Potential.

CAP Compound Action Potential.

CNS Central Nervous System.

CV Conduction Velocity.

EC Ephaptic Coupling.

EMI Extracellular domain, Membrane and Intracellular domain.

FDM Finite Difference Methods.

FEM Finite Element Methods.

FINE Flat Interface Nerve Electrodes.

HH Hodgkin-Huxley.

LFP Local Field Potential.

LIFE Longitudinal Intrafascicular Electrodes.

MEA Micro Electrode Array.

MF Mean-Field.

MRG McIntyre-Richardson-Grill.

NAELC Non-Axonal Extracellular Longitudinal Cable.

PNS Peripheral Nervous System.

PS point-source.

QS quasi-static.

RDM Relative Difference Measure.

RN Resistor Network.

TIME Transverse Intrafascicular Multichannel Electrodes.

List of Publications

Conference Proceedings

- M. C. Juan, F. Kölbl, and F. Sepulveda, "Optimisation of the spatial discretisation of myelinated axon models," in *2016 8th Computer Science and Electronic Engineering (CEEC)*. IEEE, 2016, pp. 216–221

- F. Kolbl, M. C. Juan, and F. Sepulveda, "Impact of the angle of implantation of transverse intrafascicular multichannel electrodes on axon activation," in *2016 IEEE Biomedical Circuits and Systems Conference (BioCAS)*. IEEE, 2016, pp. 484–487

- M. Capllonch-Juan, F. Kölbl, and F. Sepulveda, "Unidirectional ephaptic stimulation between two myelinated axons," in *Engineering in Medicine and Biology Society (EMBC), 2017 39th Annual International Conference of the IEEE*. IEEE, 2017, pp. 230–233

- M. Capllonch-Juan and F. Sepulveda, "Evaluation of a resistor network for solving electrical problems on ohmic media," in *2019 11th Computer Science and Electronic Engineering (CEEC)*, Sep. 2019, pp. 35–40

Journal Articles

- M. Capllonch-Juan and F. Sepulveda, "Modelling the effects of ephaptic coupling on selectivity and response patterns during artificial stimulation of peripheral nerves," Unpublished manuscript; submitted to PLOS Computational Biology on 5/6/2019

Chapter 1

Introduction

1.1 Overview

Human body is formed by sets of organs ensembled in systems that, interacting with each other, provide the necessary functionalities for its correct operation. Whenever one or more organs suffer an injury, dysfunction or removal, they become an obstacle for such correct operation, usually limiting a person's ability to interact with the environment.

A common strategy along history to alleviate the effects on the life quality of people with organ-related limitations has been to attempt to restore the compromised functionalities. In cases where tissue loss or malfunction does not represent an important portion of an organ, this goal can be achieved using repairing techniques or implanting new tissue. When the loss is more severe, the strategy is usually to use replacement organs coming from other living bodies or technological devices aimed to provide approximate replacement for the missing functions. This set of techniques conforms what is commonly known as implants.

The nervous system is an essential component of the human body which is as much at risk of suffering injuries and amputations as any other. However, the implications of damages in the nervous system are generally different in nature to those of other systems, and can lead to very severe impairments that may span from sensory, motor and cognitive to vital body dysfunctions. In particular, sensory and motor dysfunctions limit a person's capabilities to normally interact with her environment, which can produce serious discomforts and decrease life quality. If sensory and motor dysfunctions are severe enough, and if the person is not living in a controlled environment, they can even lead to death.

Neural implants are becoming nowadays a major technique to restore functions
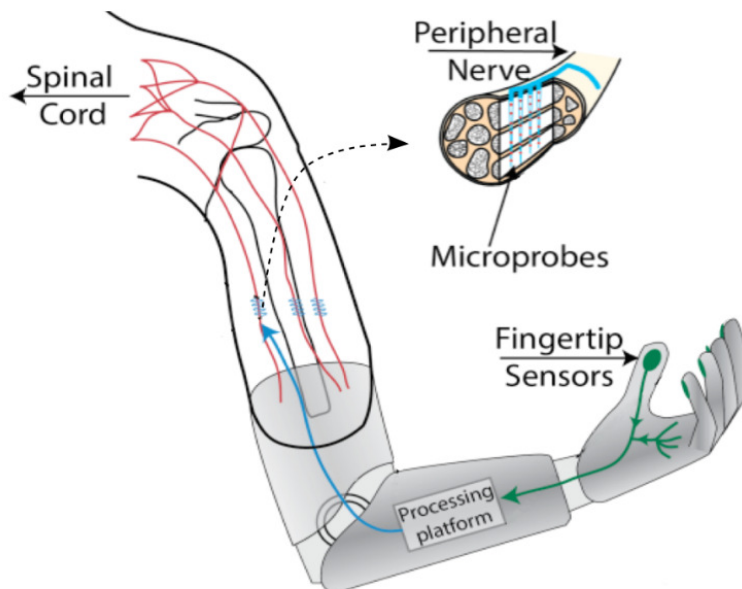
Figure 1.1: Overview of somatosensory feedback as implemented in the SenseBack (UK's EPSRC) project. The electrical signal generated by sensors is processed and translated into stimulation waveforms applied in peripheral nerves by transverse intrafascicular electrodes to stimulate sensory axon fibres. [1]

of the nervous system that have been lost or damaged. They span an extensive range of applications that responds to the wide variety of functions and organs that the nervous system contains. Implants aimed to recover motor or sensory functions are connected either to the Peripheral Nervous System (PNS) or to the Central Nervous System (CNS).

Neural injuries are varied in their nature, and so are the strategies adopted to overcome them. For instance, when a nerve is locally damaged or cut, implants can create a bridge between the two sides of the injury. This can be done by implanting a healthy piece of another nerve to fill a gap [16,17], tubulisation [18], neurorrhaphy with suturation [19], or by implanting an electronic system such as a brain-machine-spinal cord interface (BMSI) [20–22], which communicates the brain with the spinal cord below an injury. Loss of sensory functions can be overcome with sensory substitution techniques. These include prostheses and devices for restoring audition (cochlear implants [23–25] or auditory brainstem implants [26]), vision (implantable retinal prostheses [27]) and connected to the PNS, prostheses for tactile sensation and proprioception (the latter two are discussed below). Other connections to the CNS for restoring or enhancing auditory, visual, cognitive functions and even motor control involve cortical implants [28–30], which are in direct contact with the affected area of the cortex. Amputations require a different approach to injuries because the treatment involves the substitution of lost organs. For a patient, loss of limbs

implies the loss of movement, perception of the surrounding environment and proper physical interaction with the world. In the last century, the restoration of motor control and sensory feedback in limb prostheses have started being addressed thanks to the rapid growth of technological innovations.

A common technique to control the movement of artificial limbs is the use of electromyography (EMG) [31,32]. Other more experimental methods do not involve attaching prostheses to the body, and make use of brain-computer interfaces (BCI) to control robotic devices [30]. Motor control is a feature that has been achieved in limb prostheses to a reasonable level of success [31].

Somatosensory perception of the environment is natural to healthy functional limbs, and it is a very important element for movement calibration during motor control. Sensory feedback is called so since it feeds information back to the nervous system during movement in order to assist motor function. This feedback comes in the form of perception of the objects that are in contact with the body and the posture of one's own body. Without it, calibration of movements relies only on visual and auditory stimuli, which are generally not enough on their own to assist it. A rich and in-depth discussion about the importance of sensory feedback restoration can be found in [33]. Sensory feedback has long remained the last feature to be effectively addressed and implemented in limb prostheses. It can be achieved through indirect or direct methods, the former including, for instance, somatically or motionally stimulating a different part of the body when a prosthesis is used [34], and the latter, providing it directly through electrical artificial stimulation from a prosthesis.

This latter goal of providing sensory feedback through electrical artificial stimulation has only been accomplished in very recent years [35–39]. In all these works, a prosthesis or sensory substitution system (an assistive device) is connected to the PNS of a patient using electrodes that are aimed to stimulate sensory nerve fibers. The complexity of the behaviour of the PNS makes the prediction of its response to electrical artificial stimulation a real challenge, but this can be guided by the use of machine-nerve interface models. Predictions help the design of optimal interfaces between assistive devices and PNS, and modelling has thus become a valuable tool for the design of systems for providing sensory feedback. As an example, the achievements in [38] are supported by numerical simulations in [40].

1.2   Problem Statement and Rationale

1.2.1   Social Relevance of Sensory Feedback Restoration

The use of limb prostheses that lack sensory feedback, which is the case for most of the available prostheses today, provides users with new motor abilities that help them interact with the world and perform daily tasks. However, they are perceived by users as an external tool or an accessory rather than a substitute for their missing limb [33]. The feeling of embodiment of the prosthesis, which means that the prosthesis is perceived as part of one's body, hence letting users recover a sense of having a new limb, is nowadays a pursued goal in limb prosthetics design. This feeling of embodiment acts at a psychological level and entails a considerable enhancement of life quality for users. Today, embodiment is only possible through an appropriate provision of sensory feedback from the prosthesis [37, 41]. Sensory feedback lets users gain awareness of the surrounding world through somatosensory perception and through the perception of their own body—also known as proprioception—, without the need to rely on visual and auditory inputs; this allows users to release themselves from a high conscious attention to the prosthesis. Perception of one's own body entails awareness of its existence, and recovering this awareness is greatly beneficial for the psychological trauma subsequent to an amputation. Somatosensory perception and proprioception greatly improve movement calibration and fine motor tasks. The successful provision of natural-like sensations through an artificial prosthesis, even in laboratory experiments, has led users to 'feel' their lost hands [37]. This is why great efforts are being made in order to design prostheses with a natural-like sensory feedback.

Compared to exclusively motor prostheses, using a prosthesis with sensory feedback allows users to perform daily tasks with an improved level of proficiency. Users likely see an improvement in their self-esteem thanks to the new level of autonomy. However, this benefit is not exclusive to users: as they gain autonomy, they also gain independence from other people that assist them. Both the physical and psychological improvements in the life of users also have a beneficial impact on the quality of life of the people surrounding them.

For amputees, limb amputations imply limitations for undertaking a normal job, and in many cases, impairments prevent them from having any job. Not only does this deprive them from a normal life, but also drives a certain pressure on governments and societies to take care of the injured and to palliate the economical impact that this causes. This is why it is of special interest for the society to work on the recovery of motor abilities of injured people, since that would empower individuals with better competence and allow them to be reinserted as active agents in the economy.

1.2.2   The SenseBack Project

"Enabling Technologies for Sensory Feedback in Next-Generation Assistive Devices" (shortcut as "SenseBack") is a UK-national project funded by the EPSRC with the participation of Newcastle University, Imperial College London, the University of Southampton, Keele University, the University of Leeds and the University of Essex. The aim of the SenseBack project is to provide sensory feedback to assistive devices such as arm prostheses that recreates the natural feedback associated with a real arm [1].

Sensory feedback is provided through prosthesis-nerve interfaces that connect the machine with the PNS. The interfaces under design in this project rely on predictions made with numerical simulations. This thesis undertakes the task of modelling these interfaces in order to simulate their effects on the peripheral nerves. The simulation involves modelling the electrical connections of the prostheses electrodes to the nerve's tissues and fibers, the consequent stimulation on the fibers exerted by these and the propagation of elicited signals towards the CNS.

1.2.3   Peripheral Nerves Modelling

Peripheral nerves need to be modelled down to axonal level, with models including valid representations of axonal anatomy and physiology, including axoplasm, myelin sheaths and membranes with voltage-gated channels. Models of individual axons and other types of neurites have been developed during the last half of the past century until now, first for unmyelinated [42], and later for myelinated fibers [43–47], aided by numerous experimental [48–52] and analytical [53,54] works. These models have been invaluable for revealing axon properties and accumulating knowledge about the geometrical structure of nerve fibers, their physiology, biochemistry and the interplay of all these elements in fiber behaviour. Vast knowledge has also been gained regarding stimulation and propagation of signals. However, models of entire nerve trunks have been developed only in very recent decades [8,55–57], when technology in computation has allowed for it.

Stimulation in peripheral nerve trunks has been simulated in previous studies [40,55,58], but these focus on predicting how many and which axons in a bundle are activated by the stimulating field generated by the electrodes, a measure known as selectivity. They use the occurrence of propagation of elicited APs along axons as the criterion for axon activation, but in general, they do not focus in detail on the processes following activation and their potential consequences on selectivity. Other works make use of more simplified models for predicting axon activation [59,60], which are useful thanks to their low computational requirements, but at the expense of their ability to model complex axon behavioural phenomena.

1.2.4   Ephaptic Coupling

Neurons interact with each other through gap junctions and through endogenously generated electrical fields. This latter form of interaction is known as EC [9, 61, 62], which consists on the interaction or cross-talk between cells due to the mutual stimulation that they exert on each other via their endogenous electrical fields. For fibers in most mammalian nerves, it is commonly assumed that EC is negligible [11, 63]. This, of course, means that it is assumed that EC has no effects on the behaviour of axons during stimulation and propagation and therefore, on axon activation (selectivity). Findings from more recent numerical simulation studies [64–66] and experimental evidence [67] question this assumption, since they provide evidence for the possibility of important consequences of the ephaptic interactions in myelinated axons.

Despite the works from [65, 66] and the more recent [68] are a good start on the study of these interactions in axon bundles, as they provide valuable insights, they study very ideal cases of regular bundles of homogeneous axons, stimulated by internal current injections. Furthermore, they all use the mean-field approximation, which assumes that, at every position along the length of a bundle, the extracellular medium is isopotential. The magnitudes of endogenous fields from neural activity have a dependence on the distance from the neural sources, and they can be obtained using volume conductor theory [69]. Works on pyramidal cells in the cortex model endogenous extracellular fields using this theory [70]. The anatomical shape of a bundle, different in nature to cell networks in the cortex, reasonably supports the choice of a Mean-Field (MF) approach. However, in a bundle with a complex geometry, containing a large number of fibers and perineurial tissue separating different fascicles, it is worth assessing the correctness of this choice and determining whether it is accurate enough or, on the contrary, whether a geometry-dependent model such as [69] is needed. Another disadvantage of using a MF model is its incompatibility with the simulation of extracellular fields generated from electrodes. In such case, it becomes an insurmountable obstacle if both electrode stimulation and EC are intended to be included in a simulation. After carrying out a literature review, no study has been found that aims to quantify the effects of EC inside more realistic models of peripheral nerves, including fibers of varying diameters and geometry-dependent simulation of extracellular fields.

Assessment of the effects of EC in a realistic nerve trunk model under artificial stimulation from electrodes may help quantifying any possible effects it may have on fiber recruitment, CV and information encoding through synchronisation of APs, thus helping to clear out the doubts about its role and relevance. For this reason, we believe that the field of sensory feedback restoration would benefit from a study that addresses the problem of determining the importance that this usually underestimated factor may have on the results of artificial stimulation, by using modern computational techniques and geometrical approximations to a real nerve.

1.3 Objectives

This work has two main objectives: 1) to quantitatively assess the effects of ephaptic interactions between axons in a mammalian peripheral nerve model on the neural responses generated by stimulating electrodes; and 2) to develop an open-source, highly customisable framework to build entire nerve trunk models and simulate their activity with various types of stimulating and recording electrodes.

1.3.1 Scientific Questions: Assessing the Effects of Ephaptic Coupling in Mammalian Peripheral Nerves

Our first objective is to better understand the nature and role of EC in mammalian peripheral nerves. Three scientific questions were addressed in this study in order to gain understanding on the nature of three aspects of EC between nerve fibers. These questions are listed below.

I. Distance Dependence of Electrical Interactions.

The MF model may be unsuitable for large nerves and is incompatible with the presence of fields resulting from external stimulating electrodes. A model of ephaptic interactions with a dependence on the separation distance between nodes of different fibers is necessary to obtain a better quantification of their effects. Hence, the spatial dependence of EC was studied in this work using a distance-dependent model and the validity of a MF approximation under different scenarios was assessed and discussed.

II. Quantification of the Effects of Ephaptic Coupling on Propagation.

Firstly, we wanted to assess whether EC has any chance to be effective on a nerve. In order to do so, the effects of EC were studied between groups of two and three fibers using two different models for computing the ephaptic fields, one taken from the literature and another developed in this work. Effects on the propagation velocity and, consequently, on AP locking and synchronisation, were studied for these numbers of fibers. Secondly, we aimed to simulate the effects that EC can have on propagation of APs in a realistic nerve trunk model, and determine whether these can effectively alter relative timings between APs and even elicit recruitment of inactive fibers. For this, a study was made using a full nerve trunk model with different fascicles filled with fibers of different diameters. The model also includes an explicit representation of stimulating and recording cuff electrodes and various neural tissues. Simulations

with and without EC were compared in order to assess the extent of the influence of EC during propagation in the nerve model. The existing knowledge for the simple cases of a low number of parallel identical fibers was compared to the results for the nerve model and its validity was discussed. Knowledge gained on this can aid understanding how motor and sensory information is processed during propagation in peripheral nerves.

III. Quantification of the Effects of Ephaptic Coupling on Stimulation.

Another objective of this study is to quantify to what extent EC can modify the known results of artificial stimulation from electrodes on axons in a nerve. This is, whether EC can drive additional axons to fire when results are compared to non-EC simulations, how many can these axons be, and the effects on AP elicitation delay that EC can have on the recruited axons. In particular, we aim to understand whether EC can shorten the response times of axons to artificial stimulation, making them fire APs in a more synchronous way, or if instead EC can have inhibitory effects on axons during stimulation. Understanding the potential role of EC during artificial electrical stimulation is key to decide whether it can be dispensed with or, on the contrary, whether it should be taken into account in stimulation studies.

1.3.2 Technological Contribution: Open-Source Framework to Model Nerves and Electrode-Nerve Interfaces

Our second objective is to develop an open source software consisting of a framework for building and simulating nerve models (Fig. 1.2). Such framework was created in this work, and it allowed us to run the simulations presented in this study. We aim to provide this software as a publicly available tool in order to facilitate other researchers running simulations with their own nerve models. The framework is aimed to come with mainly three features which are described below.

I. Anatomically Detailed Model.

In order to carry out the necessary simulations described above and to facilitate researchers and modellers simulating the behaviour of a nerve trunk under many stimulation scenarios, a model builder of a nerve trunk was created. This model builder includes fascicles, axons, and anatomical and electrical distinctions between the different constitutive tissues: endoneurium, perineurium and epineurium.

II. Flexibility at Modelling Anatomy, Biophysics and Electrodes.

The model builder allows users to create a nerve with the cross-sectional shape, size and components of their choice; this enables the building of models with cross-sectional shapes obtained from histological data. The framework allows users to define axon anatomy, physiological and biophyisical properties, as well as using pre-existing axon models. A method to declare and describe the stimulation and recording electrodes was designed so that these can be defined in a flexible way. This allows users to choose which types of electrodes to use (Utah, cuff electrodes and TIME), where to place them, what shape and properties to assign to them and what stimulation protocols to use.

III. Compatibility with Finite Element Methods and Other Solvers.

The framework's default method to model the extracellular space uses a Resistor Network (RN), which is coupled to the neural models. This permits the simulation of stimulation and recording from electrodes as well as EC. However, computation of fields using an external tool, such as an external Poisson solver or a Finite Element Methods (FEM) tool, is permitted. The framework allows using the results of the electric potential coming from any method capable of solving the fields over a volume. These results can be used to exert stimulation on the neural models in the framework or, inversely, the currents from the neural models can be saved and used as boundary conditions for the external solver in order to compute extracellular recordings.

1.4   Contributions of this Research

The work presented here is situated within the context of simulating neural activity under and after stimulation with electrodes, while taking into account the ephaptic interactions between fibers. Although several approaches have been proposed that allow the simulation of these scenarios in self-consistent Extracellular domain, Membrane and Intracellular domain (EMI) models [71–73], none of them addresses the particular problem we have for peripheral nerves. On the other hand, existing studies that address this or very similar problems, while being able to provide valuable clues and insights at a low computational cost, use oversimplifying assumptions based on the MF model that are not compatible with the complexity and depth of the approach that has been adopted in this work. Under these circumstances, the work carried out here brings a number of contributions that are listed below:

- This work provides a variant of a self-consistent EMI model fully implemented
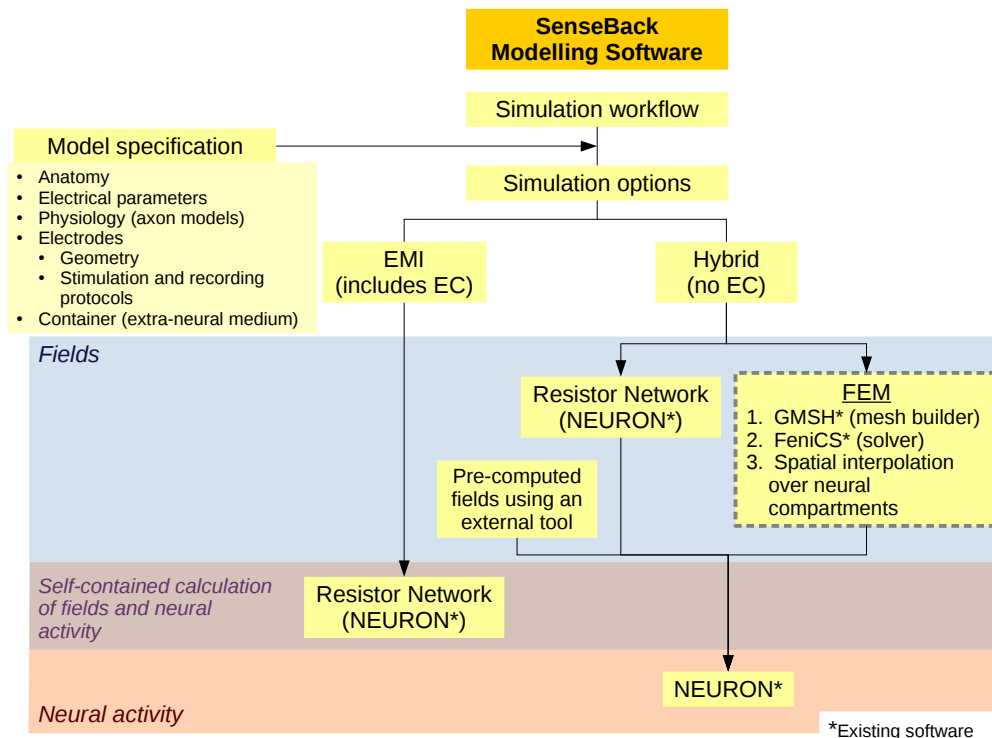
Figure 1.2: Overview of the SenseBack modelling software workflow. The software can simulate the activity of a nerve model either by using an EMI approach with the RN or by using a hybrid field-neuron approach, for which the RN, FEM or pre-computed fields can be used. Specification of the nerve model includes custom choices of cross-sectional anatomy, tissue electrical properties, electrode configurations with stimulation and recording protocols, and extra-neural space (container embedding nerve and electrodes). Stars (*) indicate existing third-party open source software tools that are used in the modelling framework (NEURON [2], GMSH [3] and the FEniCS FEM solver [4]). The implementation of the FEM (box with grey dashed contour line) has not been used in this thesis, but it is related work. An example of its use at an early implementation stage can be found in [5].

in NEURON [2] that permits the simulation of stimulation from electrodes, neural activity and recordings in a single run and under a realistic geometry and set-up defined by the users. The EMI approach implemented in NEURON guarantees numerical stability throughout simulations. The model can also use a hybrid field-neuron approach, where fields are computed in a static simulation and used afterwards for axon stimulation.

• The present work is, to our knowledge, the first to address the study of tissue- and geometry-dependent EC during stimulation and propagation in arbitrary and more realistic models of nerve trunks that include several bundles of fibers of varying diameters. Ephaptic stimulation between fibers was quantified against the inter-fiber distances, and the effect of the presence of perineurial

membrane separating fascicles was also studied.

- The effects of EC on fiber recruitment after electrode stimulation for a nerve trunk model including a large enough number of fibers were studied, and they were found to increase recruitment by a non-negligible amount. This is a useful finding to be taken into account for further stimulation studies. Additionally, EC was found to decrease the response times of axons to stimulating fields.

- A new method is provided here in order to define nearest-neighbour electrical interactions among fibers based on weighted Voronoi tessellations in the Laguerre geometry. This method has never been applied before in this field, and it has demonstrated to be a valid and convenient method that can systematically define electrical contacts between nearest-neighbours given any possible configuration of fiber positions and diameters. It can also be used for any other neuron populations in either two or three dimensions, not only in axon bundles.

1.5   Assumptions, Constraints and Shortcomings

The results and reach of this work are constrained by a series of factors that need to be mentioned. Although these will be discussed in detail in later chapters, they are introduced here so the reader can keep them in mind from the onset.

Assumptions   The model uses a series of assumptions regarding the nerve's nature, such as the assumption of cylindrical and parallel fibers, the use of the one-dimensional cable equation and compartmental modelling, and also the neglect of the capacitive properties of connective tissues. Although the capacitive nature of extracellular tissues is known (see, e.g., [74] for the perineurium in frogs), it is generally assumed that the quasi-static (QS) approximation, which removes time-dependent components of the potential from the equations, can be used in most neural applications, since the frequencies of neural oscillations normally lie below 1 kHz [75, 76]. Also, the error of applying the QS approximation when stimulating with the square pulses from electrodes generally used in this work (near 200 μs long) is small [75]. Further work regarding the topics covered in this research, but including axon tortuosity—which has been investigated in previous studies with different conditions—and capacitive properties of tissues, could provide yet more accurate results and richer insights. In addition, the model disregards the accumulation of potassium ions in the interstitial space between fibers and ionic diffusion through the extracellular space, which are known to be sources of inter-fiber interactions.

Shortcomings While the framework uses a RN which was theoretically validated under simplified conditions, it does not make use of FEM simulations. A FEM solver was under development during this project, which was meant to be coupled to the neural models. However, due to time and human constraints and considering that our intended FEM solver, as well as all the software we have developed, was meant to be open-source —which implies giving up on the swiftness of using available commercial solvers—, this task could not be finished. Therefore, this framework lacks a FEM solver which would allow the calculation of fields from stimulating electrodes using the most commonly used and thoroughly validated method. Nevertheless, we consider that the RN acceptably serves the purpose.

Constraints Using a RN requires a high amount of computational power and time. Even when saving computational costs is not one of the main purposes of this thesis, this should be accounted for at the time of using this model, especially if users need fast results for quick analysis. It is left as suggested work to further investigate on how to optimise simulations using RNs.

1.6 Overview and Structure of this Thesis

This thesis contains seven chapters and it is structured as follows:

Chapter 1 presents an introduction of the study.

Chapter 2 describes the state of the art in the growing technologies for sensory feedback restoration and PNS modelling. It focuses on the currently existing models, together with their properties and advantages. Afterwards, a literature review of the currently available knowledge about EC in myelinated nerves and the PNS is provided, making a special remark on the relevance that this has for modelling for practical applications.

Chapter 3 presents a preliminary study where EC is studied for the case of very few fibers (2 and 3). The one-to-one ephaptic interactions and effects on propagation are quantified, and the results are used to create a simplistic particle model that serves to infer the possible consequences of these interactions in larger bundles.

Chapter 4 presents a RN that creates an EMI model of a bundle of fibers and its extracellular space, meant to overcome the numerical stability issues found in Chapter 3. The RN and its new nearest-neighbour electrical connection model are explained here. The RN is validated against expected solutions from FEM and analytical equivalents. Following this, the RN is used in bundles of fibers in two scenarios in order to test its usability: First, it is used to study the effects of several

anatomical variables of the fibers in a bundle and of RN implementation choices on the responses of the fibers to electrode stimulation. Next, it is used to study the behaviour of a low number of identical fibers ephaptically coupled in order to contrast the results against preceding knowledge.

Chapter 5 presents the first study of the effects of EC on stimulation with cuff electrodes and propagation of APs along several bundles and a model of a peripheral nerve trunk that includes fascicular perineurial membranes, anisotropic extracellular conductivity and myelinated fibers of different diameters based on mammal diameter distributions. EC is also assessed under the dependence on inter-fiber distances and presence of perineurial membranes. This chapter uses an extension of the RN in order to run these studies.

Chapter 6 provides an in-depth discussion on the findings of this work, remarking both the novelty and relevance of its contributions, and also providing a critical review of this work and its limitations.

Chapter 7 provides the main conclusions of this work.

Chapter 2

Background

2.1 Existing Methods for Sensory Feedback Restoration

A variety of methods have been used to provide sensory feedback. In general, methods for sensory substitution consist in using either: neural interfaces, which ultimately aim to stimulate the peripheral sensory nerve fibers in order to send to the CNS the exact sensory information that is aimed to be evoked; or by providing stimulation to functional sensory organs, in order to make a substitute for the intended information.

2.1.1 Variety of Sensory Substitution Techniques

A number of approaches for sensory substitution includes cutaneous electrical stimulation [77–79], mechanical stimuli on the skin (which includes vibrotactile [78] and mechanotactile [80] stimulation of the skin), auditive systems to encode positional information [81,82] and a technique known as skin reinnervation [83], which consists of surgically redirecting the remainders of the sensory afferents of the missing limb to the skin of a different part of the body. See [84] and [33] for broader reviews on sensory substitution techniques; note however that these reviews are bound to 2013 and 2015, respectively.

Most of these techniques and approaches have, to some extent, been successful at providing certain improvements in movement control, but few have ever had a practical applicability outside laboratories [33]. Vibrotactile feedback has been successfully implemented in myoelectric prostheses [84]. Body-powered prostheses,

which were some of the formerly developed around the beginning of the 20th century, offer one type of mechanotactile or haptic (force) but effective feedback provided by the pressure that the movement of the prosthesis exerts on the body (elbows, shoulders, etc) [85]. This type of early and purely mechanically originated feedback has, ironically, a higher rate of acceptance amongst users than all others (not including direct neural stimulation), and these prostheses have therefore been accepted even more than the more modern myoelectric ones, which usually lack a proper sensory feedback system [84, 85]. Other more indirect forms of sensory feedback include, for example, mechanically stimulating another, or a reciprocal, part of the body (e.g. if a hand prosthesis is in use, the other hand is stimulated for feedback) [86].

2.1.2   Neural Interfaces

All the techniques listed above, except body-powered prostheses, commonly share their difficulty of being applied outside laboratory settings, and that the quality of their feedback is not modality-matched. I.e., the actual sensations generated by these methods do not match the intended natural sensation. In order to provide this natural feedback, only neural prostheses have so far been successful [37–39]. Furthermore, they have managed to provide a certain stability and durability [87].

Although reconfiguration of neural pathways occurs in the CNS after an amputation, the mapping of the missing parts of the body remains. Therefore, the brain virtually retains the ability to identify sensations associated with the missing parts [35]. Hence, the remaining nerves of the missing limbs can be physiologically stimulated, and the brain will still map sensations to missing tissues.

Neural interfaces for sensory feedback are relatively new. The first work we have found where electrical stimulation was directly exerted on a peripheral nerve was [88], where the median nerve was stimulated and subjects could feel sensations correlated to the inputs.

A variety of peripheral neural interfaces have been developed during the past decades. They can be classified according to their level of invasiveness and selectivity, which unfortunately are somewhat positively correlated (see [89], [90] and [91] for thorough reviews on existing neural interfaces up to 2005, 2010 and 2018, respectively). The least invasive of direct neural interfaces for peripheral nerves, (and some of the first developed), are cuff electrodes [90]]. These are the least invasive since they wrap the nerve without damaging it, but are also the least selective, meaning they are the least capable of targeting specific axons separately from others. There is, however, one interesting type of cuff electrodes, the Flat Interface Nerve Electrodes (FINE) [92], which increase their selectivity by compressing the nerve flat and thus gaining proximity from the active sites to the targeted fascicles [8]. They were used in [37] to deliver sensory feedback in a prosthesis. Cuff electrodes are not

invasive to the nerves, but they are invasive to the body (i.e. they need to be surgically inserted in the body in order to connect them to a nerve). A prosthesis that uses cuff electrodes to deliver sensory feedback was developed by [39]. Other neural interfaces are all invasive. Probably one of the least invasive are the the Longitudinal Intrafascicular Electrodes (LIFE), which are introduced longitudinally inside the fascicles. This offers a good degree of selectivity, since they can be introduced in the fascicles of choice. The works [35] and [93] were the first in using LIFE, connected to the PNS of amputees, to deliver sensory feedback. Transverse Intrafascicular Multichannel Electrodes (TIME) [94] consists of one needle with multiple active sites that is inserted transversally in the nerve. They have been successfully used in prostheses to provide sensory feedback for closed-loop control [38]. Their level of invasiveness and selectivity present an interesting trade-off when compared to other electrodes [90]. UTAH electrodes [95] and their slanted design [96] consist of an array of electrodes that are also inserted transversally in the nerve. Being an array of needles, they are both highly selective and invasive. Finally, sieve electrodes can be highly selective, but are the most invasive design [97].

2.2   Computational Modelling of Peripheral Nerves

2.2.1   Necessity of Models for Understanding Neural Physiology

Our understanding of the physiology and behaviour of the nervous system is strictly dependent on developing conceptual and mathematical models of neurons in order to imprint and test on them and their simulated behaviours our knowledge about the neurons. Models comprise all the knowledge we have about the neurons, including their properties and both their individual and collective behaviours, as well as our knowledge about complex phenomena that arise as a result of their collective behaviours. Modern technologies in computation allow us to numerically simulate the behaviour of our models under conditions of our choice, and therefore quantitatively assess potential or hypothesised neuronal behaviour and its consequences.

2.2.2   Evolution of Nerve Fiber Models

The PNS has been (and is still being) studied extensively using computational models. It started with individual modelling of its basic units, the axons, and the complexity and richness of models has been increasing over the years. When a spatial representation of neurons is needed in order to account for the dependence of the currents and potentials on the geometry of the neuron, the cable equation is the

staple model in use. It was first used in the study of neurons by [98] and [99], and has since been extensively used by many others (see [100] for a review; see also [69]). This equation, with all its elaborated versions, has allowed researchers to study many aspects of neuronal behaviours through neuron membranes, especially regarding electrotonous potentials and propagation. The study of the membranes with the cable equation has facilitated the study of the membrane ion channels, responsible for the active propagation of APs, about which knowledge has increased every year. Around the mid-20th century the works of [101] and [51] set a cornerstone for the modern study of ion channels, and their models have been thoroughly used to the present day.

Models of membranes with voltage-gated ion channels have been thoroughly used, studied, and improved during the past century. They started with simple RC circuits, acquired the level of [101] and [51] for squid and frogs, and eventually started including properties of mammalian nerves. This step involved the study of myelinated axons and the role of myelin in conduction in myelinated nerve fibers.

Departing from knowledge on other animals, experimental studies have provided insights about properties of mammalian nerve fibers (as representative examples for rat nerve fiber ion channels, see [102–105], among many others), and the knowledge about them has accumulated over the years. The properties of myelin sheaths need to be thoroughly understood in order to attain a complete picture of their role in the physiology and behaviour of mammalian nerve fibers. A myelin sheath acts in close interaction with the voltage-gated ion-channelled membrane that it surrounds. Compartmental models (compartmental modelling consists of lumping the membrane properties of the axons in order to discretise its length to aid numerical simulations [100]) of myelinated fibers were first run in numerical simulations by [46] using a lumped form of a myelinated axon, which consists of lumping the nodes of Ranvier and adjacent internodal compartments in order to save computational power. Later works used this and improved models in order to study different aspects of myelinated fibers. For example, [45] studied the relationship between CV and diameter with numerical simulations, [10] studied this relationship with internodal length, and [106] and [59] used their newer models to study the response of myelinated axons to a field generated by an extracellular electrode. Computational and experimental studies have aided accumulating knowledge about myelinated axons. Knowledge was acquired regarding new ion channels, paranodal regions, and myelin longitudinal currents on rat myelinated axons [103,104,107]. This eventually led to more complex models, such as the McIntyre-Richardson-Grill (MRG) [108], where paranodal regions and periaxonal space are accounted for in a double cable model that simulates the longitudinal currents. The model from [108] has been commonly used since [109,110], even when models for human myelinated fibers had been proposed in the past [111,112] —although the latter have also been used relatively recently [40,56]. The MRG model has also recently been the basis for a new model describing sensory fibers [113].

Newer models are questioning the implications of the cable equation, studying the often neglected effects that its assumptions have when modelling situations of interest. The acknowledgement of ephaptic currents is probably one of the most remarkable examples [69, 114] —although these works do not necessarily deal with myelinated axons. Also, the effects of the assumption of angular isopotentiality or rotational invariance of the membrane have been assessed through modified models of the cable equation which incorporate transverse components for polarisation [115–117]. However, it has generally been found that this assumption is valid for the majority of practical applications [117].

2.2.3 Models of Peripheral Nerve Trunks
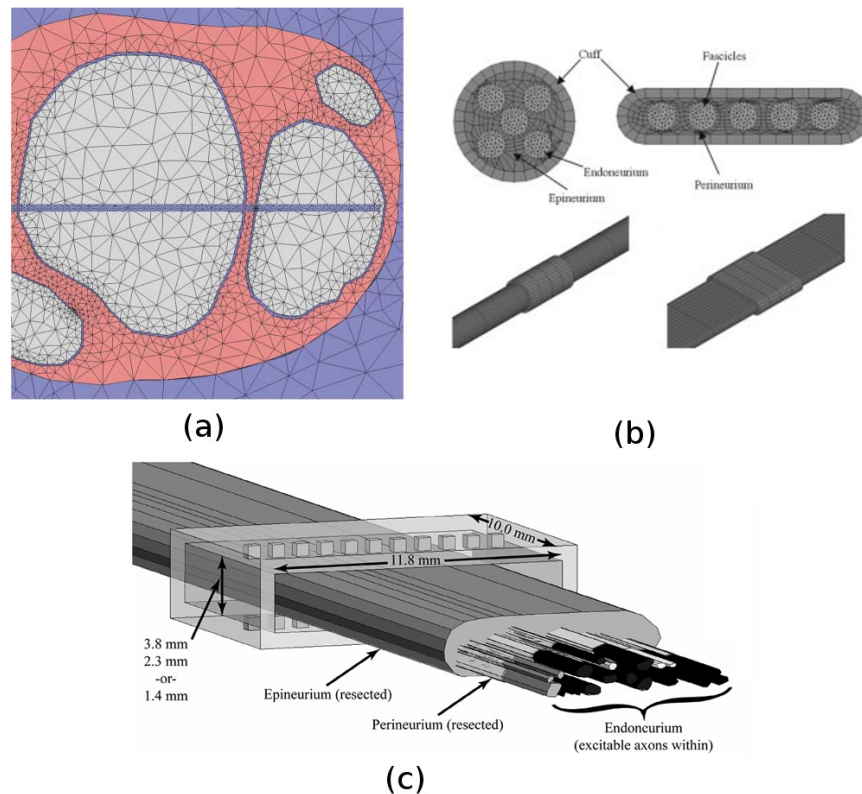
Figure 2.1: Examples of existing nerve models implemented to solve their fields in FEM. Models and figures taken from (a) [6], (b) [7] and (c) [8], respectively.

Models of fiber bundles and nerve trunks are relatively recent. They were first designed as part of theoretical studies, or as computational volume conductor models which included numerous simplifications [55, 118, 119], then later as more detailed models including separate fascicles in complex geometries [120–122]. FEM are very convenient for computing fields resulting from electrodes over the geometry of a nerve trunk. They were proposed early for this purpose [123], although they started being

used later with greater frequency in models with somewhat complex geometries and distinction of tissues [7, 120, 124]. Since then, they have been used as the most powerful tool for modelling the electrode fields [8, 40, 110, 125]. The complexity of peripheral nerve models has been increasing in recent years. After previous models in which fibers in bundles were all identical, fibers of differing diameters (although with only a few values) were taken into account [120]. Eventually, fascicles with fiber diameters randomly allocated, following experimentally measured distributions [8], were used. Other anatomical aspects, such as tortuosity, were also included [110], and more complex axon models such as the MRG were embedded in these larger nerve models [109, 110, 126].

2.2.4   Existing Tools for Neural Modelling

Computational modelling of neurons and neural systems has underseen the creation, development, and use of numerous models that aim to simulate most parts of the nervous system and many of its relevant aspects —physiology, anatomy, computational function of individual cells and networks, etc. Most models have been developed in close relationship with experimental studies that provide necessary data, knowledge, and parameters model designs. They are mostly based on the cable equation, established as the most utilisable theory for modelling the shape and physiology of individual neurons due to its ease of understanding and implementation. Early computational studies of neurons which focused on their anatomical (including the main parts of neural morphologies —somas, dendrites [127–129], axons [10, 45, 46, 100, 106], branching points [130], etc.) and physiological properties (such as membrane ion channels [128, 130] and synapses [127, 131]) were based on this theory, and it has been thoroughly used until the present day. During this time, both simple [59, 60] and sophisticated [108] cable models have been included in larger nerve models [8, 40, 68, 108, 110, 132, 133], and basic models for cortical cells based on the cable equation like [129] are still used today—in fact, this model is arguably one of the most popular—to expand the knowledge about them, is such areas as those regarding their artificial stimulation [76], EC [70] or recordings of their activity [134] (note that these references are only examples of works on these respective fields; a more thoroughly intended review should include all the deserved references).

Following the proliferating use of the cable equation and, more generally, neural models, programmatic tools have been developed in the last few decades to facilitate the modelling of neurons. These tools were developed with the idea of reducing redundant design efforts [135], allowing modellers to define detailed anatomical and physiological properties of individual neurons and neural systems with relative ease, and saving them the burden of implementing the cable and membrane equations from scratch. There are therefore common aspects to these tools: their open source philosophy and the availability of their code. Most of the tools discussed here are

open source.

Two tools developed between the late 1990s and early 2000s are NEURON [130] and GENESIS [135]. These tools were centred on modelling the detailed morphology of neurons, something barely achieved at that time (except for the dendritic trees models of [129], for instance) and which was definitely not available in the form of a programmatic tool; in order to run their simulations, every research group had to implement their models in computer programs from the start. These tools also permit configuring neural networks and parallel computing of their simulations (see [136] for NEURON and [135] for GENESIS). More recently, NEURON has been updated with a Python interface [137], which makes the definition of models and simulations easier for users.

NEURON and GENESIS use compartmental modelling of the cable equation in order to build neural models. These two tools have been by far the most relevant and widely used in the field of neural modelling in recent decades. They have facilitated the modelling of many cells and systems closely based on experimental observations, which has greatly widened the knowledge about the nervous system. For lists of works using NEURON and GENESIS see [130] and [135], respectively. Note that these are only until 2001 and 2003, respectively. This present study makes exclusive use of NEURON for the peripheral nerve models and also individual fiber models, and we have taken advantage of its Python interface.

Other tools have been developed recently which also use the cable equation. Examples of these are shortly summarised in the following. Neurite [138] was recently developed as a tool to simulate signal propagation in neurites under mechanical loading, which can be used to simulate the behaviour of damaged neurites. Neurite also allows the definition of complex neural morphologies and parallel computing of the simulations. Also worth mentioning are NEST [139], similarly developed in the early 2000s, and the more recent Brian [140], implemented as a Python package. These two tools allow the simulation of networks of spiking neurons, although they have less focus on detailed neuron morphologies.

The existence of these tools has facilitated researchers building complex neural models, and the development of more sophisticated tools based on the original. A clear example involved in modelling PNS is PyPNS [110]. This software uses NEURON to simulate bundles of both unmyelinated and myelinated fibers in peripheral nerves, allows the use of pre-computed fields to stimulate the fibers (either coming from FEM simulations or by other means), and uses FEM and analytical solutions to simulate electrode recordings of neural activity. Regarding the morphological properties of axons, it allows for the inclusion of detailed models of the double cable circuit from MRG and, on a larger scale, it furthermore simulates axon tortuosity in the bundle, which permits studying into the effects of tortuosity on stimulation and recordings. It lacks, however, a model of EC among fibers and, therefore, it does not use a EMI approach. It uses NEURON for the neural models and Python as a

wrapping language. Another application of NEURON is not involved directly with the generation of more complex models than the existing, but is aimed at computing the Local Field Potential (LFP) from any desired model. LFPy [134] uses NEURON in order to simulate the activity of any number of neuron models provided by users, and uses the simulated membrane currents to compute the extracellular field over space. The aim of this tool is limited in scope, in the sense that it is not intended to explicitly study aspects of neural activity other than the extracellular potential. But it does serve a very useful purpose, since the LFP generated by neural activity at a point (such as the location of a recording electrode) is of great interest.

2.2.5   Use of Computational Modelling for Sensory Feedback Restoration

Designing neural interfaces for sensory feedback restoration requires knowing how the PNS responds to such interfaces, so that the sensory information that can be elicited with them can be predicted. The PNS is an intricate system, and predicting its response to artificial stimuli is arguably difficult, yet it is necessary in order to avoid excessive trial and error experiments on patients. Trial and error approaches when using certain neural interfaces directly on human subjects exist in order to calibrate the stimulation parameters necessary for evoking different sensations. See [38], who mapped injected electric charge through TIME electrodes to reported sensation intensity by the user, and [37], where the stimulation parameters were found by matching induced sensation of pressure with a pressure reported by the user. However, none of these works do so without previous prediction studies; see [40] as a previous study to [38] and [58] to [37]. These latter are guided by machine-nerve interface models, where the behaviours of axons in nerves are simulated under conditions that imitate those that, ideally, take place in real scenarios, mainly involving the implantation of an electrode in a peripheral nerve. Simulations using these models allow in-detail observations of both individual and collective axon behaviours in response to the simulated stimulation from electrodes. They allow us to observe which fascicles in the nerves get the highest number of fired axons. This, together with a theoretical map between fascicles and somatosensory regions, provides an indication of where artificial stimulation can elicit sensations in the human body. Also, observation of axon firing rates can help elucidate the quality of the evoked sensations [141]. These variables depend on the stimulation parameters in play. There are geometrical parameters (type of electrodes, nerve anatomy and active site locations) and electrical (the time series used by the active sites to inject charge into the nerve, which can include any waveform, although the most common are square monophasic or biphasic pulses [142]). In these, relevant parameters are pulse amplitude, width and frequency. As nerve response can be predicted based on the values for these parameters, numerical simulations can assist optimal choices for them, ultimately helping the design of interfaces between assistive devices and PNS.

Simulations of Collective Axon Response to Extracellular Stimulation

Predictions of collective axon response to artificial stimulation use nerve trunk or bundle models like those described in Section 2.2, including models of the electrode designs under study. They include varying levels of detail with regards to variety of fiber types and sizes, inclusion of different tissues (some of which may have anisotropic conductivity), and fascicle shapes, amongst other aspects. But they share a common intention: to model nerve segments with several separate fascicles, and simulate which axons are activated by the different stimulation protocols under study. The selectivity is the level of accuracy with which an electrode can stimulate the targeted groups of fibers of a nerve, in order to generate certain sensory information or to elicit the movement of certain muscles of a patient. Stimulation performed with insufficiently selective electrodes could induce unwanted muscular movements or sensations in the patient. Selective stimulation of axons has often been an intensely pursued goal, and it has been studied within the last decades, either for targeted muscle innervation [8] or for sensory feedback [56]. The endeavours towards this goal, aided by simulation studies, has led to various designs for neural interfaces as discussed in Section 2.1. During the process, a variety of numerical approaches have been adopted to study axon response and, subsequently, selectivity.

The process of simulating artificial electrical stimulation mainly consists of two parts. First, the potential fields generated by the electrodes need to be solved over the neurons, at their locations and along their geometries. And second, the neurons' electrical and physiological responses to these fields need to be simulated.

Simulating fields generated by electrodes   The electric and magnetic fields generated by stimulating electrodes on any physiological tissue are naturally given by Maxwell's equations. Neurons respond both to electric and magnetic fields. However, most practical applications in artificial electrical stimulation use fields with frequencies low enough to rely on the QS approximation. Under the QS approximation, the time-dependent components of Maxwell's equations are neglected, and therefore magnetic and inductive effects can be ignored. The QS approximation is valid for frequencies under 1 kHz [76,143]. Most aspects of known neural behaviour, including time constants and most common voltage oscillations in neuronal membranes, lie in this range or under. However, not all do, and furthermore, electrical stimulation patterns include components above 1 kHz. Therefore, the validity of the QS approximation has been assessed [75,143], although it has been determined that for most practical applications in electrical stimulation, the QS approximation accurately describes the fields generated by electrodes [75,76].

Under the QS approximation, the variable of interest from these equations is the electric field or the electric potential, and it is generally found by solving the Poisson

equation over a domain. Even in this case, solving this variable on neural tissue is generally not an easy task, due to the morphological and electrical complexities of the tissues. Analytical solutions exist for approximated cases. The simplest of them is the point-source (PS) approximation, used by [144] to compute the potential field over a volume from a current injected by a monopolar point electrode. The potential field over a volume is obtained as follows:

$$\phi(\mathbf{r}) = \frac{1}{4\pi\sigma} \frac{I_S}{|\mathbf{r} - \mathbf{r}_S|}, \tag{2.1}$$

where I_S is the current at the source, $\mathbf{r}$ is any point in space, $\mathbf{r}_S$ is the position of the source (the electrode), and σ is the conductivity of the space.

There are also analytical solutions which are approximated to the scenarios of interest. For stimulation in fiber bundles, there are solutions for PS electrodes in cylindrical conductors [145] (see [76]).

These approaches, although they are computationally very efficient and in many cases convenient, entail restrictive assumptions and simplifications and hence do not account for the complexities of nerve anatomy and electrical properties. Thus, they are practically unsuited to model complex anatomical and biophysical structures. Numerical solutions are needed in cases with more complex problems. Finite Difference Methods (FDM) and FEM have been widely used to model the electric fields over tissues with complex geometries, heterogeneous distributions of tissues and anisotropic conductivities. FDM were initially used (see [112,146] for modelling the dorsal root). However, complex geometries are better represented by the meshes used in FEM than the regular meshes used in FDM. FEM have been used since early works [120, 123] and have recently acquired great importance, being currently the main, if not practically the only, tool for solving the Poisson equation over nerve models. They have been widely used in nerve electrical stimulation studies in order to simulate the performance, especially focusing on selectivity, of cuff electrodes [7,124], FINE [8] and TIME [40] (amongst many other works). They have also been used to model electrode recordings from neural activity in peripheral nerves [110]. FEM are also used to simulate stimulation in the CNS [147], where the performance of Micro Electrode Arrays (MEAs) is studied.

Simulating neuronal responses to fields   The collective neuronal response to applied stimulating fields is, of course, computed from the individual responses of each of the neurons or axons in the model, which are simulated using the methods described in Section 2.2.2. The general practice to combine those individual models with a larger framework that includes bundle models and electrode configurations is to use the so-called hybrid field-neuron models [40], which first simulate the fields using a Poisson solver for the electrical fields over the nerve's volume

as described above (structural modelling, generally using FEM in the last years), and later use the resulting fields as a stimulation forcing on compartmental models of neurons (normally using the NEURON simulation environment [2], although other methods exist) to study their response, according to the locations and orientations of the compartments. The framework for hybrid field-neuron models was started with the FEM simulations of [123], and it was followed by other works [8, 120, 148]. The exceptions to this generalised practice are EMI models (EMI standing for extracellular-membrane-intracellular domains; see [114]), where both fields and neuronal responses are computed self-consistently at every time step of the simulations, and the recent bi-directional models [149], which couple 3D models of unmyelinated [150] and myelinated double-cable models [151] with an extracellular space, also self-consistently, and solve their interactions using FEM.

Within hybrid field-neuron models, the methods and models for simulating neuronal response differ according to the type of neurons accounted for and the level of detail given to the models. The most common model for the spatial representation of neurons is the cable equation, and this is solved numerically using compartmental models. In the most explicit neuron models that use the cable equation, this is combined with models for non-linear dynamics of the ion-gated channels of the neuron membranes, represented with circuit models. They also include explicit circuital representations of the myelin sheaths of the axons and the close surrounding extracellular space. NEURON allows the implementation of these models, and has been frequently used for this purpose. This is the case, for instance, of the selectivity studies carried out on PNS models by [8], who performed simulations of the stimulation of a model of the human femoral nerve using FINEs, in order to study their selectivity at stimulating motor fibers for muscular movement, or [40], who ran a similar study for a rat sciatic nerve model using TIMEs.

There are other ways to predict excitation in axons without the need of computing membrane processes and solving the full cable equation. These are approximations known as linearised models [152] or estimators [76]. They eliminate the non-linear terms of the ion-gated channels from the cable equation, which can be computationally expensive, and make the prediction of the membrane polarisation under an extracellular stimulating field much easier. These methods are very useful when ion-gated properties of the membranes are unknown, or are not aimed at being computed, in order to make quick estimations of recruitment in bundles containing large numbers of axons. The most basic method within this set of approaches is to use purely linear, or passive, cable models. Using these, the activation of an axon is predicted when the induced membrane depolarisation reaches the assumed threshold. This approach has the disadvantage that it assumes the threshold to be fixed and ignores the relationship between it and the stimulation pulse width [121, 153]. An early estimator of this kind, aside from the mentioned passive cable models, is the Activating Function (AF), developed by [59]. It predicts the membrane sub-threshold polarisation of an axon to be proportional to the second spatial derivative of the extracellular field, and because it needs only knowledge on the

extracellular potential, the location, and orientation of the axon, it can make such prediction avoiding the computation of passive cable models. Examples of the use of this method can be seen in [43, 154, 155]. The assumptions inherent in this method, however, make it prone to errors, and other works have developed other linearised models which address these weaknesses. The model from [153] uses the AF in combination with cable models, and accounts for intracellular longitudinal currents, which are known to affect the transmembrane potential after a few μs from stimulation onset [153] (see more on [76]). Other so-called linearised prediction models were developed by [60], who introduced the excitation function, different to the AF, and [152], who added more detail on the activation thresholds, including dependence on the extracellular potential, fiber diameter and stimulating pulse width. Also, [147] developed the mirror estimate, which takes into account the boundary conditions in finite axons, while the AF assumes infinity of axon length, and can compute activation from fields whose second order derivative along the axon is null.

Although their validity is constrained by their algebraic and linear nature, these latter methods are so computationally inexpensive that they allow their usage in evolutionary or genetic optimisation algorithms for electrode design, which involve a large number of simulations. For examples on these studies, see: [154], where the AF was used to optimise a cochlear implant electrode array; [133], who used [60] to optimise the parameters for stimulation with FINEs to maximise selectivity; or [156], who used [153] for a similar study on the same type of electrode.

2.3   Ephaptic Coupling

Ephaptic coupling consists of electrical interactions between nearby cells through endogenously generated fields (see Fig. 2.2), i.e., fields generated by the activity of these cells, in such a way that the activities of these cells are intercorrelated —coupled, even in the absence of other types of connections, either synaptic or gap junctions. This type of coupling is different to synaptic connections and gap junctions, and is probably the least studied of the three, since there its relevance is under a heated debate [157]. Ephaptic coupling in the nervous system may happen between neurons in networks in the CNS or between fiber tracts, both in the CNS and PNS. Many more studies have been undertaken for neurons in the CNS than for fiber tracts [157, 158], since its relevance is well acknowledged in some regions of the CNS; it is known to be significant in the hippocampus [157] and in the cortex [159], where the high density of neurons and their laminar structure favour large LFPs [70]. In these regions, ephaptic coupling is known to play a role in synchronisation of neurons and also in the emergence of pathological neural behaviours, such as epilepsy [160]. Ephaptic coupling is also present and strong in AP propagation in cardiac cells [161–163].
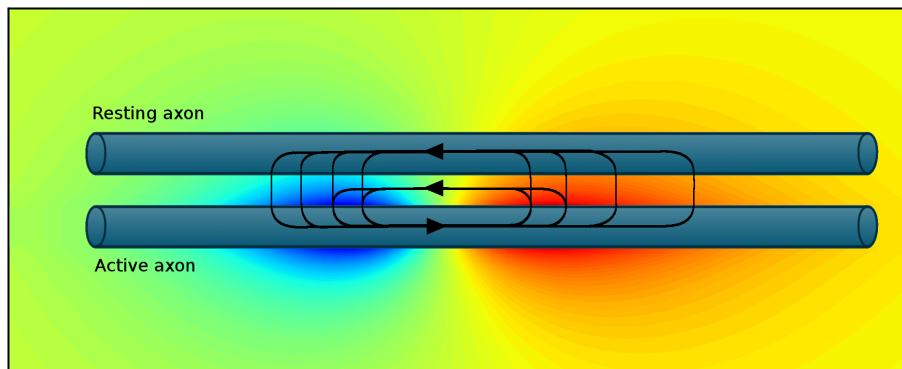
Figure 2.2: Conceptual illustration of ephaptic interactions. In this scenario, an axon carrying an AP (active axon) creates an extracellular field (color map) which stimulates the neighbouring (resting) axon. Black closed curves conceptually illustrate how currents driven by the activity of the active axon flow along the interstitial space between axons and enter inside the resting axon. Inspired on [9].

2.3.1 Existing Knowledge about Ephaptic Coupling in Fibers

The electric interactions between two unmyelinated fibers were first experimentally observed in *in vitro* preparations and studied by [9] in 1940 and [61]. Since then, electrical interactions in the absence of synapses or gap junctions (that is, due entirely to the endogenously generated extracellular potential) have already been studied, and considerable understanding has been gained for the case of two unmyelinated fibers [11, 62, 65, 164, 165]. Studies on the interaction of myelinated fibers are more recent, and interest in this phenomenon only arose within the last two decades. A possible reason for this is the work of [63], which assumed that ephaptic interactions between myelinated fibers are negligible. This assumption became accepted until subsequent studies about ephaptic coupling in myelinated axons questioned this idea. Previous to [63], first indicators about ephaptic coupling in myelinated axons came from observations on a frog's sciatic nerve by [166]. Later, a ground-setting study on the ephaptic interactions of myelinated axons was provided by [64]. By interpreting an analytical treatment of ephaptic coupling in unmyelinated nerve fibers provided by [165] into the myelinated case, they provided a theoretically justified reason for expecting coupled impulses in saltatory conduction and developed a simple circuit model which was used to study different cases of coupled propagation of pulses, as well as the effects of myelination on propagation of a single nerve fiber. In the same year, two other models for simulating ephaptic interactions in parallel unmyelinated fiber bundles were developed by [65], which are also applicable to the case of myelinated fibers: the MF model and the geometric model. The first simulation of propagation with ephaptic coupling that included more than two myelinated axons in a bundle was made by [66]. In this sense, although [65] simulates the activity of a bundle, the equations presented for the MF model are reduced to two axons, accounting only for the distinction between stimulated and

unstimulated axons. Using the MF model taken from [65], [66] studied the effect of myelin damage and level of ephaptic interaction in signal propagation, as well as other aspects as temperature. The results of these works showed synchronisation between fibers in the propagation of pulses. That is, pulses in different fibers tend to adjust their speeds and synchronise and travel together, although this occurs at the expense of a decrease in the velocity of propagation. Also, [66] found that damaged fibers with conduction block could be brought into conduction by the activity of other nearby fibers. The works of [64] and [66] found that ephaptic coupling may be especially strong for damaged fibers, especially after demyelination, since loss of myelin removes insulation layers between fibers. These results are in agreement with the observations from [166].

Later works, which usually use the work of [66] and almost invariably that of [64] as references until 2013, focus on mathematical treatments of systems of coupled network differential equations and use ephaptic coupling as an application or example for their studies [167–170]. Others use ephaptic coupling for studying health issues, such as conduction difficulties by loss of myelin or axon damage [171]. Some of the mentioned works with mathematical treatments address ephaptic coupling in a more direct way, thus providing useful insights in some of the many relevant aspects of the problem. For instance, [168] used the models of [165] and [64] to study the effect of the alignment of the nodes of Ranvier on the range of propagation failure due to ephaptic coupling. They found that the alignment of the nodes increases the range of the parameters in the models between which failure could occur, whereas staggering diminishes it. Also, [169] studied the coupling effects of two non-identical fibers and found phenomena such as soliton-like collisions between pulses, recombination of solitary and synchronised pulses and overtaking. These more mathematics-aimed works provide scope for the study of ephaptic coupling of myelinated axons.

2.3.2   Existing Modelling Techniques for Ephaptic Coupling between Fibers

All the approaches developed to date for modelling the ephaptic interactions between fibers intend, with varying levels of explicitness, to model the extracellular space where the fibers are embedded as a volume conductor. Some models have more of a strictly mathematical approach, like [167–170], while others focus on a somewhat detailed modelling of geometries and tissues. Below, the most relevant of the latter approaches for this work are described. It is worth noting that, in general, each one of these main approaches is preferred for a particular application (e.g., although there are exceptions, the MF model is preferred for bundles of parallel axons, classical electrostatics models are preferred for cortical neural networks, and resistor networks are preferred for cardiac cells).

The Mean-Field Model

The model from [64] consists of a cable that is shared between two axons as their extracellular domain, and both membranes are connected to it. This is probably the most basic model of extracellular connection between the two axons (at least for the myelinated case) that has been presented to date, which allows longitudinal currents to flow along the extracellular space (cable) and thus the flow of current from one axon to another. [64] used only two axons. Essentially the same idea was used in the same year by [65], who modelled a bundle of unmyelinated axons in the olfactory nerve as a set of parallel and identical axons whose extracellular domains were all directly connected to the same cable. This case, however, necessitates of the explicit assumption that the extracellular space is isopotential at any cross-sectional layer, so that all axons share a mean field at every layer. This eliminates any transverse currents between axons from the equations and leaves only the longitudinal currents along the shared extracellular cable.

When considering N identical axons in the bundle and N_S of them are stimulated simultaneously, the cable equations of all of them are coupled in such a way that the whole bundle can be reduced to the equations for two axons A (stimulated group) and B (unstimulated) [65]:

$$c_m \frac{\partial V^A}{\partial t} = \frac{a_{11}}{D}\frac{\partial^2 V^A}{\partial x^2} - \frac{a_{12}}{D}\frac{\partial^2 V^B}{\partial x^2} - I_{ion}^A + I_{stim}$$

$$c_m \frac{\partial V^B}{\partial t} = -\frac{a_{21}}{D}\frac{\partial^2 V^B}{\partial x^2} + \frac{a_{22}}{D}\frac{\partial^2 V^A}{\partial x^2} - I_{ion}^B$$

$$a_{11} = r_i + r_e(N - N_S)$$

$$a_{12} = r_e(N - N_S)$$

$$a_{21} = r_e$$

$$a_{22} = r_i + r_e$$

$$D = r_i^2 + Nr_i r_e$$

$$(2.2)$$

where c_m is the membrane capacitance, $V_{A,B}$ and $I_{ion}^{A,B}$ are the transmembrane potentials and membrane ionic currents of axons (or groups of axons) A and B, respectively, $r_{i,e}$ are the intracellular and extracellular resistances, respectively, and I_{stim} is the injected current in axon A.

The extracellular potential V_e does not actually need to be computed, since it leads to the equations above for the coupling of the transmembrane potentials of the axons. The only parameter that controls the properties of the extracellular space is r_e, which depends on the extracellular longitudinal conductivity of the medium and

the cross-sectional area of the extracellular space. As it can be seen in the equations, this parameter, along with its ratio with r_i, controls the strength of the ephaptic coupling between the axons. Note that the limit $r_e = 0$ implies $\frac{a_{12}}{D} = a_{12} = 0$, so the system in Eq. 2.2 becomes two uncoupled cable equations for axons A and B. This is the case where the assumption of the standard cable equation that the extracellular resistance is very low is met, so ephaptic interactions can be neglected [11].

The only dependence of this system on the extracellular space is on its longitudinal component. Its transverse component is ignored. This implies that V_e is common to all axons, regardless of the separation distance between them, and so is the strength of the ephaptic coupling between any two axons.

This model was used shortly after by [66] using a bundle of parallel and identical myelinated axons having all their nodes of Ranvier aligned. Their treatment and simulations depart from such a restricted and simple case of having only two groups of axons separated by their stimulation, and in some of their simulations, axons are stimulated individually at different times. Hence, this can—not with unjustified discussion—be considered as the first work in actually simulating a bundle of many ephaptically coupled axons. Also, the ephaptic current is explicitly included in their equations. More recently, this model was also used by [68].

The works of [65, 66] are concerned with synchronisation of APs, AP phase locking and effects on CV. The work of [68] is more concerned with polarisation effects due to ephaptic coupling, as well as synchronisation of neurons. In any case, but especially when studying synchronisation, applying this model to identical axons greatly simplifies the problem because it eliminates accounting for transverse currents, along with the intricate complexity of currents in the extracellular space that would arise from them. Axons of equal diameters have equal CVs, and therefore, observations in the deflections in CV and AP synchronisation are easy to observe. This model, despite its simplicity, clearly manages to simulate CV deflections that occur in order to reach AP synchronisation and the eventual AP synchronisation itself. It can also make predictions on recruitment of damaged fibers by the activity of healthy neighbouring ones. However, its core assumption presents a most important drawback: any variations of the extracellular potential over the bundle's cross-section cannot be modelled. These are actually very relevant in certain situations of interest, such as situations where extracellular stimulating electrodes are present, for which spatial dependence of the fields has been so much studied, and thick nerves where many fibers are present (and where this assumption may lose its validity).

Distance-Based Models

As known from basic electrostatics, the potential generated by a finite-sized current source varies across space, decaying with the distance from the source. The MF model only takes this into account in one direction. This is convenient for a bundle of parallel fibers which favour such configuration. But when potential variations along other directions needs to be accounted for, this is not a good approach. This is the case, for instance, of neural networks that do not have this geometrical characteristic length. Unless it is assumed that neural activity can generate an extracellular field that is isopotential across the entire volume of the network, a MF model is not suitable for this scenario, and distance dependence of the electric potential has to be taken into account. Also, simulations of electrical stimulation from extracellular electrodes become practically pointless if a MF model is used, since the spatial details of the electrode fields cannot be captured by such model.

Modelling the spatial change of the electric fields can be done in various ways, the most relevant of which are described below.

Classical Electrostatics Models

Compartmental modelling of neurons generally regards each neuron as a sequence of compartments, which can also be referred to as nodes, over each of which all the relevant variables in a neuron are constant, from geometrical properties and channel densities to electrical properties. Each compartment is therefore regarded as a current node in a circuit, and can be regarded as a current point source when seen from the outside.

The electric potential generated by a current point source S in an isotropic medium where the ground is assumed to be infinitely far away is given by Eq. 2.1. This and more complicated versions of it have been used by many who have studied the electric fields over tissues generated by electrodes, first by [144] and subsequently by others who also computed electrode fields [59] and fields generated by neuronal activity [134, 172] in order to simulate electrode recordings. But it was [69] who first applied this as a model of the extracellular potential generated by the activity of neurons. Each neuron, consisting of N compartments, would generate a potential at a point $\mathbf{r}$ given by:

$$\phi(\mathbf{r}, t) = \frac{1}{4\pi\sigma} \sum_{n=1}^{N} \frac{I_n(t)}{|\mathbf{r} - \mathbf{r}_n|} \tag{2.3}$$

Also, a line-source approximation is given in [69] which is suitable for long

straight axons.

This simple model can be used for any neuron model of any shape and complexity, and it is widely used because it is especially convenient for cells where axons and dendritic trees are modelled as departing from a soma, such as pyramidal cells. It has been used to study ephaptic coupling and AP synchronisation between these cortical neurons [70].

This is a non-costly model that can easily be implemented in numerical simulations. However, it is based on the assumption of an infinitely large extracellular domain, and has a singularity at the centre, which means that values of the potential computed very close to the source can be unrealistically high. This latter problem presents a difficulty when working with cells which are very close to each other, since it can compute unrealistic values of the extracellular field. Eq. 2.3 can be modified to account for anisotropies in the extracellular conductivity, although the complexity of any model cannot easily get much further than that. Accurate computing of the fields over complex geometries may be difficult to achieve.

Despite these inconveniences, this approach is still the basis of the calculations of LFPs from neurons [134], and it is also still highly relied upon for computing ephaptic fields [173].

Finite Element Methods

Modelling the endogenous extracellular fields with FEM is likely to be the most accurate method to date for this purpose, just as FEM are used to model the electrode fields in so many works. FEM are not only a reliable mathematical and computational tool; they also allow, in principle, for modelling the fields in any geometrical configuration and with the presence of any tissues of interest. Although FEM simulations are not exceedingly computationally expensive for electrical stimulation studies, where one simulation is enough to compute the electrode fields, it is so for simulations including EC. Either implementing neural models and extracellular space as EMI-type models [114], or using hybrid field-neuron [40] models (i.e., coupling other non-FEM neural models to FEM meshes for the extracellular space), needs at least one FEM computation of the fields to take place at every time step or between every two time steps of a simulation of the desired system. This has been done by [72,114,174], generally for neurons with complex shapes and with a remarkable success in obtaining a fine level of detail in the spatial distribution of the fields, membrane potentials and ephaptic interactions, but they used models which include a very small number of neurons in order to save computational costs. Nevertheless, these methods need to be kept in mind if high detail simulations are needed in the future, and might become especially interesting if the computational costs of FEM simulations are reduced in the future.

Resistor Network Models

Resistor network models for volume conductors discretise the space in nodes which are interconnected between resistors. The resistors are given values in accordance with the geometry and electrical properties of the volume conductor.

One of the simplest examples of this in axons is [11], where the extracellular longitudinal cables of two core-conductor axons are connected by transverse resistors. Several models of cardiac tissue that involve ephaptic coupling between cells use this approach [161, 163, 175, 176]. Also, note that the MF model for parallel axons can be viewed as a very simple case of this approach where the extracellular common cable comprises the whole network.

Just like FEM meshes, this approach permits modelling any complex geometry and tissue configuration at will if proper characterisation of the space is done, i.e., if a general model for the values of the resistances is used for any random geometry, as is done in this dissertation. Again, its main drawback is the high computational cost it entails. However, its circuital configuration permits an easy coupling with currently used neural simulation environments like NEURON [2], which are also circuit-based, and an EMI-type model can be built. This is done in this dissertation, and was also done recently by [73].

2.3.3 Relevance for Sensory Feedback Restoration

The studies that have used computational models of nerve trunks or fiber bundles in order to assess the selectivity of different electrode configurations [8, 40, 120], especially those ultimately concerned with sensory feedback restoration [40], are not concerned with the potential effects that ephaptic coupling may have on actual results of neural activity in their situations of interest. Experimental evidence of ephaptic interactions between peripheral nerves in rats has very recently been found [67]. In the works [64, 66, 166], ephaptic coupling seems to be most important between damaged fibers, yet not so much for undamaged ones. However, the findings of [67] evidence that these are also present between undamaged fibers. In [67], ephaptic coupling appears not to be very strong between and within peripheral nerves outside the dorsal root, and it is suggested that the epineurium may be preventing such interactions between fascicles (note however, that ephaptic interactions between fibers inside fascicles may still be strong). Within the dorsal root, however, the ephaptic coupling was found to be stronger. This alone, whilst accounting for the still open possibility that it is strong between fibers inside fascicles, is enough to consider modelling ephaptic coupling in computational models, otherwise important effects on the interaction between fibers during stimulation and propagation may be overseen.

These effects can be taking place during stimulation or propagation, or during both. The work of [67] finds an increase in excitability of the fibers in a nerve when a compound signal from a neighbouring nerve travels near it. This, in fact, is in agreement with findings using numerical simulation in this dissertation (see Chapter 5). Hence, repeating the conditions of previous studies [7, 8, 40] including ephaptic interactions in the models may yield higher recruitment values than the original works and thus, selectivity performance of the studied electrode configurations would need to be at least slightly revisited. The effects of ephaptic coupling on propagation are known from numerical studies [64, 66, 68]. These mainly consist of synchronisation, AP phase locking, and reduction of the conduction velocities. Also, to a different extent, they may include recruitment of inactive or damaged fibers [66]. This could further affect selectivity. But more importantly, synchronisation is postulated to be a mechanism for information processing. Little is known yet about how the PNS encodes sensory information [141], and given the currently existing clues about the synchronisation mechanism in the PNS, it could be worth modelling them in order to study their role in sensory information encoding before entrance into the CNS.

Chapter 3

Conduction Velocity Adjustments During Propagation in Fibers

The contents of this chapter are adapted from [13] and [177], publications leaded by the author of this thesis as detailed in the List of Publications.

3.1 Introduction

The work of [64] found that two neighbouring myelinated axons tend to match their Action Potential (AP) Conduction Velocities (CV) in such a way that their APs travel together synchronously. Hence, Ephaptic Coupling (EC) is expected to modulate AP CVs and adjust the frequency of the Compound Action Potential (CAP) via synchronisation or locking of APs. Hence, the work of [64] provided a justification for expecting coupled impulses in saltatory conduction. Qualitatively similar results were found by [66] for a bundle of parallel myelinated axons. The works [64,66] use a Mean-Field (MF) assumption to compute the extracellular field for ephaptic interactions. However, the amplitude of this field is, naturally, thought to depend inversely on the distance from the source axon [69]. Although the MF assumption is useful for bundles of axons in simple conditions, it is not suitable for other scenarios, such as those including extracellular electrodes or those where large axon bundles are considered, such that inter-axonal distance may be too large for the assumption to hold.

In this chapter, we aim to test the effects of EC under a distance-dependent model of the extracellular potential, and we thus used a distance-based model based on [69]. We found that in simulations of two and three neighbouring axons, these tend to match their AP CVs and propagate their APs synchronously.

This chapter is divided in two main sections. In the first section, we demonstrate the influence of axonal activity on neighbouring axons by simulating the activity of two parallel, neighbouring and identical axons, in which the activity of one of them (axon 2) is influenced by the activity of the other (axon 1) through the electrical currents generated by the latter in the extracellular medium that both axons share. This interaction takes place only in one direction, so axon 2 has no influence back on axon 1. This allows us to isolate the effects of individual axons and avoid the effects of mutual interaction. Our simulations show that the activity of axon 1 influences the CV of axon 2 (v_2) so that, under certain conditions, the AP of axon 2 approaches the AP of axon 1. In the second section, we address the effects of EC in the synchronisation of the APs of three identical, parallel myelinated fibers. Results show how the CVs of the three fibers change in order to couple the APs of the three axons. The findings in this chapter are in general agreement with the findings on AP synchronisation in [64, 66, 68].

The novelties and contributions of this chapter are the following:

- Using numerical simulations, we provide a quantitative measure of the effects of the ephaptic influence from one myelinated axon on the CV of a neighbour. This quantity is measured against i) the relative timing between the APs of the two axons, ii) the inter-axonal distance between the axons, and iii) the conductivity of the surrounding medium.

- We show that the known synchronisation mechanisms between myelinated axons apply also for a distance-based model.

3.2   Unidirectional Ephaptic Stimulation between Two Myelinated Axons

3.2.1   Materials and Methods

Myelinated Axon Models

We use axon models described by the one-dimensional cable partial differential equation along the x-axis, given by

$$c(x)\frac{\partial}{\partial t}V(x,t) = \frac{1}{r_a}\frac{\partial^2}{\partial x^2}V(x,t) - i_m(x,t) \tag{3.1}$$

where V is the transmembrane potential, r_a is the axial resistance of the axoplasm per unit length, $c(x)$ is the membrane capacitance per unit length at the position[1] x, so that it is equal to:

- the membrane specific capacitance at the nodes of Ranvier (NR), or

- the membrane and the myelin sheath specific capacitances in series in the internodes (IN),

and i_m is the ionic total current per unit length crossing the membrane. In the IN, this current is computed using a passive model:

$$i_m(x,t) = g_M \left(V(x,t) - E \right) \tag{3.2}$$

with g_M being the myelin conductance per unit length, and E the resting potential. At the NR, this current is driven by the Hodgkin-Huxley (HH) equations [101]:

$$i_m(x,t) = \sum_k g_k \left(V(x,t) \right) \cdot \left(V(x,t) - E_k \right) \tag{3.3}$$

where for a voltage-gated channel k, g_k is the channel's non-linear function describing the conductance per unit length, and E_k is the corresponding reversal potential.

Values for the capacitance and conductance of the myelin sheath were obtained from [10].

Computation of Ephaptic Stimulation

Influence of axon 1 on axon 2 was obtained by calculating the extracellular potential resulting from the activity of axon 1 along the length of axon 2. This was done in a three step process:

1. A simulation of the activity of axon 1 for a time span of 27 ms is performed and the results of its net membrane currents $I_n(t)$ for every compartment n and every time step are stored.

2. Next, the stored values of $I_n(t)$ are used as current point sources to calculate the extracellular potential over the positions of the compartments of axon 2 for every time step, $\phi(\mathbf{r}, t)$, using Eq. 3.4.

---

[1]It should be noted that in this chapter, the axons are aligned with the x-axis. This will change in subsequent chapters, where axons will be aligned with the z-axis.
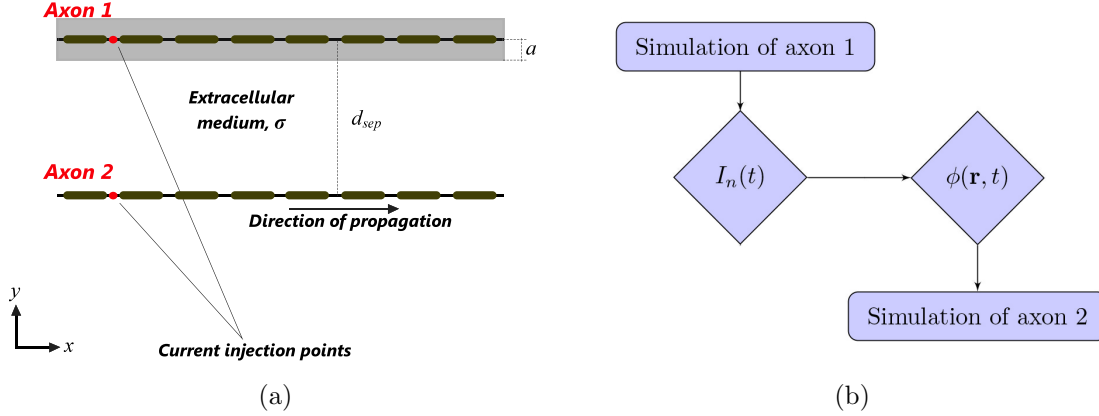
Figure 3.1: (a) Schematic of the arrangement of the axons. Axons are placed in parallel, separated by a distance d_{sep} and with their NR aligned. Red dots indicate points of current injection, which is the trigger for the APs. This point is at $x \approx 1$ cm for both axons, which corresponds to the 6th NR (INs are $2mm$ long and NRs are 3.183 μm long; this value has been obtained from [10]). The APs propagate in the direction of the arrow. The figure is not to scale. (b) Workflow diagram of the simulation framework. The membrane currents of axon 1 are used to compute $\phi(\mathbf{r}, t)$. To avoid divergent values near axon 1, the field is not computed inside the grey area in (a), which has the same width as the diameter of the axons. Although this choice is arbitrary, it serves as a reference of what would be the values of $\phi(\mathbf{r}, t)$ expected to be on the surface of axon 1.

3. Finally, the activity of axon 2 is simulated using both the computed $\phi(\mathbf{r}, t)$ and the current injection for stimulation.

Fig. 3.1 shows the geometrical arrangement of the axons and summarises the process.

Calculation of the extracellular potential   After simulating axon 1, extracellular potential was calculated in an offline process onto every one of the positions $\mathbf{r}$ of the compartments of axon 2 using Eq. 2.3, which is repeated and explained in more detail below:

$$\phi(\mathbf{r}, t) = \frac{1}{4\pi\sigma} \sum_{n=1}^{N} \frac{I_n(t)}{|\mathbf{r} - \mathbf{r}_n|} \tag{3.4}$$

where $\mathbf{r}_n$ is the position of the nth compartment of axon 1, $I_n(t)$ is the net membrane current of the nth compartment of axon 1, the sum is for all N compartments in axon 1, and σ is the conductivity of the medium.

Conductivity of the extracellular medium We have used two values for the conductivity. First, the known transverse conductivity of a nerve, $\sigma_T = 0.085$ S/m [178], and second, a smaller conductivity $\sigma = 10^{-3}$ S/m, to simulate a more resistive medium. As follows from Eq. 3.4, a more resistive medium increases the values of $\phi(\mathbf{r}, t)$, so it is expected to enhance the ephaptic effects.

Numerical Simulations

Numerical simulations of axons were performed using the NEURON simulation environment [2]. We used the Crank-Nicolson method for integration over time of equation 3.1. The time step used in the simulations is 0.025 ms, and each simulation spans a time lapse of 27 ms. This time lapse allows to minimise the margins of error in the calculation of the CVs.

3.2.2   Results

Simulations consist of the propagation of an AP on axon 1 and axon 2 during a time span of 27 ms.

In all simulations, both axons are stimulated with a square-shaped internal current injection with an amplitude of $1nA$ and a duration of 2 ms situated at the 6th NR, at $x \approx 1$ cm. This current can be injected in axon 2 at a different time ($t = t_2$) than in axon 1 (in which the current is injected at $t = t_1$). This time difference is expressed as $\Delta t = t_2 - t_1$. Thus, $\Delta t < 0$ means that current in axon 2 has been injected before in axon 1, and vice versa. Although it needs not be necessarily the case due to ephaptic stimulation in early stages of the simulations, we can regard $\Delta t < 0$ as the case when the AP of axon 2 is ahead of that of axon 1.

The CV of axon 1 is $v_1 = 13.82 \pm 0.03$ m/s. Both axons are identical in all their morphological and physiological properties (with the exception that axon 2 can be stimulated by an extracellular potential, unlike axon 1) and are stimulated with an equivalent current injection pattern. Therefore, simulations of axon 1 can serve as control simulations for axon 2, and in the absence of the ephaptic effect, $v_1 = v_2$. Thus, the difference in the CV between both axons $\Delta v = v_2 - v_1$ is indeed a measure of the strength of the ephaptic stimulation.

The CV of axon 2 can change with time as the APs of the axons change their relative positions, so the trajectory of the AP of axon 2 in the $x - t$ space is not necessarily a straight line. However, despite the deflection of this trajectory from a straight line is negligible, v_2 must be understood as the average of the CV over the length of axon 2 excluding its boundaries (to avoid the influence in the results of

the boundary conditions), which is 6.93 cm.

Dependence of the Strength of the Ephaptic Stimulation with the Delay between Axons
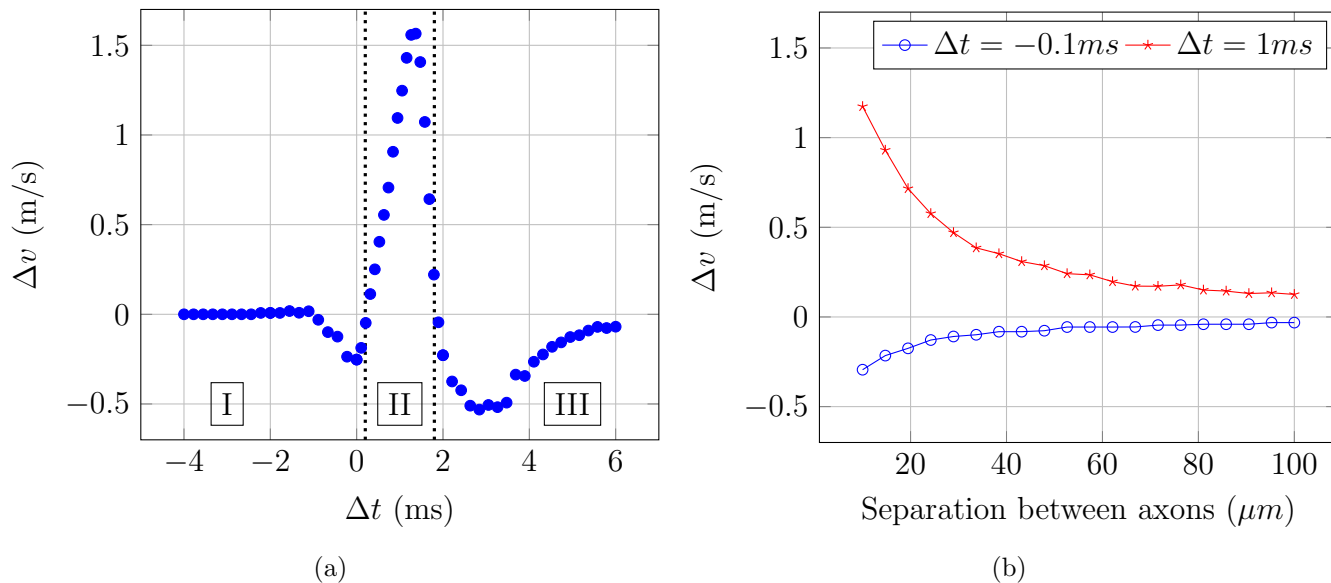
Figure 3.2: (a) Difference in the average CV between axons 2 and 1 depending on Δt and for a separation $d_{sep} = 10$ μm. The dotted lines separate the regions I, II and III mentioned in the text. (b) Difference in the average CV between axons 2 and 1 depending on d_{sep}. For both figures, $\sigma = 10^{-3}$ S/m.

We have run simulations with a variable Δt and a fixed separation distance between the two axons (d_{sep}) of 10 μm. Results for Δv (Fig. 3.2(a)) show a small slowing down effect for $\Delta t < 0.2$ ms (region I), a high peak corresponding to a speeding up effect for $0.2ms < \Delta t < 1.7$ ms (region II) and a subsequent slowing down effect for $\Delta t > 1.7$ ms (region III). Ephaptic stimulation beyond the limits $\Delta t < -2$ ms and $\Delta t > 6$ ms is very small and can be neglected. These ranges are approximate.

The comparison of Δv between regions I and II suggests that an AP in axon 1 is much more effective at speeding up a delayed AP in axon 2 than at slowing it down when the latter is ahead. In the mutual ephaptic interaction case, this can have the consequence of increasing the synchronised group velocity of both APs compared to a situation in which both slowing down and speeding up had the same effect. In other words, in order to make the AP in axon 2 reach the AP in axon 1 and achieve synchronised propagation, speeding it up is prioritary over slowing down the AP in axon 1.

Region III is wider and stronger than region I. Although a more thorough study

needs to be done to fully understand what the physical meaning of this region is, it suggests that axon 1 may be preventing APs in axon 2 that are delayed beyond a certain Δt (around 1.7 ms) from reaching it, thus keeping an increased separation between them and allowing only synchronisation with those APs of axon 2 that lie within $\Delta t < 1.7$ ms. This way, trains of well defined synchronised groups of APs could be travelling along a bundle of axons without mixing up.

In all cases that lie in region I, the AP of axon 1 eventually overtakes that of axon 2 at a distance that depends on the strength of the ephaptic interaction. However, overtaking has not been observed yet in the case when axon 2 is sped up. In fact, results in Fig. 3.2(a) suggest that axon 2 cannot overtake axon 1 under these conditions. Despite these observations, we can hypothesise that for $\Delta t < 0$, in the case of a mutual ephaptic interaction, axon 1 would not be able to overtake axon 2, as can be followed after [64].

Simulations with $\sigma = 0.085$ S/m (not shown) report a qualitatively similar pattern to that in Fig. 3.2(a), but in this case, Δv has a maximum of 3 cm/s and a minimum of -1.2 cm/s. However, in this case results do not present the smoothness of the curve in Fig. 3.2(a) and region I is not observed, probably because the values become of the same order of magnitude as the margins of error.

Dependence of the Strength of the Ephaptic Stimulation with the Distance between the Axons

Eq. 3.4 indicates an inverse dependence of $\phi(\mathbf{r}, t)$ on $|\mathbf{r} - \mathbf{r}_n|$. Therefore, it is reasonable to expect an inverse dependence of the ephaptic stimulation with d_{sep}. To check this, we have run simulations with varying values of d_{sep}.

We show the results of our simulations for two different cases: $\Delta t = -0.1$ ms and $\Delta t = 1$ ms, which are meant to study the effects of axon 1 on axon 2 when the latter is propagating an AP ahead and behind the former, respectively. In both cases, $|\Delta v|$ decreases with d_{sep} (Fig. 3.2(b)). This decreasing trend is consistent across simulations, so we can confirm that, as expected, the ephaptic effect is present and that its amplifying decays with the separation distance.

3.3 Conduction Velocity Effects Due to Ephaptic Interactions between Myelinated Axons

3.3.1 Materials and Methods

Myelinated Axon Models

We used the model for myelinated axons described in the previous section, which is based on the model by [10] and uses the Hodgkin-Huxley (HH) model [101] for the membrane of the nodes of Ranvier. We used axons with a diameter of 10 μm and an internodal distance of 2 mm. Internodes (IN) were partitioned into 10 segments each.

Computation of Ephaptic Coupling

EC was simulated by computing the extracellular potential field, ϕ, generated by the membrane currents of all the axons, and using this field as a stimulation input for the axons. The extracellular potential was calculated at every time step and on every position, $\mathbf{r}$, of all axons' compartments by using Eq. 3.4.

Details of the Numerical Simulation

The simulation was performed in NEURON and the integration method and time step size were the same as in the previous section (Crank-Nicolson; time step 0.025 ms). The simulation spans a time lapse of 45 ms.

The simulation comprised three parallel myelinated fibers with their central axes placed on the vertices of an equilateral triangle of side $a = 15$ μm as shown in Fig. 3.3(b)). The number of neurons was chosen to provide insights into multi-axon interaction without loss of generality while keeping the model simple and computationally fast. All the axons were identical in their physiological and morphological properties, and their nodes of Ranvier were perfectly aligned as shown in Fig. 3.3(a). The conductivity of the extracellular medium was set to $\sigma = 10^{-3}$ S/m.

Each simulated axon was independently stimulated with an intracellular square-shaped current injection with $1nA$ amplitude and 1.5 ms duration applied at the 31th node of Ranvier (position $x_{inj} \approx 6$ cm) and at times t_1, t_2 and t_3, respectively, being $t_1 < t_2 < t_3$. In order to avoid ephaptic effects during internal current stimulation and hence, avoid firing times different to those induced solely by the
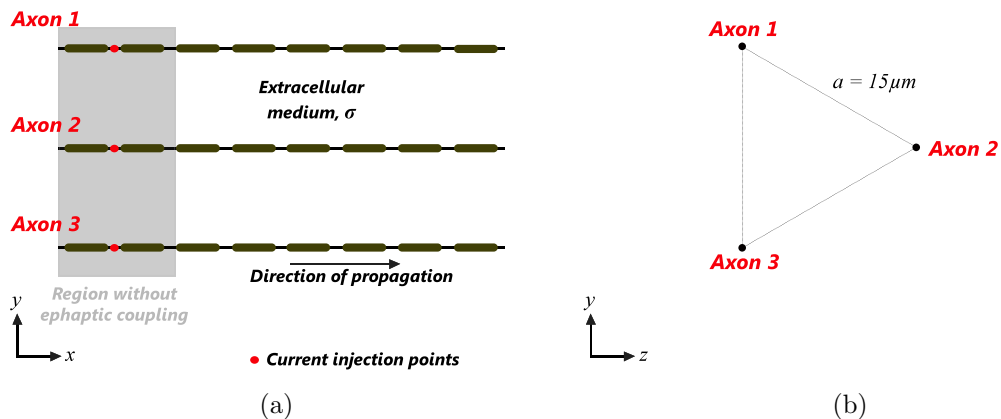
Figure 3.3: Geometrical arrangement of the axons in the simulation. (a) Longitudinal view. Fibers are parallel and the nodes of Ranvier are aligned. (b) Cross-sectional view. Axons are placed on the vertices of an equilateral triangle of side $a = 15\,\mu$m. The figures are not to scale. The axons are immersed in an extracellular medium of conductivity $\sigma = 10^{-3}$ S/m. Red dots indicate that the sites of current injection are at the same value of x (and in the same node of Ranvier) for all axons. The grey area indicates the region where ϕ is set to zero and ephaptic effects are suppressed. The horizontal arrow indicates the direction of propagation of the APs.

current injection at t_1, t_2 and t_3, ϕ was set to zero for all axons from $x = 0$ to an arbitrary safe distance $x = 2x_{inj}$, which also allows to calculate the velocity of propagation without EC. The stimulation times for axons 1, 2 and 3 were $t_1 = 0.1$ ms, $t_2 = 1.1$ ms and $t_3 = 2.1$ ms, respectively.

3.3.2   Results

Calculation of the Conduction Velocity

Conduction velocity was variable along distance and time in simulations with EC. The values of $v(t)$ for every time step in the simulation were obtained from the position x of the AP peaks (captured at the nodes of Ranvier) and the time instant when they occur. These data are shown in Fig. 3.4(a), after the $v(t)$ curves were smoothed as follows:

- Firstly, a 21-point moving average was applied to the position and time values of the AP peaks, and

- Secondly, a value of v for every point was obtained from the slope of a linear regression using the 40 surrounding points.

This smoothing process was necessary since computing $v(t)$ merely from the x and t values of each NR and its adjacent nodes generated a high number of artefacts. However, it limits the range in which $v(t)$ can be plotted to $t \in [3.82, 36.28]$ ms.

Ephaptic Interactions
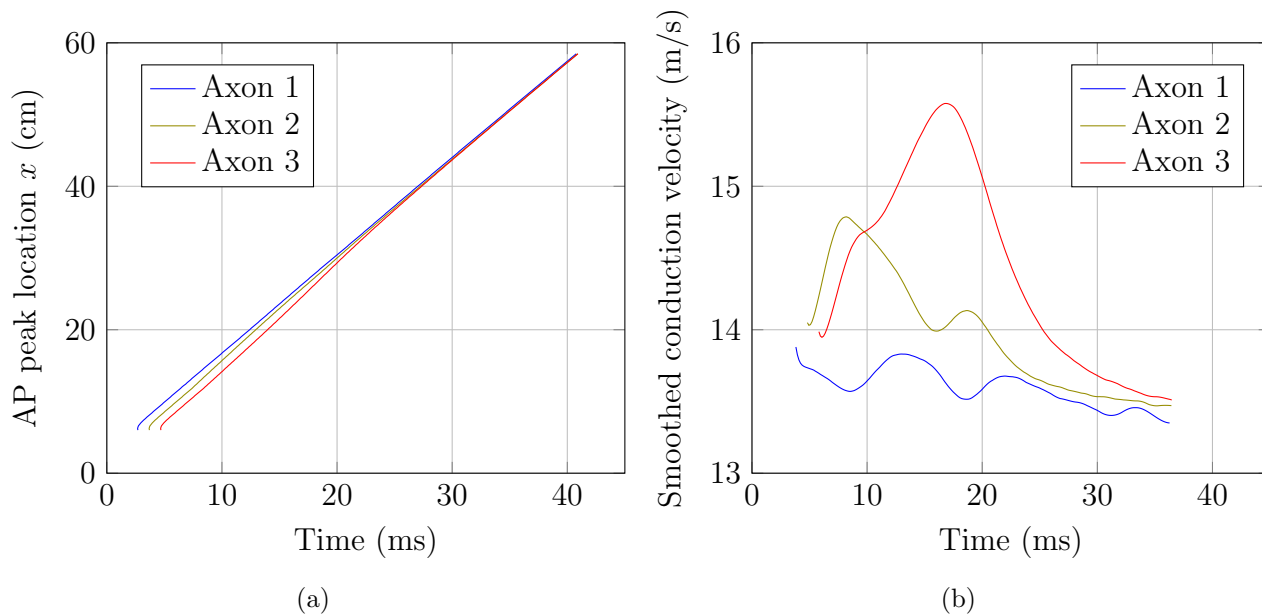
Figure 3.4: (a) Trajectories of the AP peaks in the x-t plane for the different axons. (b) CV as a function of time for each of the axons after the smoothing process was applied.

Although it is not visible in Fig. 3.4(b) due to the smoothing effect, at the beginning of the simulation all axons start with the same CV: $v_0 = 13.82$ m/s. As the ephaptic interactions start having an effect over the axons, CV is influenced. Curves in Fig. 3.4(b) suggest that the attraction effect of the action potential wave (APW) of the axon that has been fired first (axon 1, hence APW1) is dominant compared to those of APW2 and APW3. The first axon has no physiological difference compared to the others that could cause this advantage. The cause for this is rather related to the timing difference between APWs.

The velocities in axons 2 and 3 rise rapidly once the ephaptic interactions start, whereas v_1 decreased, and at a smaller rate. This suggests that axon APWs exert a stronger attraction over those which are delayed by about 1 ms behind them than over those which are ahead by a similar amount. As such, APW2 approaches the velocity of APW1 within approximately 2.6 ms. Once their velocities get closer, APW2 starts to slow down and eventually reaches synchronisation with APW1. Synchronisation for these two waves appears to occur after approximately 18 ms of the start of their ephaptic effects begin to play a significant role.

When APW3 enters the region of ephaptic interaction effects ($x > 2x_{inj}$), APW2 has already started its trend towards synchronisation with APW1, so the delay between APW2 and APW3 increases to more than 1 ms. It appears that the consequence of this is a slight decrease in the acceleration of APW3.

APW3 keeps increasing its velocity whilst attracted by APW1 and APW2, until it finally approaches the entangled positions of the two latter waves, and then it starts to slow down. Up to this point, APW3 has increased its velocity by more than a 13% of its original value due to the summed attraction exerted by APW1 and APW2.

After $t \approx 35$ ms, all APW maximums follow a closer trajectory and their velocities tend to equalise towards a certain value highly biased towards APW1. At this stage, synchronisation of the three axons is reached, and the final group velocity of the axons is 13.4 ± 0.2 m/s, about 0.4 m/s lower than v_0. This decrease in the group velocity is consistent with the findings of [64] and [66].

Apart from the above observations, the curves in Fig. 3.4(b) show other fluctuations. These are specially obvious in the curves for the velocities of axons 1 and 2 all through their descending trend, preventing them from monotonicity. Also, a momentaneous inflection point is observed in v_3 at $t \approx 10$ ms, i.e., once APW2 has just started to slow down. Further investigation needs to be undertaken to determine the origin and nature of these fluctuations.

Numerical Stability Issues

This simulation was carried out using three models of axons separated by 15 μm each and using a time step of 25 μs. We also performed simulations with different numbers of axons, separation distances and time step sizes. We found that simulations with a number of axons higher than three, with three or more axons separated by 20 μm or more, or with a smaller time step generated numerical instabilities in the values of ϕ. Thus, a careful choice of these three parameters must be made in order to avoid instabilities (e.g., unexpected asymptotic behaviour). Such errors are likely to be related to numerical truncation effects, but further investigation will be necessary to reveal the sources of the instabilities. This will then determine the limits of applicability of the model.

3.4   Discussion

In this chapter, we studied the EC between myelinated axons through the use of a model. First, in Section 3.2, the ephaptic stimulation of one axon over another

was simulated. Subsequently, we simulated in Section 3.3 the ephaptically coupled propagation of APs in three axons. The model presented here uses a different approach to [65] and [66] with regard to the electrical coupling between the axons. While [65, 66] used a longitudinal resistance parallel to the fibers and shared by all of them, leading to a MF model, we used an inverse distance dependence of the extracellular potential, thus taking into account transverse variations of this potential.

3.4.1   Unidirectional Ephaptic Stimulation between Two Myelinated Axons

It has been shown in Section 3.2 that the ephaptic stimulation performed by the AP wave of axon 1 on axon 2 slows down or speeds up the AP wave of axon 2 depending on the separation on the x-axis with which these two waves travel. The net effect is that axon 1 attracts the AP wave of axon 2 towards its own AP wave. These observations support the hypothesis of [64] for myelinated axons.

The strength of ephaptic stimulation for $\sigma = 10^{-3}$ S/m affects the CV of myelinated axons by up to 11.75%. However, in less resistive media with conductivities which are more similar to those of the endoneurium ($\sigma = 0.085$ S/m), the strength of this effect reaches a maximum of 0.2%.

Ephaptic stimulation depends inversely on the conductivity of the extracellular medium and the separation distance between the axons. Results from this chapter show that ephaptic effects are present, and strongly suggest the different features of its role in the regulation of CVs and, potentially, in the occurrence of synchrony between APs of different axons. This may regulate the firing frequencies and so be a mechanism for coding sensory information [65].

Despite the evidence of ephaptic stimulation in the simulations, the small magnitude that it shows for $\sigma = 0.085$ S/m opens the question of what the total net effect of the ephaptic interactions in an entire nerve trunk may be. The large number of fibers in a peripheral nerve trunk may have the effect of amplifying these ephaptic interactions but, on the other hand, the large separation between distant axons can limit these amplifications. The net effect of the interplay of these two factors needs to be studied in a medium with a more realistic conductivity value.

3.4.2 Conduction Velocity Effects Due to Ephaptic Interactions between Myelinated Axons

Despite the definitory difference between the MF model and the distance-based model used here, results with the distance-based model, presented in this chapter, are consistent with those of the cited contributions which use the MF model [65,66]. Simulations showed synchronisation of the APs of all of the axons involved in the mutual ephaptic coupling simulations. Locking of APs and synchronisation during propagation was observed as well as the decrease in the final group velocity. The general behaviour of the EC obtained from our results is qualitatively similar to that in [66], albeit with differences in time and space scales due, most likely, to the differences in the axon models. The reason for this apparent similarity between the two models is that in the geometry of our simulation, axons are all separated by the same distance. I.e., in this chapter, we have not yet tested for differences in the strength of the EC between axons due to different inter-cell distances. It is expected, however, that simulations of fascicles in nerve trunks with hundreds of axons will provide a noticeable difference with respect to simulations that use the MF model.

In order to obtain more realistic simulations of propagation in peripheral nerve trunks in mammals, our models of myelinated axons need to be improved with more species-specific neural models and validated with experimental data.

3.5   Conclusion

A distance dependent model for the extracellular potential generated by the activity of axons has been used to model the ephaptic interactions of groups of two and three parallel myelinated fibers via extracellular potential. In the case of two fibers, the effects on CV of the unidirectional stimulation that the ephaptic field generated by one fiber exerted onto the second fiber was studied and quantified against the relative timings between the APs in both fibers, the transverse distance separating the fibers and the conductivity of the extracellular medium. Results show that an AP in the first fiber attracts or repels an AP on another fiber depending on the relative timings on the two. Also, the strength of this effect decreases with inter-axonal distance and with the conductivity of the extracellular medium.

In the case of three fibers, a further simulation was run of AP propagation under mutual EC using the same extracellular potential model. Results show synchronisation between APs and the adjustments of CVs that lead to this synchronisation, in accordance with existing literature. Due to the numerical instabilities that grew rapidly with the number of axons in the simulations, we were not able to extend

our simulations to bundles of more axons. For this reason, in the next chapters we implement a different model of ephaptic interactions which allows us to study EC in bundles of any number of axons and even in realistic nerve models.

Chapter 4

The Extracellular Space as a Resistor Network

4.1   Introduction

Existing approaches for modelling ephaptic interactions between populations of neurons not only include the point or line-source approximations. As seen in Chapter 3, this approach, while still usable, may present numerical stability issues due to close distances between fibers [177], which results in unrealistically high extracellular potentials. Either a computational method to avoid numerical instabilities or an alternative model are needed.

In order to study EC for fiber bundles, a Mean-Field (MF) approach was developed by [65], where every layer along the z-axis of the extracellular medium is assumed to be isopotential. This has been useful to provide insights about the nature and consequences of EC in bundles [65, 66, 68]. However, this approach is incompatible with simulating fields coming from extracellular electrodes, which vary across the cross-section. A more sophisticated approach which allows modelling all the systems involved (electrode and endogenous fields) and permits modelling the complex geometrical structures of the tissues (which is difficult by using the point or line source approximations only) is discretising the system in meshes and using approximate numerical methods to simulate the fields. FEM are widely used for computing the electrode fields [179] over complex geometries thanks to their reliability. However, they have rarely been used for modelling EC due to the high computational cost it would take to run time-dependent FEM simulations that took into account all the aspects of the system. So far, [71] and [72] have adopted such approach, but limited their studies to systems of just a few neurons, normally less than five.

Although FEM are enough, in principle, to simulate both electrode and endogenous fields in an EMI-type model —EMI meaning that it simulates the Extracellular, Membranes and Intracellular domains in a single run [114], it is also possible to exclusively use NEURON [2] for this purpose. Given that experimentally validated and up-to-date models are already available for this framework, we wanted to take advantage of its modelling capabilities and created a Resistor Network (RN) which allows embedding any fiber models in an EMI model.

The RN developed in this chapter is entirely implemented in NEURON. It uses the Delaunay triangulation of any given discretisation of a cross-sectional geometry and its dual Voronoi tessellation [180] in order to build the properties of the RN, including its longitudinal resistances, perpendicular to the cross-section. The use of these methods for the RN allows us to realistically simulate the fields from electrodes over extruded geometries, which are suitable for bundles of parallel fibers. Although the idea of using these tessellation techniques to study electrical phenomena in RNs has already been studied [181], and RNs have been used in studies of neurophysiology [73, 182], we have found no work that combines both approaches in order to tackle the non-uniform positions of fibers over a bundle's cross-section. Only [73] built a RN (also implemented in NEURON) to study EC in muscular cells, but no such tessellation techniques were used; instead, a very regular lattice of cells was used.

Using Voronoi tessellations for building a RN in order to model an ohmic medium—specifically, the extracellular space of a fiber bundle—has two main novel advantages:

- They are capable of meshing geometries that uniform Finite Difference (FD) meshes cannot represent reliably.

- The use of Voronoi tessellations to build the properties of the RN results in a nearest-neighbour electrical interaction model that quantifies ephaptic links based on geometrical and physical quantities concerned with each pair of fibers, and consequently constructs a distance-based EC model for the whole bundle which does not follow the restrictive assumptions of a MF model.

Another advantage of the RN which is not necessarily related to the Voronoi tessellations is its full implementation in NEURON, which avoids coupled simulations between NEURON and any other FEM or Poisson solver and thus ensures numerical stability when computing the extracellular fields.

It must be noted that this RN uses only resistive connections among nodes, since it is developed to solve fields in neural applications under the QS approximation. Hence, no capacitive components of the media are accounted for. Although this is outside the scope of the present work, capacitive properties of the extracellular media can still be modelled in NEURON and included in the connections of the RN.

The RN developed in this chapter needs to be validated. For this, results from numerical simulations using the RN were compared to their equivalents in FEM and analytical solutions. We show that this RN method is a valid technique to study ohmic media and therefore use it in relevant applications.

We used the RN to study how fibers react to extracellular stimulating fields and how they interact ephaptically between them during propagation. For this, the effects of a number of variables—distance from the fibers to the source, node-to-pad misalignments and RN model choices—on the response of the fibers to stimulation from an external electrode are studied. Next, the RN was used in a simple study of the effects of EC on AP conduction for bundles of few identical and parallel fibers. Finally, it was used to record the activity of one axon from a cuff electrode.

We found that the RN can be used to model stimulation and recordings from electrodes on a bundle. When studying the response of the fibers (measured in this work with the delays with which APs fire after a stimulating pulse is applied) to the stimulating fields from extracellular electrodes, we found that, as we increased the anatomical complexity of the bundle, such as misalignments between fibers, the dependence of these responses with the distances between the fibers and the electrode was generally not smooth, whereas this is the case when all fibers in a bundle are identical. We were interested in elucidating the causes of the complex relationship between responses and distances, and thus we carried out a study to isolate certain anatomical variables and study how they can deflect this smoothness. The study concludes that the node-to-pad misalignments, which are defined as the distances along the z-axis between the Ranvier nodes and the stimulating electrode, and model choices for locating the transverse resistors in the RN, have major effects on the fiber responses. Because it is known that fiber diameters do have an effect on this through axonal excitabilities, we were not concerned with this variable in the study, although if considered, it would modify the node-to-pad misalignments.

We also found that the RN can simulate EC between parallel fibers. We used it to test how the RN simulates EC in bundles of 1-4 identical fibers in order to contrast the results with previous studies [66, 68], since these cases are approximately equivalent to using a MF model. Although we use different fiber models and extracellular medium choices, results do show a qualitative agreement with previous findings, and the basic observed phenomena can be easily explained.

The main contributions of this chapter are aligned with the four sets of results that it presents:

- The creation of a Resistor Network (RN) to model a bundle of fibers embedded in an extracellular medium, and in which stimulation and recordings from electrodes can be modelled.

- A method to quantify nearest-neighbour electrical connections for any distri-

bution of fibers.

- The validation of the RN against theoretical solutions.

- The assessment of the effects of anatomical variables on the response of fibers to fields, which finds a strong effect due to node-to-pad misalignments.

- The assessment of the effects of EC on AP propagation for bundles of few identical fibers with the use of the RN.

This chapter is divided as follows: The next section presents a formal description of the RN, how it is used to model bundles of fibers and volume conductors and the demonstration of its equivalence to a Finite Difference Methods (FDM) for the case of a uniform rectangular mesh. The Results section is divided in four: the first subsection describes the results of the validation process for the RN; the second subsection studies the effects of anatomical and model variables on fibers responses to stimulating fields; the third subsection provides the study of the effects of EC on AP conduction in small bundles, and the fourth subsection shows the recordings of the activity of an axon from a cuff electrode.

4.2 Materials and Methods

4.2.1 Resistor Network Formulation

The contents in this section are adapted from the Materials and Methods sections of two manuscripts: [14] (published in CEEC 2019) and [15], submitted to PLOS Computational Biology (not published yet; as at this writing, revisions from the reviewers are being addressed and the final paper may differ in content from this chapter).

The extracellular volume of a nerve, or a bundle of fibers, is modelled with a RN which uses the extracellular connective RN between two axons from [11] as the basic model for connecting two cables. Our RN is an adaptation from such model that suits any number of myelinated axons and also volumes in the nerve that contain no axons.

The model from [11] consists of two parallel core-conductor (unmyelinated) axons linked by a grid of resistors (Fig. 4.1). Each axon is coupled to its parallel (longitudinal) extracellular cable through its membrane compartments, and the two longitudinal extracellular cables are linked to each other by transverse resistors R_T —perpendicular to the axons, at each compartment's position. Each longitudinal

extracellular cable is a series of resistors with value R_L located one at each compartment.
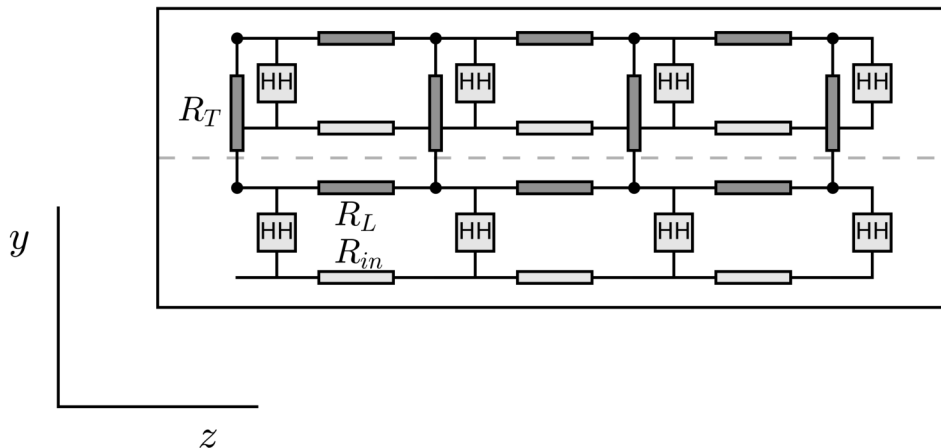
Figure 4.1: Circuit representing the connective RN model of [11] for two parallel axons. The intracellular resistances of the axons are represented as series of light grey resistors (long horizontal rectangular boxes labeled as R_{in}). Each of these cables is connected to its corresponding extracellular cable (parallel dark grey resistors, R_L) through the membrane compartments (boxes labeled as HH). The extracellular cables of the two axons are connected with transverse resistors, R_T. Schematically, in this figure the circuits of the two axons are separated by the dashed line. This figure is not to scale. The y-axis can be substituted by any direction co-planar with the x-y plane.

The RN developed here is conceived to extracellularly couple parallel fibers that are randomly scattered in a bundle using this approach. For this, this axon-to-axon interaction model is replicated for every pair of neighbouring axons. This way, the RN suits any cross-sectional geometry for a bundle —as long as this is made of parallel fibers, and hence the bundle's shape is an extrusion of its cross-sectional surface. This is facilitated by the implementation of the extracellular properties of the cells in NEURON.

The aim is to model the extracellular electrical properties of a bundle of fibers. However, this method can also be used to model volume conductors where fibers are not present. This is the case of the validation tests we ran in this section. For this reason, we will refer as "bundle" to any such geometry for the remaining of this and the validation sections, regardless of whether it contains fibers or not.

The following is an explanation of how the geometry of a bundle is discretised in a mesh and how the resistances of the network are calculated from this discretisation.

(a)

(b)

(c)
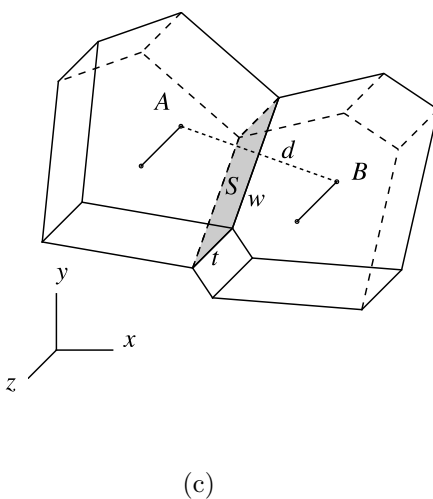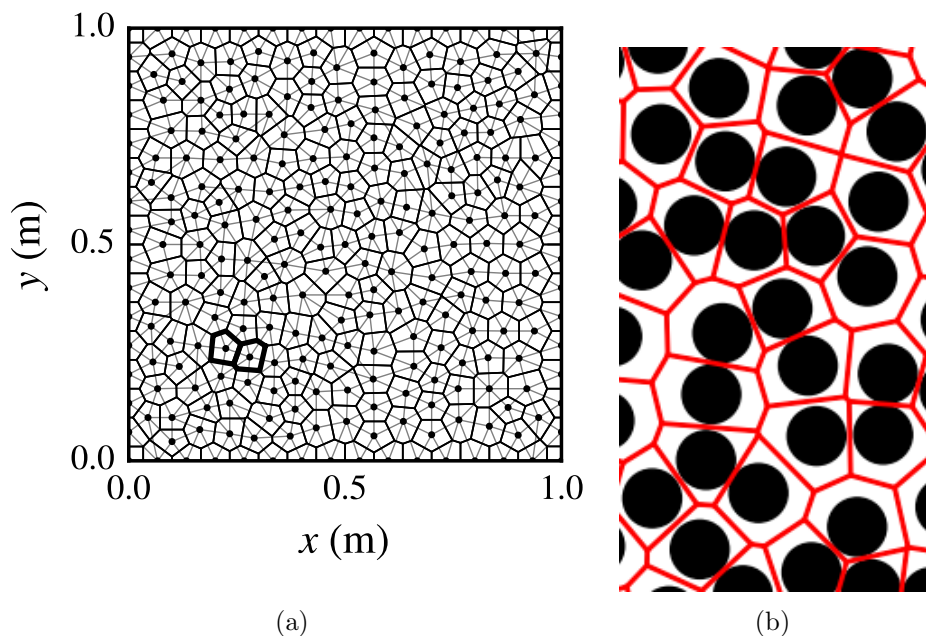
Figure 4.2: (a) Representation of mesh *RN-Delaunay-1*, used in the Results section to run a simulation. The mesh is built from the set of contour points and the central point for current injection. From this, a new set of points is added by building a Delaunay triangulation. The contour of the domain is shown with a thick black line. Dots represent all the points in the mesh. The connections between them, denoting the positions of the resistors, are shown in thin grey lines. The dual Voronoi diagram, which assigns a polygon to each point and defines the contact width between each, is shown in thin black lines. The two cells highlighted with thicker black lines correspond to the cells shown in (c). (b) Example of a Voronoi diagram of a set of circles or cylindrical fibers of equal diameter. (c) Detail of the physical connection model between two polygonal prisms corresponding to cables A and B. The two points are separated by a distance d, and their cells have a contact surface with width w, depth t and area S. In this case, t is the length in which the z-axis is discretised (the length of one segment).

Discretisation of the Bundle's Cross-Section (x-y Plane)

The meshing method divides the cross-sectional surface of the bundle in individual regions, one for each fiber. Given a random distribution of fibers across the cross-section, a natural way to do this division is to compute the Voronoi diagram of the fiber positions set, assuming all fibers have equal diameter. This divides the cross-section in a set of convex polygons with the fibers located at their orthocenters (see Fig. 4.2(b)).

In case of a volume without fibers, we need to fill the cross-section of the bundle with a non-uniform cloud of points. The points may be assigned random positions or be given by a tessellation technique. Since a Delaunay triangulation can provide triangles that generally avoid sharp angles, we used a Delaunay triangulation over this surface in order to generate the point set. Then, its dual Voronoi tessellation is built (Fig. 4.2(a)). Note that the Voronoi diagram of a set of fibers also defines the connections between fibers from its dual Delaunay triangulation.

Using this method, each point or fiber —depending on the case, has a corresponding polygon assigned to it, and the cross-sectional surface of the bundle is discretised in a set of interconnected polygons (Figs. 4.2(b) and 4.2(a) for fibers and points, respectively).

When extruding this concept to the bundle's length, the polygons become polygonal prisms that extend the whole length, and the points or fibers become cables in the interior of these prisms (Fig. 4.2(c)). In order to implement the cables that model prisms not containing fibers, we designed the Non-Axonal Extracellular Longitudinal Cables (NAELCs) in a NEURON cell template. They are defined as passive cables with a dummy value for the diameter (1 μm), a very large intracellular resistivity (ideally infinite; for this, we used 10^9 $\Omega \cdot$ cm, which we assumed to be a sufficiently large value), null membrane capacitance and a passive mechanism (*pas*) with null reversal potential and a very large conductivity (ideally infinite again), in order to allow injected currents to flow directly to its extracellular cable. Its actual extracellular properties are implemented on its extracellular cable (*xraxial*). This model forms a linear resistive cable that can be used to model any prism of the discretised extracellular space.

The prisms are all connected to their neighbours by contact surfaces, one perpendicular to each of the Delaunay triangulation's segments. Naturally, each pair made by a Delaunay segment and its corresponding contact surface represents an electrical contact between two neighbouring points (Fig. 4.2(c)). We then need to define and implement a resistor in order to quantify such a contact. For this, we assumed, as done before by [181], that its resistance is directly proportional to the length of the Delaunay segment, d, and inversely proportional to the area of the contact surface, S:

$$R_T = \rho \frac{d}{S} = \rho \frac{d}{w \cdot t}, \tag{4.1}$$

where the subscript T stands for transverse —transverse to the bundle, refer-ring to the resistors which are co-planar to the bundle's cross-section, and ρ is the resistivity of the medium.

The values of the resistances in this transverse network are implemented in ex-actly the same way as [73], using NEURON's tool *LinearMechanism*.

Discretisation of the Bundle's Length (z-axis)

Unmyelinated fibers can be discretised along the z-axis in compartments of equal length. Therefore, when the bundle is made by NAELC or by unmyelinated fibers, the length of the bundle is simply divided in *nseg* segments of equal length t (see Eq. 4.1 and Fig. 4.2(c)), on each of which a copy of the cross-sectional network is connected, thus having *nseg* layers of cross-sectional networks.

NEURON allows the assignment of an extracellular resistive cable along every cell, whose resistance per unit length is implemented through the variable *xraxial*. This is used by NEURON to compute the total resistance of each segment. We made the assumption that this resistance is inversely proportional to the corresponding Voronoi or cross-sectional polygon's extracellular area, A_E:

$$r_L = \frac{\rho}{A_E}, \tag{4.2}$$

where the subscript L stands for longitudinal.

The polygon's extracellular area is the difference between the polygon's total area (A_P) and the fiber's area if a fiber is present:

$$A_E = A_P - A_C \tag{4.3}$$

The subscript C in A_C stands for "cable", denoting that the value of A_C is zero when a fiber is not present and equal to the fiber's cross-sectional area if it is present.

In case a 2D problem needs to be solved, the RN must still include the z-axis, since NEURON needs to provide a length for the cables. However, it is enough with assigning $nseg = 1$, thus having only one layer for the cross-sectional RN.

Resistor Network for Bundles of Misaligned Myelinated Axons

Symbol	Units		Description
N_k	None		Number of nodes of Ranvier in fiber k.
$M_{k,l}$	None		Total number of transverse resistors between fibers k and l.
$z_{T,(k,l)}^n$	cm		Location of the transverse resistor number n between cables k and l.
$Z_{T,(k,l)}$	None	(members: cm)	Set of locations along the z-axis of the transverse resistors between cables k and l.
Z_k	None	(members: cm)	Set of locations along the z-axis of the nodes of Ranvier of fiber k.
$c_{k,l}^n$	cm		Length (along the z-axis) of the transverse resistor number n between cables k and l.
$r_{L,k}$	Ω/cm		Resistance per unit length of the extracellular cable k.
$R_{T,(k,l)}^n$	Ω		Value of the transverse resistor n between cables k and l

Table 4.1: Variables used for the resistor network.

Two important adaptations from this approach are needed in case the model includes myelinated axons with misaligned nodes of Ranvier (Fig 4.3): First, transverse resistors can be connected at any location along the axons' extracellular cables. Second, there are two options for how to connect the transverse resistors: The first one is to locate them at regular intervals along the z-axis, as done for unmyelinated axons and empty volumes. The second one consists of connecting them at the locations of the nodes of Ranvier of both axons. This is the case shown in Fig 4.3[1]. In this case, the set of transverse resistor locations along the z-axis between any two fibers k and l is $Z_{T,(k,l)}$, which is the union of the sets of positions of the nodes of the two axons:

$$Z_{T,(k,l)} = Z_k \cup Z_l, \tag{4.4}$$

and therefore, it contains $M_{k,l}$ elements (which means there are $M_{k,l}$ transverse resistors between the two axons; see table 4.1 for a list of all the variables used here), i.e., the sum of the number of nodes of Ranvier of the two axons minus the number of pairs of nodes which share the same location on the z-axis (because such case, obviously, means there is only one resistor for two nodes):

$$M_{k,l} = N_k + N_l - \sum_{i=1}^{N_k} \sum_{j=i}^{N_l} \delta\left(z_{NR,i} - z_{NR,j}\right), \tag{4.5}$$

---

[1]For generality purposes, Fig. 4.3 depicts this method for two axons with different internodal lengths, which naturally have their nodes of Ranvier in misalignment.
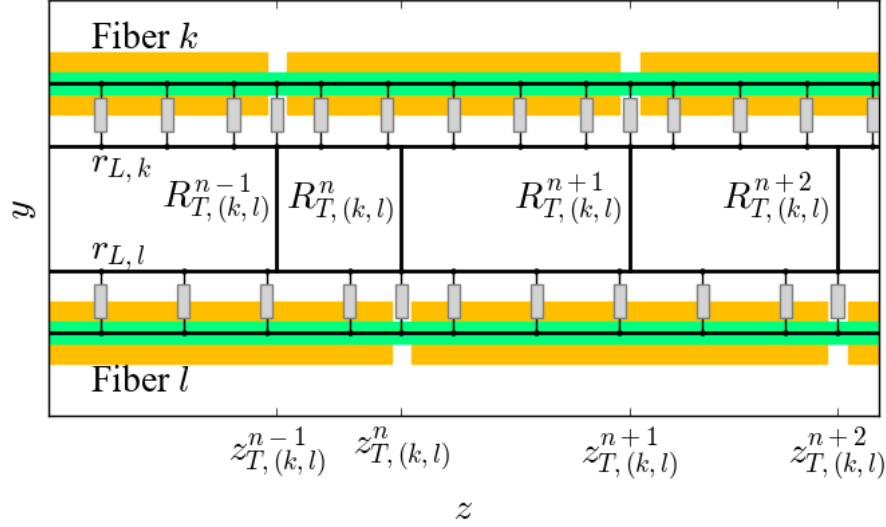
Figure 4.3: Example of resistor network connecting two myelinated fibers ephaptically. Conceptual (not to scale) representations of two myelinated fibers are shown as axons (green) wrapped by the myelin sheaths (dark yellow). Thick black line segments represent purely resistive connections. Grey boxes represent membrane compartments, either nodal or internodal (in which case, they also include the myelin sheath in series). As in Fig. 4.1, the y-axis has been used on the ordinate axis in this figure for simplicity, but given our model, this can be any direction co-planar with the x-y plane. The resistance per unit length of each longitudinal extracellular cable $r_{L,k}$ is the r_L given by Eq. 4.2. The k subscript simply helps distinguishing the different fibers in the figure.

where $z_{NR,i}$ ($z_{NR,j}$) is the position of the i-th (j-th) node of Ranvier of fiber k (l).

The length along the z-axis of one transverse resistor n is given by:

$$c_{k,l}^n = \frac{z_{T,(k,l)}^{n+1} - z_{T,(k,l)}^{n-1}}{2},$$ (4.6)

being $z_{T,(k,l)}^n$ a member of $Z_{T,(k,l)}$:

$$z_{T,(k,l)}^n \in Z_{T,(k,l)} \forall n \mid n \in [1, M_{k,l}]$$ (4.7)

The transverse resistors connecting myelinated axons need to be reformulated to account for the misalignments. The variable t in Eq. 4.1 needs to be substituted by the length of the resistor, $c_{k,l}^n$. Hence the value of the n-th extracellular transverse resistor between two fibers k and l is:

$$R_{T,(k,l)}^n = \rho \frac{d}{w \cdot c_{k,l}^n} \tag{4.8}$$

4.2.2 Equivalence between the Resistor Network and the Finite Differences Method for a Rectangular Mesh

In the case of a rectangular uniform mesh, this RN method is equivalent to the FDM for such mesh. In order to show this, we demonstrate how using this approach is equivalent to the FDM when solving the Laplace Equation on any point (indexed with i and j) inside the domain (not on the boundaries).

Consider a point (i, j) and its four points in contact $(i-1, j)$, $(i+1, j)$, $(i, j-1)$ and $(i, j+1)$ on a rectangular network where points are separated by a distance Δx on the horizontal direction and by Δy on the vertical direction.

The Laplace Equation in FDs on point (i, j) on a mesh with such specifications is:

$$\frac{\phi_{i-1,j} - 2\phi_{i,j} + \phi_{i+1,j}}{\Delta x^2} + \frac{\phi_{i,j-1} - 2\phi_{i,j} + \phi_{i,j+1}}{\Delta y^2} = 0 \tag{4.9}$$

On a 2D RN under the same discretisation, the resistance per unit length (in $\Omega \cdot$m) between any two neighbouring points in a horizontal direction is, by applying Eq. 4.1 and neglecting the z-axis (hence, the units are $\Omega \cdot$cm instead of Ω):

$$R_x = \rho \frac{\Delta x}{\Delta y}, \tag{4.10}$$

where ρ is the medium's resistivity. Equivalently, the resistance between any two neighbouring points in the vertical is:

$$R_y = \rho \frac{\Delta y}{\Delta x}, \tag{4.11}$$

Kirchhoff's current balance equation on point (i, j) is:

$$\frac{\phi_{i-1,j} - \phi_{i,j}}{R_x} + \frac{\phi_{i+1,j} - \phi_{i,j}}{R_x} + \frac{\phi_{i,j-1} - \phi_{i,j}}{R_y} + \frac{\phi_{i,j+1} - \phi_{i,j}}{R_y} = 0 \tag{4.12}$$

Grouping terms, we have:

$$\frac{\phi_{i-1,j} - 2\phi_{i,j} + \phi_{i+1,j}}{R_x} + \frac{\phi_{i,j-1} - 2\phi_{i,j} + \phi_{i,j+1}}{R_y} = 0 \qquad (4.13)$$

Using (4.10) and (4.11), we get:

$$\frac{\phi_{i-1,j} - 2\phi_{i,j} + \phi_{i+1,j}}{\Delta x / \Delta y} + \frac{\phi_{i,j-1} - 2\phi_{i,j} + \phi_{i,j+1}}{\Delta y / \Delta x} = 0 \qquad (4.14)$$

Dividing by $\Delta x \Delta y$, we finally obtain:

$$\frac{\phi_{i-1,j} - 2\phi_{i,j} + \phi_{i+1,j}}{\Delta x^2} + \frac{\phi_{i,j-1} - 2\phi_{i,j} + \phi_{i,j+1}}{\Delta y^2} = 0, \qquad (4.15)$$

which is exactly the Laplace Equation in FDs for point (i, j) (Eq. 4.9).

4.2.3   Stimulation and Recording from Electrodes

The RN allows the definition of cuff electrodes for stimulation and recording within its domain.

When modelling fiber bundles or nerves, these are embedded in a cylindrical container containing a saline bath, which provides a current path to the electrical ground. The electrical ground is located across the cylinder's surface and its bases. The insulating sheath of cuff electrodes is modelled by adding its resistance to the paths to the electrical ground from the NAELC on the bundle's contours. The active pads of the electrodes, whether for stimulation or recording purposes, are modelled by setting up their positions according to the cuff's rings. Stimulation from the pads is simulated using current point sources on the bundle or nerve membrane's NAELC in contact with the desired pads. Recordings are simulated by reading the value of the potential on the locations of the desired pads. Electrodes are not regarded as surface, but as point, current sources, and their contact surface impedance, including capacitance, is not modelled since we work under the QS approximation.

The current path between the points on the bundle's membrane and the container's walls is assumed to be purely radial (hence no longitudinal currents are allowed across the bath or the cuff insulators). For this, all points in the discretised bundle lying on its membrane (which are given by the triangulation hull in the cross-section) are connected to the container's cylindrical wall using radially aligned

resistors. The resistance per unit length for each of these resistors is estimated from the geometry of the bath (see tables 5.2 and 5.3 for variables and parameters):

$$R_G = \frac{\rho_I \Delta_I + \rho_S \Delta_S}{(\pi D_N / n_H)}, \tag{4.16}$$

where:

$$\Delta_I + \Delta_S = \Delta_C \tag{4.17}$$

In the regions of the bundle (along its length) not covered by the cuffs, the membrane was directly in touch with the saline bath and Eq 4.16 then becomes:

$$R_G = \frac{\rho_S \Delta_C}{(\pi D_N / n_H)} \tag{4.18}$$

All NAELC and extracellular cables of fibers are connected to ground on both ends since they are assumed to be in contact with the container's bases. The ends of the intracellular domains of the fibers, however, are treated as sealed ends and do not have such connections.

4.3 Results

4.3.1 Validation

The contents in this section are based on a manuscript published in CEEC 2019 [14].

Poisson Equation

We have validated the RN by running simulations with different configurations of the RN and comparing their results with a FEM simulation, used as a reference for being a well known method for providing an accurate approximation to the actual result. The simulation is run on a 2D square domain of side 1 m where a current source of 1 A is located at the centre ((0.5, 0.5) m). The four sides of

the square—all the points on the contours—are connected to ground. The domain contains a medium with a sheet resistance of 1 Ω/sq. As the z-axis is necessary in our NEURON implementation of the problem, we implemented the domain as a cube of side 1 m with a resistivity of 1 $\Omega \cdot$ m.

In these simulations no fiber or biological cell models are used. Hence, for the remaining of this validation section, the word cell will be used to refer to the individual regions in which the domain is discretised by using meshes.

The FEM simulation was implemented and run using the FEniCS Project software [4]. The domain uses a uniform square mesh with $\Delta x = \Delta y = 0.025$ m. Apart from the FEM simulation, three simulations using the RN were run (Fig. 4.4): one using the same uniform discretisation (*RN-Uniform*) and two using discretisations given by Delaunay triangulations (*RN-Delaunay-1* and *RN-Delaunay-2*). Differences in the results between the simulation with *RN-Uniform* and the FEM simulation are negligible. The peak difference is of the order of 10^{-7} V. This shows that the RN is indeed valid for this type of mesh, in line with the demonstration provided above, assuming that the results with a FDM would be very similar. The mesh *RN-Delaunay-1* contains 94 points, excluding the points on the contours, where the solution is trivial, while the mesh *RN-Delaunay-2* has 1310 points. For comparison, *FEM* and *RN-Uniform* have 1521 points. The only point that is necessarily in common in the two meshes, apart from the contours, is the current source point.

The first thing that can be noticed from Fig. 4.4 is that all simulations are capable of modelling the basic shape and magnitude of the field over most of the domain. However, it is visible how modifying the mesh resolution affects the accuracy in the results. Simulation with *RN-Delaunay-1* shows visible deflections on the potential curves near the injection site. On the other hand, results from simulation with *RN-Delaunay-2* are difficult to distinguish from results with *FEM*. Simulation with *RN-Delaunay-1* has a difference with FEM at the central cell of -0.14 V, which makes a relative difference of -19.07%. However, the Relative Difference Measure (RDM) for the whole domain, computed using the expression from [182], is 0.041. This shows that the location of the highest discrepancies is near, and especially at, the central cell. Simulation with *RN-Delaunay-2* has a much lower difference with FEM at the central cell, of $-2.64 \cdot 10^{-2}$ V, which makes a relative difference of -0.89%. The RDM in this case is 0.011, comparatively not so much lower than *RN-Delaunay-1*.

Given the domain was extended infinitely, this problem would have the analytical solution of a current point source [183], with an inverse dependence on the square of the distance from the current source. In a simulation on a discretised domain, however, the current is applied on one cell of the mesh, over the surface of which the potential is assumed to be constant. The analytical solution for the ideal case can be obtained from the divergence theorem, based on which, by using the mentioned assumption of isopotentiality over the whole cell in the case of a mesh, we can predict
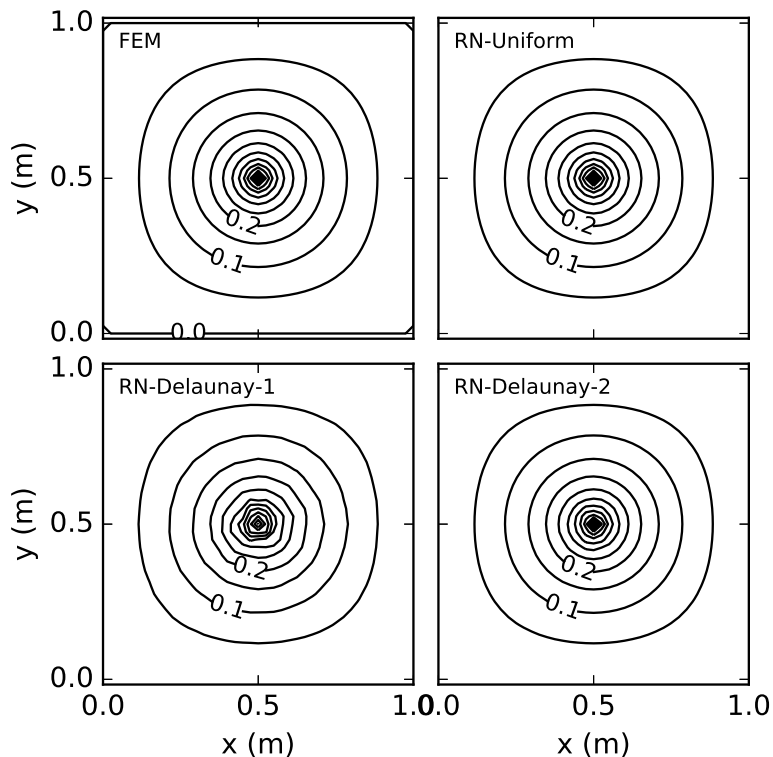
Figure 4.4: Results of the potential distribution across the domain for four different simulations: Top Left: FEM; Top Right: *RN-Uniform*; Bottom Left: *RN-Delaunay-1*; Bottom Right: *RN-Delaunay-2*. The contours indicate the potential distribution at intervals of 0.05 V, and the units in their labels are Volts.

that the value of the potential at the cell where the current is applied has an inverse relationship with the area of this cell. Indeed, in our simulations this peak potential value follows a linear relationship with the logarithm of the central cell's area (Fig. 4.5), which is expressed as:

$$a = log_{10} \frac{A_P}{A_D} \tag{4.19}$$

where A_P is the area of the cell's polygonal face and A_D is the area of the whole domain.

For the FEM simulations, the fitted line is $\phi_{peak} = -0.188a + 0.146$, with a standard error of 10^{-3} V and $r^2 = 0.9995$. For the simulations with the RN, the fitted line is $\phi_{peak} = -0.177a + 0.184$, with a standard error of $3 \cdot 10^{-3}$ V and $r^2 = 0.997$. Despite solutions with the RN generally yield slightly higher peak values, the fittings of the two methods are very similar. Thus, the RN can solve the Poisson equation over this domain with nearly the same accuracy as FEM.
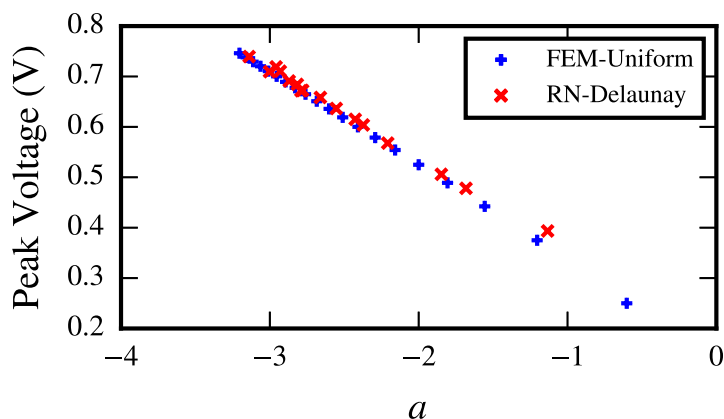
Figure 4.5: Peak Voltage from each simulation, which is located at the central cell of the mesh were the current source is applied, against a.

Cubic Linear Resistor

We tested the accuracy of the implementation of the longitudinal resistances, given by Eq. 4.2, at modelling the electrical properties of a volume along the z-axis. For this, we designed a very simple cubic domain with side 1 m. Its faces on the x-y plane were discretised with a uniform mesh of 6×6 points. For each point on this plane mesh, a NAELC was set up with $nseg = 5$ along the z-axis.

A distributed current of 1 A/m^2 was applied uniformly across the face with $z = 0$ (left face; the distributed current summing 1 A over the whole surface), and all the points on the face $z = 1$ m (right face) were connected to ground. The distributed current was applied in the following way: each point on the left face was applied a current source that was weighted by the ratio between its polygonal area A_P and the total face area (1 m^2):

$$I_P = I_T \frac{A_P}{A_S}, \tag{4.20}$$

where I_T is the total current (1 A) and A_S is the total face area (1 m^2).

The analytical solution for this problem is:

$$\phi(x, y, z) = 1 \cdot (1 - z), \tag{4.21}$$

for all x and y inside the domain, and where the units of ϕ are Volts and the

units of z are m.

It must be noted that NEURON applies all point processes like current sources on the centres of the sections' segments where they are assigned. Therefore, the current source on the first segment of each NAELC would be found at $z = 0.1$ m. In order to fix this issue, two additional sections were attached at both ends of each NAELC. The current sources were then applied on each of the additional sections on the left, while the ground connections were made on each of the additional sections on the right. These additional sections were 1 μm long, so the total length of the domain was 2 μm longer than it should be, and the distance along the z-axis between the current sources and the ground was 1 μm longer. Although this was a necessary addition, it could be a source of error in the model. Nevertheless, given the size of our domain, this error should be negligible.

Results from the simulation yield a RDM of $1.43 \cdot 10^{-6}$ compared to the analytical solution, and a Magnification Factor (MAG) [182] of $1 + 2 \cdot 10^{-6}$. Therefore, the solution to this simple problem when using the RN is sufficiently accurate, suggesting that our implementation of the values for *xraxial* (Eq. 4.2) is justifiably correct. Note that the order of magnitude of the RDM is the same as the error in length that the two additional sections add (1 μm over 1 m).

4.3.2 Variables Influencing Axon Activation

We were interested in studying the relationship between axon activation, using AP firing delay as its measure, and the relevant variables that may influence it under electrode stimulation, as well as the interplay between them. Two well known of such variables are the axon to electrode distances and the axons' excitabilities, which are directly dependent on the diameters. Another variable, which may be not as obvious as the former, is the level of misalignment between the nodes of Ranvier of an axon and an electrode's active pad. We have studied this third variable and found a close relationship between it and the AP delays.

Apart from these three physical variables, model design choices for numerical simulations also affect the results of AP delays. In particular, as will be shown here, results vary depending on the choice between the two different options we have for locating transverse resistors in the RN to model the ephaptic connections between axons —i.e., placing them directly on the nodes of Ranvier or placing them at regularly spaced locations.

Here we show the results of two simulations that were run in order to assess these relationships. Unless otherwise specified, the simulations are run on a circular bundle of 51 axons of equal diameter, 7 μm, scattered at random locations over the bundle's cross-section. Using axons all of equal diameter makes all them identical

and removes any differences between their excitabilities from the study. The bundle is 2 cm long and it is wrapped by a 4.25 mm long cuff near its left end, centered at $z = 3.875$ mm, which has one active pad at the middle of the cuff, that is, at the position ($x = 0.075$ mm, $y = 0$, $z = 3.875$ mm). The active pad exerts a square stimulating current pulse with an amplitude ranging roughly from -0.42 μA to -0.5 μA, depending on the simulation, and a duration of 0.2 ms. Both simulations run 1 ms of neural activity. We made the assumption that the stimulation effects beyond the cuff's ends are negligible. Therefore, the RN is connected only in the region within the cuff's ends (or under the cuff). The reason why the bundle is extended longer than that is to avoid the effects of the boundaries.

All axons have a certain degree of nodal misalignment between each other (Ranvier node misalignment between axons)[2]. This is modelled by giving each axon a random position along the z-axis for its first node of Ranvier, that can go from 0 to $a \cdot \Delta x$, where Δx is equal to the sum of the internodal and nodal lengths and a is a factor ranging from 0 to 0.5 at our choice. For axons of equal diameter, their mutual misalignments are very easy to control with the value of a: $a = 0$ means their nodes are perfectly aligned, while $a = 0.5$ means they can have their maximum degree of misalignment. For axons of different diameters, their internodal lengths are different and therefore a complete alignment of all the nodes is impossible. Even choosing a certain degree of alignment is not possible unless their internodal lengths are very similar and the bundle's length is short enough.

In the first simulation (simulation 1), the transverse resistors are connected at the locations of the nodes of Ranvier and we use $a = 0.5$. Figs. 4.6 and 4.7 show the relevant results for this simulation. The maximum absolute values of the extracellular field over the axons—or absolute field maxima—are used in the horizontal axis of the top right panels and in the vertical axes of all bottom panels in both figures. However, the values for this variable are sampled differently for each figure: Fig. 4.7 samples this variable along the entire length of the axons to its maximum resolution (i.e. over all the axon compartments; this will be symbolised with ϕ from now on), whereas in Fig. 4.7, the field was sampled only over the nodes of Ranvier, so the absolute field maxima correspond only to the nodes of Ranvier (hence, ϕ_N). This makes a difference in the dependence of the absolute field maxima on distances and node-to-pad misalignments and on the dependence of AP delays on absolute field maxima.

It can be seen in Fig. 4.6 (top left) that the AP delays, while showing an overall positive dependence on the distances between the axons and the source, do not follow a very smooth relationship with this variable. They follow a much smoother relationship with ϕ_N (Fig. 4.6, top right). From the activating function theory [59], we can infer that the AP delays do not strictly depend on ϕ_N, hence the irregularities

---

[2]Do not confuse this type of nodal misalignment with the node-to-pad misalignment that is discussed later on.
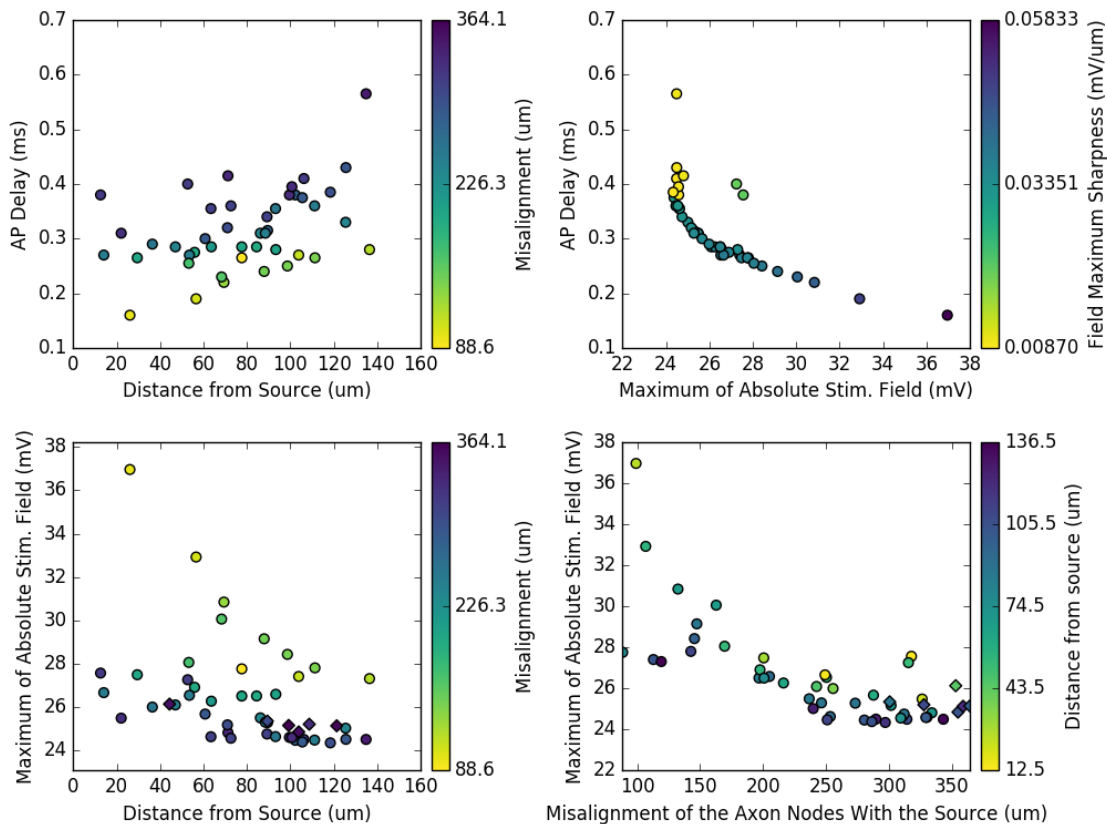
Figure 4.6: Results for simulation 1. Top left: AP delays vs. distances from the axons to the source. Top right: AP delays vs. ϕ_N. Colormap: sharpness of the field where the field of each axon is maximum. This variable may have some influence in the AP delays. However, this is not clear because it is very correlated to ϕ_N. Bottom left: ϕ_N vs. distance. Colormap of this and top left panel: nodes misalignment with respect to the source (node-to-pad misalignments). Bottom right: ϕ_N vs. node-to-pad misalignments. Colormap: distances from the axons to the source. Top panels show data for fired axons only, whereas the bottom panels show data for all axons. In these two latter, circles correspond to fired axons and diamonds correspond to axons that did not fire APs.

that break the smoothness of the graph. Nevertheless, the absolute field maxima are a suitable variable to be taken into account as an intermediate variable when studying the relationship between AP delays and distances, since we may assume there is a close relationship between AP delays and absolute field maxima and in turn, between absolute field maxima and distances. Despite this, we can observe in Fig. 4.6 (bottom left) that the relationship between ϕ_N and distances is not smooth. The distinction between ϕ_N and ϕ is made because while the AP delays follow a close relationship with ϕ_N, it is ϕ, more than ϕ_N, which follow a closer relationship with the axon-source distances (compare the bottom left panels of Figs. 4.6 and 4.7).

As was mentioned above, the third variable influencing the AP delays is the node-to-pad misalignments. For each axon, this is defined as the component along
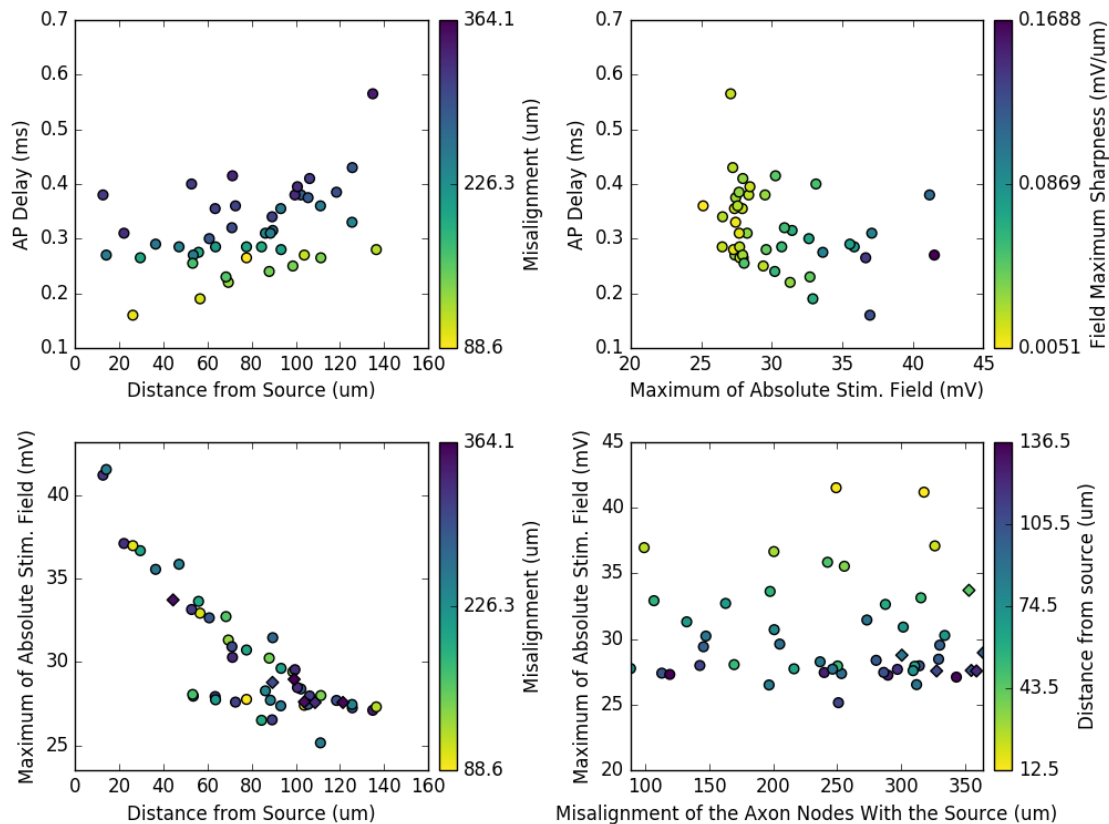
Figure 4.7: Results for simulation 1. Same as Fig. 4.6, with the difference that the fields include data from all the sections on the axons (including paranodal regions and internodes) as opposed to data from the nodes of Ranvier only. Note how the ϕ lose their dependence on the node-to-pad misalignment. Also, the AP delays have a weaker dependence on the ϕ than on ϕ_N, since ϕ is not necessarily located on the nodes of Ranvier.

the z-axis of the distance between the source (active pad) and the axon's closest node of Ranvier. Every axon has, then, a particular value of node-to-pad misalignment, whose maximum possible value is $\Delta x/2$. The ϕ do of course not follow any relationship with the node-to-pad misalignments but only on the axon-to-pad distances (Fig. 4.7, bottom right), but the ϕ_N do follow a decreasing trend on these (Fig. 4.6, bottom right). The points with lower misalignments in the bottom left panel of Fig. 4.6 show an interesting behaviour, where they form a smoother front, indicating that groups of nodes with similar misalignments may follow smoother curves. The AP delays show in turn a positive trend, where delays are longer for greater misalignments (both figures, top left panels).

Despite the above, the relationship between ϕ and the axon-source distances shows irregularities, while in theory it should be completely smooth. This is a direct consequence of the choice of placing transverse resistors on the nodes of Ranvier only. For axons having a completely random misalignment between their nodes ($a = 0.5$),

the three-dimensional RN formed by the transverse and longitudinal resistors is considerably irregular. This can quickly induce a loss of field resolution along the z-axis with the distance from the source, which leads to very visible inaccuracies in stimulation far from the source. One way to solve this problem is to place transverse resistors at regular intervals along the z-axis, which creates a much more regular network. Simulation 2 was run using all the same parameters as simulation 1, except for the transverse resistor locations, which were placed at regular intervals of 200 μm. After this change, the relationship between ϕ and the distances is substantially improved (Fig. 4.8).
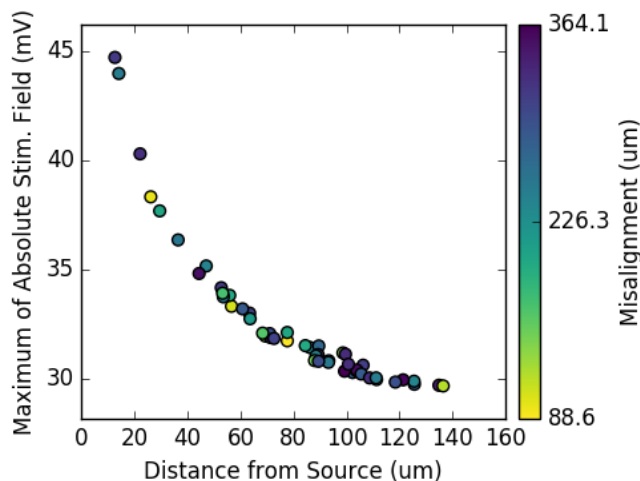
Figure 4.8: Results of ϕ vs. distance for simulation 2.

4.3.3   Effects of Ephaptic Coupling on Action Potential Propagation along Parallel Fibers

We used the RN to run simulations of bundles that range from one to four parallel fibers in order to study the effects that EC between them has on the propagation of their APs. All fibers were identical MRG motor fibers with a fiber diameter of 10 μm and their nodes of Ranvier were completely aligned. Transverse resistors were connected on the nodes of Ranvier. In this case, as all the nodes were aligned, this is equivalent to connecting them at regular intervals equal to Δx of the fibers. Fibers were intracellularly stimulated at their left-most Ranvier nodes using a square pulse with an amplitude of 10 nA, a duration of 10 μs and with a start time difference of 0.1 ms between each fiber. The walls of the bundle are isolated so current is not allowed to flow radially to a distant ground. However, the ground is connected to the extracellular space at the ends of the bundle, so the path to ground for any current is longitudinal.

In all simulations, the ratio between the total cross-sectional axoplasmic and

Symbol	Value	Description
ρ_A	70 $\Omega \cdot$ cm	Axoplasmic resistivity (MRG [108]).
r_F	5 μm	Fiber radius.
g	0.679	Axon to fiber diameter ratio. This is the approximate value for a MRG 10 μm diameter fiber. Obtained by interpolation.
α	2.865	Ratio between total cross-sectional areas of the bundle and the fibers.

Table 4.2: Parameters used for the simulations.

extracellular areas was preserved, so we controlled the ratio (β) between total extracellular (R_E) to axoplasmic (R_A) longitudinal resistances simply by changing the value of the extracellular longitudinal resistivity (ρ_E^L). This ratio was controlled in the following way:

$$\beta = \frac{R_E}{R_A} = \frac{\rho_E^L}{\rho_A} \frac{g^2}{\alpha - 1}, \tag{4.22}$$

where ρ_A is the axoplasmic resistivity, g is the axon to fiber diameter ratio, and

$$\alpha = \frac{A_T}{A_F}, \tag{4.23}$$

where A_T is the total cross-sectional area of the bundle and A_F is the sum of the cross-sectional areas of the fibers. Being r_F the fiber radius and n the number of fibers,

$$A_F = n\pi r_F^2, \tag{4.24}$$

Table 4.2 shows the values of these variables.

The parameter β determines the proportion of current that flows to ground through the extracellular space compared to the current that flows through the axoplasmic resistances. Therefore, low values of β denote a low extracellular resistance and therefore, a small strength of EC, and vice versa.

The trajectories of the APs of all the axons in the simulations were graphed for visualisation. These were found by identifying the time for each node of Ranvier where the transmembrane potential reached 15 mV.

For the bundle with two axons, in the simulation with $\beta = 1$ the two axons manage to lock their APs and reduce their CVs (Fig. 4.9(b)). The simulation with

$\beta = 0.1$ is shown as a reference when the EC is very small and there is nearly no interaction between the axons (Fig. 4.9(a)).

(a) (b)
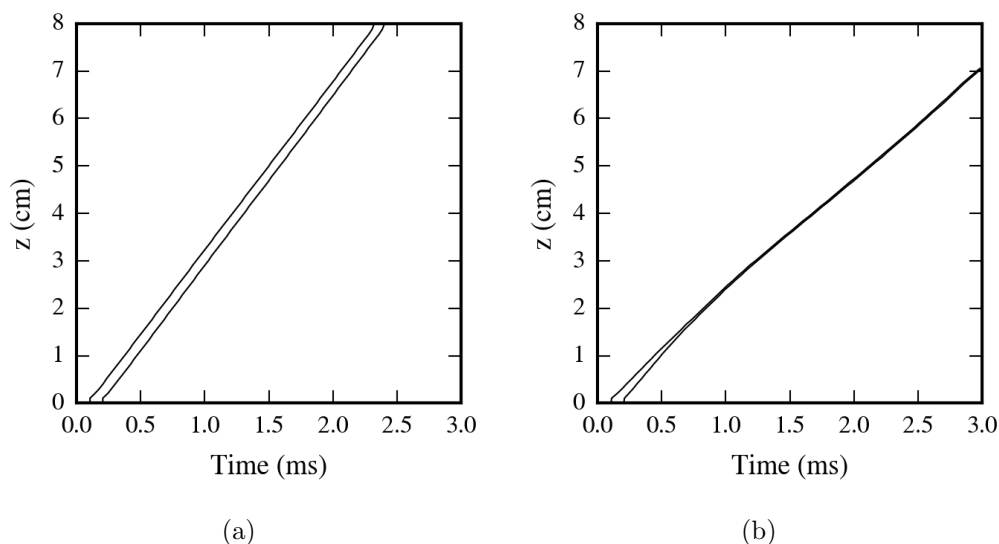
Figure 4.9: Trajectories of the APs of the two axons in this bundle. (a) is for $\beta = 0.1$, and (b) is for $\beta = 1$.

For the simulations with three and four axons, only the case $\beta = 1$ is displayed (Fig. 4.10). If these results are compared to the simulation with two axons (Fig. 4.9(b)), it can be noticed that increasing the number of axons diminishes the strength that their trajectories exert on each other. For three axons, the two last axons manage to form an AP locking, but this happens later than for two axons alone and the trajectory of the first axon is never fully incorporated to the lock. For four axons, there is a clear attraction between all the trajectories, but the lock does not happen after the trajectories have finished the length of the bundle. Furthermore, and probably due to the lack of AP lockings, the CVs of the axons do not decrease as much as with two axons. A possible cause for this observed effect is that the currents exerted by one axon alone into the extracellular space enter all the other axons and spread mostly between the axoplasmic resistances of all of them, so the higher the number of axons in the bundle, the lower the current flowing through the axoplasmic resistance of each of them, and therefore, the lower the ephaptic influence of the source axon on other axons. Additionally, it can be argued that as we are keeping a constant value of α, increasing the number of fibers also increases the cross-sectional extracellular area, which reduces the strength of EC.

This approach of sequential stimulation of the axons is in general not presented for higher values of β (we tested with $\beta = 10$ and above) because for these, stimulation of the first axons always induced a premature AP in the remainder and this generated complex behaviours. However, we considered interesting to show the case $\beta = 10$ for four axons (Fig. 4.11). The first stimulated axon fires an AP on its own, but the other three fire simultaneously, shortly after the first. They travel

(a)   (b)
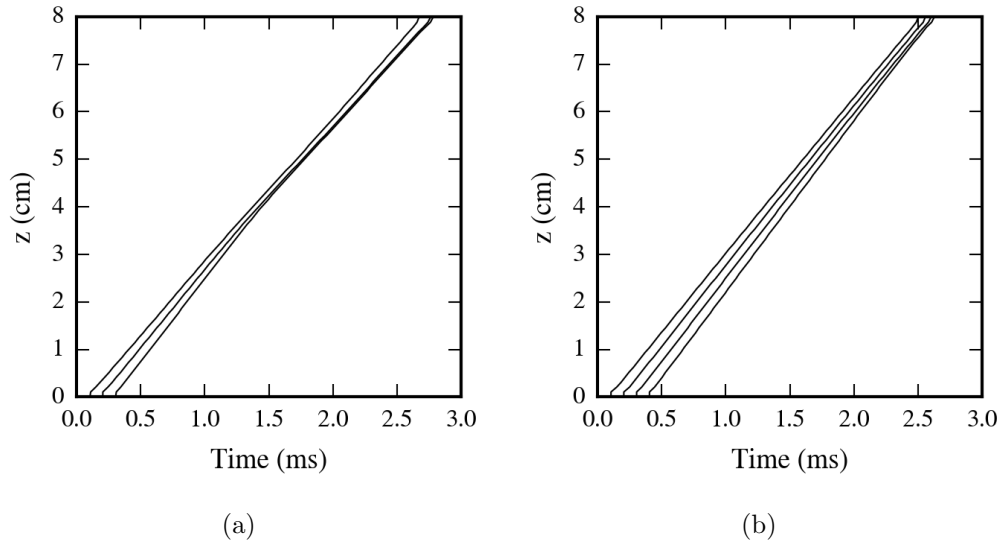
Figure 4.10: Trajectories of the APs for the bundles with three (a) and four (b) axons. $\beta = 1$.

synchronously for a distance and they start separating from the group one by one, just as will be observed in the much more complex case of Chapter 5. The shapes of these trajectories display a clear relationship between number of trajectories in a AP lock and its group CV, where more trajectories in the lock always drive a lower CV.

(a)   (b)
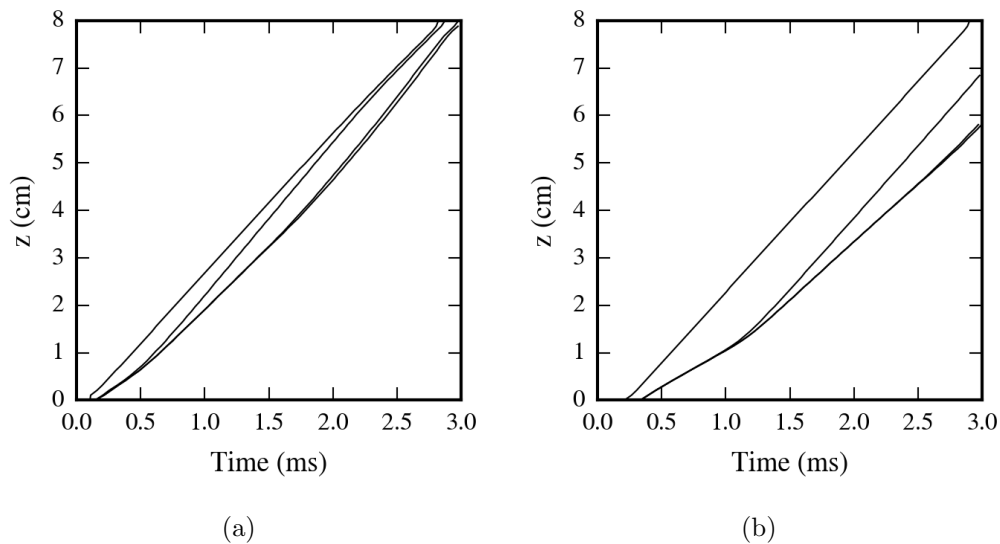
Figure 4.11: Trajectories of the APs of the four axons in this bundle. Both cases are for $\beta = 10$. In (a), the axons are stimulated with a start time difference of 0.1 ms, and in (b) this time difference is 0.2 ms.

Consequences of Transverse Resistor Location Choices

In the simulations that led to these results, the transverse resistors were located at the nodes of Ranvier of the fibers, which were perfectly aligned in all cases. If instead of choosing the locations of the nodes of Ranvier to place the resistors, we opt to connect them at regularly spaced intervals, the strength of the EC between the axons is affected if this spacing is not equal to the nodal separation of the axons. We ran a simulation in which we connected transverse resistors at every 1000 μm, where the nodal separation of the axons was 1036.6 μm. The resulting trajectories of the APs of the axons show how their CVs oscillate along the z-axis with an amplitude near 5 m/s, where the minimum value of the CV is almost 20.5 m/s (Fig. 4.12). This is an oscillation that can be higher than a 24% of the average CV. In this simulation, $\beta = 1$.
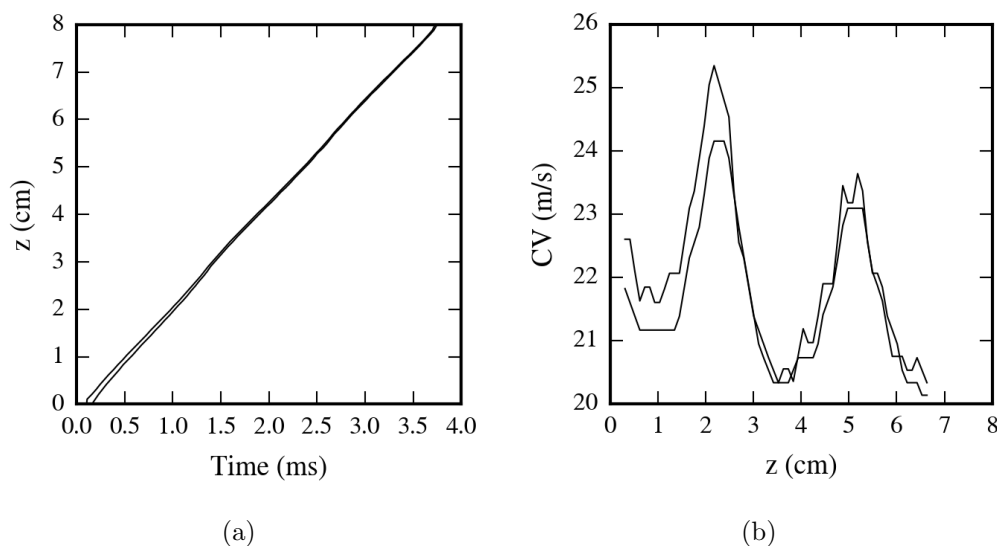
Figure 4.12: (a) Trajectories of the APs of the axons. (b) CVs of the axons during the propagation of their APs along the z-axis. The CVs in this figure were applied a moving average using a window of 10 nodes of Ranvier. Note the oscillations in the trajectories and also in the CVs.

This large amplitude oscillation in the CVs is an artefact arising from the relative positioning of the transverse resistors with respect to the nodes of Ranvier. Considering that the difference between nodal and resistor separations is 36.6 μm, the points where the best alignment between nodes of Ranvier and transverse resistor occur are separated by $1036.6/36.6 \approx 28.3$ nodes of Ranvier, which is equivalent to a distance of approximately 2.94 cm. This distance is approximately the same as the observed wavelength of the oscillation in CV in Fig. 4.12.

The presence of these artefacts are clearly a limitation to the proper simulation of EC, so while we saw that this modelling choice is more suitable for computing the fields from stimulation, it is not suitable for EC during propagation.

4.3.4   Electrode Recordings from one Axon

We used the RN to simulate the recordings of the activity of one axon on a pad of a cuff electrode. A MRG fiber with a diameter of 10 μm was located at the center of an ideal cylindrical nerve model with a diameter of 300 μm and a length of 2 cm. The nerve did not contain any other axons. The endoneurium was modelled with an isotropic resistivity of 1211 $\Omega \cdot$ cm [178]. The nerve was considered mono-fascicular (i.e., having only one fascicle), and the fascicle was surrounded with a perineurium of 9 μm thickness (3% of the fascicle's diameter [132]), and a resistivity of $1.136 \cdot 10^5$ $\Omega \cdot$ cm [56]. The cylindrical container was given a diameter of 2.2 cm, and the saline bath had a resistivity of 50 $\Omega \cdot$ cm [7]. We placed a cuff electrode for recording centered at $z = 1.5$ cm. The cuff had only one ring in the center and only one recording pad at an angular position of 0° —that is, at $x = 300$ μm and $y = 0$. The axon was given an intracellular current injection to its first node of Ranvier (on its left end) of 1 μA, and it was left to propagate an AP toward the right end of the model. The recording of the extracellular potential at the position of the cuff electrode's pad is shown in Fig. 4.13.
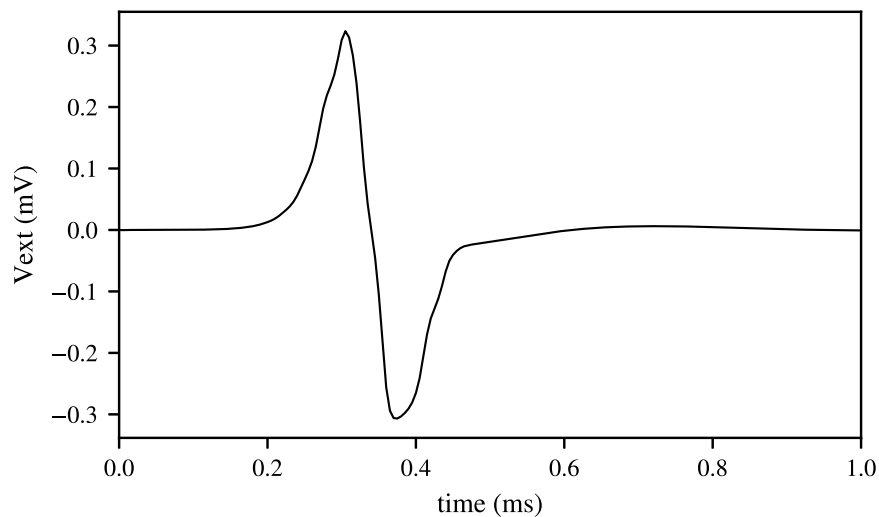
Figure 4.13: Electrode recording of the activity of a MRG fiber inside an ideal nerve model.

4.4   Discussion

In this chapter we have developed a Resistor Network (RN) to model the extracellular space of a bundle of fibers. The RN creates an EMI model of the bundle and allows the simultaneous simulation of the extracellular fields, neural activity, and electrode recordings. The RN uses a nearest-neighbour electrical connection model

for a random distribution of fiber positions based on the Voronoi tessellation of the positions. We have studied the validity of the RN by comparing its results on two simple problems to the corresponding FEM and analytical results for validation. We have tested the usability of the RN to model situations of interest, such as stimulation, propagation, and electrode recordings. For this, we studied the effects of anatomical properties of a bundle on the responses of the fibers to stimulation from extracellular electrodes using the RN. Finally, we used the RN to run simulations of EC between a small number of fibers, which is nearly equivalent to using a MF model. The results of these simulations were contrasted with previous knowledge on the effects of EC on propagation.

The RN is mathematically equivalent to a FDM in the limit of a uniform rectangular mesh. It is capable of modelling the potential distribution over a 2D domain for a simple problem where a current point source and connections to ground are present, and it yields results which are very close to results from FEM simulations. Modelling the potential along a third dimension for the simple problem of a cubic resistor where a distributed current is applied on one face and ground is connected over the opposing face is also achieved with notable accuracy when compared to the analytical result (RDM of the order of 10^{-6}). These findings support the use of the Voronoi-based RN presented here, along with its implementation in NEURON, for solving electrical problems on ohmic media and therefore, for their use in numerical simulations of neural systems involving the extracellular medium.

The RN was used to simulate bundles of fibers under stimulation and propagation scenarios. It has been shown that this method does satisfactorily simulate these scenarios.

Inside a bundle, the potential distribution that is generated from a stimulating external electrode clearly decreases with the distance from it with a monotonic trend. However, the maximum value of this field along a fiber is not the only determinant variable for its response, which can be measured with the delay between when stimulation is set off and the firs AP fires on the fiber. The relative positions along the z-axis of the nodes of Ranvier of the fibers with respect to the current source (or active pad) of the electrode has been found to strongly alter this response delay. This variable, referred to as node-to-pad misalignment, naturally affects the maximum value of the extracellular potential on a node of Ranvier, and thus affects the effective strength of the stimulation. Another factor affecting fiber response is taken into account when using the RN to model this system. The choice of placing the transverse resistors at the locations of the nodes of Ranvier instead of inserting resistor layers at regularly spaced intervals along the z-axis creates an irregular mesh which has the effect of obscuring the resolution of the potential as distance from the current source increases in the model. This, in turn, has a detrimental effect on the accuracy of the fibers' responses, especially for fibers being distant from the source.

Using the RN to model propagation in a bundle containing a small number of

fibers and choosing a large longitudinal component of the extracellular resistivity renders a very similar scenario to using a Mean-Field (MF) model for the extracellular field. EC on these scenarios makes APs of different axons attract each other and they tend to lock their trajectories. When this is achieved, their CVs are reduced. The ratio between extracellular and axoplasmic resistances controls the strength of this effect. These results hold a reasonable level of accordance with previous known results for MF EC in myelinated axons [66] if we consider that we used different axon models and parameters. This provides a degree of reliability on the RN as it behaves accordingly with known results in special case.

After these studies, the RN is presented here as a valid and potentially helpful tool for computational neuroscientists. However, three limitations, one technical and two of them regarding its applicability, need to be mentioned:

- Electrical currents through space are only modelled along the z-axis and on the x-y plane. A FEM scheme could simulate these currents more accurately.

- It has been shown how the two proposed options for locating the transverse resistors present benefits and drawbacks depending on what it is intended to model. Placing resistors on the locations of the nodes of Ranvier is based on the assumption that EC is relevant only or mostly among nodes of Ranvier. This permits simulating and quantitatively studying the effects of EC, but it is a source of inaccuracies for simulating the fields coming from electrodes since it creates an irregular RN. On the other hand, placing them at regular intervals along the z-axis permits a much more accurate simulation of the fields, while it inaccurately models EC by making it highly dependent on the relative positions between nodes of Ranvier and transverse resistors. This accidentally modifies the strength of EC along the z-axis in an oscillatory fashion, and this effect is accentuated by the increase of the longitudinal extracellular resistivity, since longitudinal currents find a great resistance outside the axons. Most likely, increasing the RN resolution along the z-axis would attenuate this unwanted oscillation. This, however, leads to a considerably higher computational workload.

- The RN presented here is conceived for cylindrical bundles of parallel axons, but it is not suitable for modelling other types of cellular arrangements. For this, however, we hope researchers will feel encouraged to extend this concept to other configurations by using tessellations in three dimensions.

Despite of these limitations, the RN method here is presented as an alternative to hybrid FEM-neural simulations that not only permits to compute fields from stimulating electrodes and on recording electrodes in a self-contained and self-consistent simulation, but also, and most importantly, permits the simultaneous simulation of ephaptic interactions between all fibers in a bundle.

4.5   Conclusion

A RN was presented in this chapter to model bundles of fibers including their extracellular medium. The RN was validated against FEM simulations for a simple problem and against analytical results. Validation results show that the RN can solve the potential field in three-dimensional ohmic media with an acceptable accuracy. Then, the RN was used in three simple scenarios: the stimulation of a bundle of parallel myelinated fibers using a cuff electrode, the propagation of APs in bundles of small number of identical and parallel myelinated fibers, and the activity recordings of an axon by a cuff electrode. For the stimulation scenario, anatomical variables (i.e., distance from axons to stimulating electrode and alignment of their nodes of Ranvier to the electrode) were related to the delay of AP elicitation from stimulation. Also, the effects of choices in the configuration of the locations of the transverse resistors in the RN on the AP delays was studied. When studying propagation in small bundles, simulations were run where the expected synchronisation effects of EC were observed, plus an observation was made that increasing the number of axons in a bundle reduces the strength of the ephaptic influence from an axon on others. We hope that this tool will be useful in further research as an available resource when considerable levels of complexity are needed in simulations of neural activity. This RN is used in the following chapter in a more detailed nerve model.

Chapter 5

Effects of Ephaptic Coupling During Artificial Stimulation of Peripheral Nerves

5.1   Introduction

The contents in this chapter are adapted from the manuscript submitted to PLOS Computational Biology [15] (not published yet; as at this writing, revisions from the reviewers are being addressed and the final paper may differ in content from this chapter). The relevant parts of the Materials and Methods section of [15] were presented in Chapter 4.

In simulation studies on electrical stimulation of peripheral nerves by electrode-nerve interfaces, the focus is generally aimed at predicting the selectivity of the electrodes (see [7, 8, 58] or [179]). Although these works use detailed geometrical representations of the nerves in their models, they rely purely on axon activation prediction to study selectivity and do not regard the effects that EC may have on the axon thresholds during propagation, nor the effects that AP propagation may have not only on the selectivity of the electrodes, but also on the frequency encoding of the signals that later reach the central nervous system. A more specific study is needed to assess the extent to which propagation can affect these variables.

In order to carry out a detailed study of propagation, ephaptic interactions should be taken into account. These are normally disregarded in peripheral nerves, but as it was explained in Chapter 2, they exist and are likely to play a role in information processing through alteration of the relative timings between APs from different axons, and possibly, in the selectivity of the electrodes. Hence, including this type

of coupling in the models might provide an improvement onto existing achievements in the predictions of electrodes' fascicle selectivity and information encoding, which would in turn lead to more accurate and more naturalistic artificial sensory feedback in neural interfaces.

We have developed three-dimensional EMI-type [114] models of both realistic and ideal peripheral nerve trunks, which use a RN in order to simulate stimulation and propagation with ephaptic interactions in a unique simulation, with the ultimate goal of using it towards making predictions of fascicle targeting selectivity, frequency encoding, and overall electrode performance, in order to optimise the designs of these electrodes.

The significance of this work lies in being the first work, to the best of our knowledge, that studies EC for a bundle of this complexity and which deviates from restrictive assumptions such as the Mean-Field (MF) model or more regular geometries [64–66, 68], and therefore intends to elucidate the relevance of EC in more realistic conditions. In comparison to Chapter 4, in this chapter we have chosen a more complete geometrical tessellation technique to model the nearest-neighbour electrical connections between fibers of varying diameters and different tissues. Also, we have added details of electrode configurations and extraneural environment to the model.

In summary, the main novelty of this work is the study of EC:

- for a nerve model containing randomly-located myelinated mammal peripheral axons with varying diameters, following both uniform and natural-like distributions,

- that departs from MF assumptions and takes the inter-axonal distances into account through a RN,

- in scenarios where the nerve models are stimulated by cuff electrodes.

5.2   Methods

The fundamental assumptions on which the model is based, the axon models in use and a detailed description of the procedures used to model the nerve's tissues are provided here.

5.2.1 Main Assumptions and Limitations

The model relies on several assumptions to simplify the implementation and computational cost while still keeping an acceptable level of accuracy:

1. Only two types of axon models are used: the double-cable models of McIntyre, Richardson and Grill (MRG) [108] for motor fibers, and Gaines & al. [113] for sensory fibers. No unmyelinated or other types of myelinated axons are considered.

2. Axons are straight, with no tortuosity (i.e., with no bends, undulations, or tapering) along their length.

3. All axons are parallel to each other.

4. Following the two above assumptions, the cross-section of the nerve's anatomy is constant along its length.

5. All extracellular tissues are purely ohmic. We work under the QS approximation, and hence we do not consider capacitive properties of the tissues.

6. The volumes of the epineurium and endoneurium are regarded as part of a three-dimensional resistor network.

7. The endoneurium was modelled as an isotropic tissue, since using its anisotropic tensor from [178] would imply an over-representation of the axons.

8. The perineurium is regarded as a surface with a nominal thickness influencing the values of the resistances that cross it.

9. Electrode impedance was not accounted for in the models.

10. The nearest-neighbour electrical connections model defines inter-axonal connections only across the x-y plane, and inter-compartmental connections along the z-axis. This is a limitation with respect to FEM schemes, which can model currents flowing in any direction.

11. The RN is computationally expensive. A very large number of axons in the model can greatly increase the simulation time to days. Therefore, although the typical diameters of human limb peripheral nerves where stimulation is studied is typically in the order of several mm [184, 185], we used smaller nerve models and axon bundles (see Fig 5.1 for more details). Also, fiber packing ratios and axon numbers were kept low.

5.2.2   Axon and Nerve Models

A number of different models were used in this chapter in order to run the different studies (see table 5.1 for a detailed list of these models). Model named Nerve 1 in this chapter uses both motor and sensory fiber models, with a proportion of 15% motor and 85% sensory fibers [113]. All other models use, exclusively, motor fibers. In all cases, we used a temperature of 37 °C. Although EC in unmyelinated axons can be relatively strong, their use in our model implied a high computational cost due to the higher spatial resolution that they require. Also, they are outside the scope of this study as our focus is on the often neglected EC between myelinated fibers. Therefore, unmyelinated fibers were not included in the models presented here.
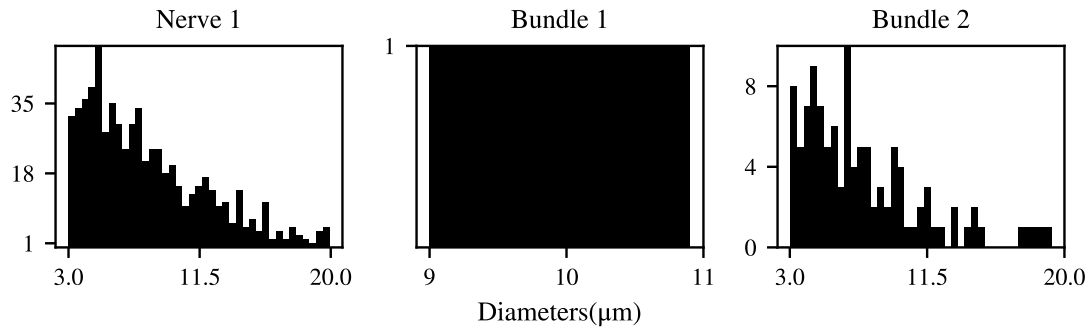
Figure 5.1: Histograms for fiber diameters of the nerve (and bundle) models used in this study, except for models without diameter variability (Bundle 3 and Nerve 2). Horizontal axes indicate diameter values in μm and vertical axes indicate the number of axons for each bin of the histograms. Note that although all histograms have the same number of bins (39), they do not necessarily share any horizontal or vertical axes. The corresponding model names are indicated on the top of each histogram.

In Nerve 1 and Bundle 2, the fiber diameters were randomly assigned, ranging from 3 μm to 20 μm, following a distribution according to the results in [186] in Nerve 1 and Bundle 2 (smaller diameter fibers were excluded due to their fine spatial discretisation requirements, which led to higher computational costs). Therefore, the nodes of Ranvier of the different axons were not necessarily aligned. The different properties of the fiber morphology that depend on the diameter —internodal length, morphology of the myelin attachment (MYSA) and paranodal (FLUT) regions and number of myelin layers, were fitted to a linear regression each, using the values from [108]. Variables whose linear regressions yielded negative values were fitted to a quadratic curve, as done in [110].

The implementation of the axon membrane models was made in the NEURON simulation environment [2].

For Nerve 1 and Nerve 2, we used a nerve model as a cylindrical body with

Model	Diameter (μm)	Number of axons	Fiber packing ratio	Intracellular to extracellular areas ratio	Length (cm)
Nerve 1	500	658			1
Fascicle 1 (Nerve 1)	156.67	82	0.282	0.205	1
Fascicle 2 (Nerve 1)	156.67	118	0.350	0.267	1
Fascicle 3 (Nerve 1)	156.67	99	0.344	0.269	1
Fascicle 4 (Nerve 1)	156.67	87	0.290	0.212	1
Fascicle 5 (Nerve 1)	156.67	98	0.330	0.251	1
Fascicle 6 (Nerve 1)	156.67	83	0.293	0.225	1
Fascicle 7 (Nerve 1)	156.67	91	0.283	0.193	1
Bundle 1	100	39	0.398	0.304	6
Bundle 2	150	110	0.347	0.267	6
Bundle 3	250	69	0.450	0.606	3
Nerve 2	500	192			3
Fascicle 1 (Nerve 2)	156.67	26	0.429	0.555	3
Fascicle 2 (Nerve 2)	156.67	28	0.462	0.634	3
Fascicle 3 (Nerve 2)	156.67	28	0.462	0.634	3
Fascicle 4 (Nerve 2)	156.67	27	0.445	0.593	3
Fascicle 5 (Nerve 2)	156.67	29	0.478	0.677	3
Fascicle 6 (Nerve 2)	156.67	27	0.445	0.593	3
Fascicle 7 (Nerve 2)	156.67	27	0.445	0.593	3

Table 5.1: Geometrical and electrical properties of the models.

seven cylindrical fascicles of equal diameter, inspired in the five-fascicle model from
[7]. In all models, the fascicles were filled with axons using a simple circle packing
algorithm designed for this purpose.

The algorithm consisted of one iterative process for each fascicle where, in each
iteration, a random diameter value D_k was chosen from the aforementioned distri-
bution for a circle (a fiber, indexed with k). For each circle, a loop for positioning
trials was then run. On each trial, a random position for the center of the circle
was chosen inside the fascicle (more specifically, inside a circle having a diameter
$D_F - D_k$, being D_F the diameter of the fascicle, in order to avoid intersection of the

circle with the fascicle's membrane). If the circle at the position had no intersections or contacts with any other circle that had been placed previously in the fascicle, the position was assigned to it and a new random circle was chosen. The algorithm stopped when a circle could not be placed at a suitable position after $10,000$ trials. For this process, a minimum allowed distance between axons was chosen to be 1 μm (which was taken into account at each contact check), so no two axons could be closer to each other than that. The fiber packing results for the different models used in this work are summarised in Table 5.1. The algorithm used here yields fiber packing ratios which are generally lower than the typical values in nerves (see, for instance, [187] for measured values in human spinal cord). However, these lower ratios prevented us from having a very high number of axons, which would increase the computational cost of the simulations. This algorithm can fill fibers given any contour, and results are not dependent on the fascicles' shapes.

Three different extracellular tissues were considered in the model (Table 5.2): The epineurium was used for the whole extrafascicular space inside the nerve, the endoneurium was used to account for all the intrafascicular spaces where axons were embedded, or interstitial spaces, and the perineurium was regarded as a surface layer that electrically separated the fascicles from the epineurium. Nevertheless, the epineurium and the endoneurium were given the same electrical properties for the following reasons, respectively: The epineurium was considered to be isotropic as in [7, 179]. The endoneurium's resistivity taken from the literature [178] is considered to be anisotropic because it accounts for the longitudinal disposition of the axons. In this RN, however, axons are explicitly represented by implementing their membranes and intracellular resistances as part of the RN. Using the known value from [178] for the longitudinal component of the endoneurium's resistivity, $\rho_{En}^L = 175\ \Omega \cdot cm$, is then not suitable for this model, since that would imply an over-representation of the intracellular resistances. Hence, given the lack of knowledge about the value of ρ_{En}^L. we made the conservative assumption of considering the endoneurium as an isotropic tissue, and used its transverse component of the resistivity, ρ_{En}^T, as the value for its longitudinal component. This value was obtained from a configuration where the transverse disposition of the axons contributed to the resistance of the nerve where it was measured [178]. Therefore, although a safe assumption of isotropy has been made here, it should be taken into account that its actual physiological value may be lower.

5.2.3   Resistor Network Model

This chapter uses the RN developed in Chapter 4. However, additional equations are provided in this chapter and incorporated to the RN in order to model anatomical properties and tissues that were not considered in Chapter 4. These model the diameter variability of fibers and the presence of different tissues. Specifically, we modelled the presence of the endoneurium, epineurium and perineurium.

Symbol	Value	Source	Description
ρ_{ax}	70 $\Omega \cdot$ cm	[108]	Axoplasmic resistivity.
ρ_{En}^{L}	1211 $\Omega \cdot$ cm	[178]	Longitudinal (z-axis) component of the resistivity of the endoneurium. See main text to understand the discrepancy with the anisotropic tensor from [178].
ρ_{En}^{T}	1211 $\Omega \cdot$ cm	[178]	Transverse (x-y plane) component of the resistivity of the endoneurium.
ρ_{Ep}^{L}	1211 $\Omega \cdot$ cm	[7, 179]	Longitudinal component of the resistivity of the epineurium.
ρ_{Ep}^{T}	1211 $\Omega \cdot$ cm	[7, 179]	Transverse component of the resistivity of the epineurium.
ρ_{P}^{T}	$1.136 \cdot 10^{5}$ $\Omega \cdot$ cm	[56]	Transverse (and only) component of the resistivity of the perineurium (value for 37°; see reference).
ρ_{I}	10^{9} $\Omega \cdot$ cm	[7]	Resistivity of the insulator.
ρ_{S}	50 $\Omega \cdot$ cm	[7]	Resistivity of the saline bath.
Δ_{P}	$4.7 \cdot 10^{-4}$ cm	[132]	Thickness of the perineurium (3% of the fascicle diameter in Nerve 1; see Table 5.1).
Δ_{I}	$2.4 \cdot 10^{-2}$ cm	[7]	Thickness of the insulating cuff.
Δ_{S}	0.85 cm		Thickness of the saline bath in the cylindrical container (in the absence of cuffs).
Δ_{C}	2.2 cm	[7]	Cylindrical container's diameter.
D_{N}	0.5 cm		Diameter of the nerve.
n_{H}	36		Number of points in the triangulation hull (or number of NAELC on the nerve's membrane).

Table 5.2: Parameters used for the RN.

Modelling the Nerve Containing Axons and Extrafascicular Regions

In this chapter, we are using the RN to model a nerve containing fibers of varying diameters packed inside fascicles which are surrounded by perineurial membranes. The epineurium, which is the space surrounding the fascicles, is free of axons and therefore, our nerve model includes both fibers of different diameters and NAELC. This is a novelty following Chapter 4, where bundles were either empty or containing equal diameter fibers exclusively.

All NAELC and fibers inside the nerve form a packing of non-intersecting circles over the cross-section (Fig. 5.2; the points corresponding to NAELC may be regarded as zero-diameter circles for this purpose).

The Voronoi diagram for sets of equal diameter circles needs now to be adapted to account for the different diameters in the new circle packing. Computing the known Voronoi diagram over the centers of the circles only may easily contain segments that intersect with circles. This would compromise the characterisation of the electrical parameters of the model, since a prism could contain fragments of different circles. To solve this problem, we need to compute the power diagram, described as the

Symbol	Units	Description
$a_{k,i}$	None	Fraction of cross-sectional area of tissue of type i present in polygon k.
$b_{k,l}^i$	None	Distance crossed through a tissue of type i by the transverse resistor between k and l as a fraction of the total distance between the membranes of k and l.
$A_{P,k}$	cm^2	Cross-sectional area of polygon k.
$A_{E,k}$	cm^2	Extracellular cross-sectional area inside polygon k.
D_k	cm	Diameter of fiber k (zero for NAELC).
$c_{k,l}^n$	cm	Length (along the z-axis) of the transverse resistor number n between cables k and l.
$d_{C,(k,l)}$	cm	Distance between the centers of fibers k and l.
$s_{k,l}$	cm	Length of the segment in common between polygons k and l.
$\rho_k^{Lu,L}$	$\Omega \cdot$ cm	Longitudinal component of the lumped resistivity for polygon k.
$\rho_{k,l}^{Lu,T}$	$\Omega \cdot$ cm	Transverse component of the lumped resistivity between cables k and l
$r_{L,k}$	Ω/cm	Resistance per unit length of the extracellular cable k.
$R_{T,(k,l)}^n$	Ω	Value of the transverse resistor n between cables k and l
R_G	$\Omega \cdot$ cm	Resistance to ground from a point on the nerve's membrane per unit length.

Table 5.3: Variables used for the resistor network.

Voronoi tessellation in the Laguerre geometry [180]. This assigns a convex polygon to each circle, be this corresponding to a fiber or a NAELC, and therefore assigns an extracellular cross-sectional area $A_{E,k}$ to each fiber and NAELC.

Polygons containing the points on the nerve's membrane are cropped so that they do not intersect the nerve's outer space.

Longitudinal resistances of the RN The polygons of the tessellation can intersect more than two regions corresponding to different tissues. I.e., one polygon can intersect endoneurial and epineurial regions of the nerve. To account for this, the longitudinal resistivity of the polygonal prism is determined using a lumped value of the resistivities of the tissues intersecting its polygon.

$$\rho_k^{Lu,L} = \sum_i a_{k,i} \cdot \rho_i^L, \tag{5.1}$$

where k indicates the cable or polygon, i indicates the type of tissue and then,
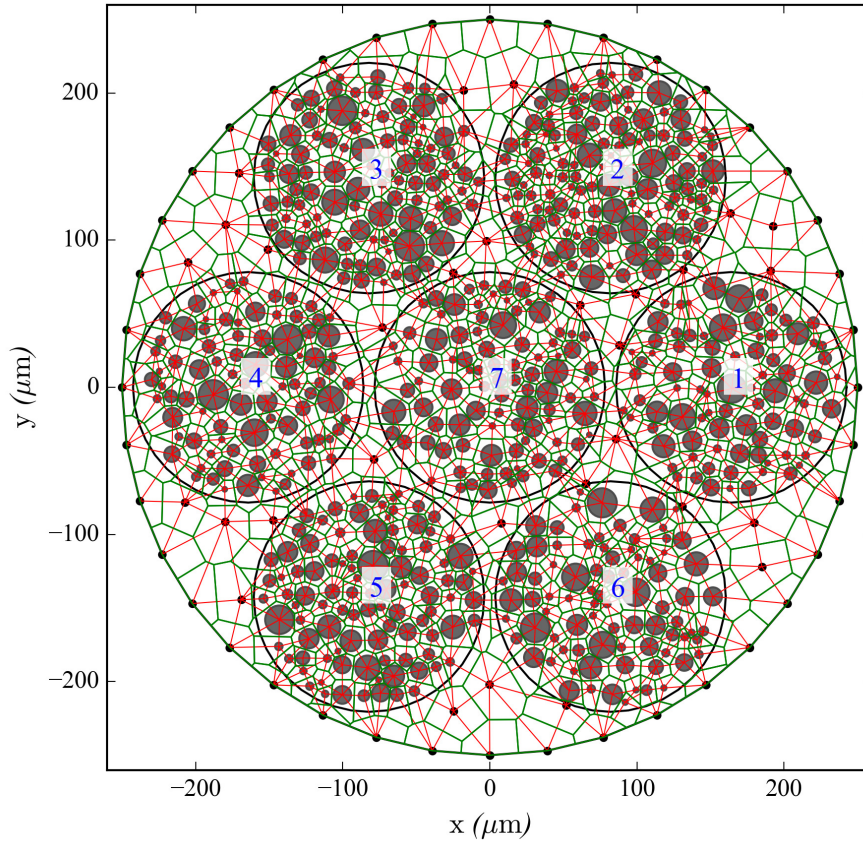
Figure 5.2: Discretisation of a nerve model's cross-section blue(Nerve 1blue) in poly-
gons using a power diagram (green). Grey circles indicate the locations and diameters
of the axons, which are embedded in seven fascicles (the blue labels number the fasci-
cles). Black dots indicate points resulting from a Delaunay triangulation to discretise
the epineurium, indicating the locations of NAELC. The dual Delaunay triangulation to
the power diagram representing the connections with transverse resistors is represented
with solid red thin segments. Note that while the nerve's contour contains NAELC, the
fascicles contours do not. This model is used in simulations in this work (see Nerve 1 in
Fig 5.1 and Table 5.1).

$a_{k,i}$ is the cross-sectional area of tissue type i present in polygon k as a fraction of
the total extracellular area enclosed by the polygon (this is, scaled over $A_{E,k}$). In
theory, in this study, this sum is made over two types of tissue: endoneurium and
epineurium ($i \in \{En, Ep\}$). However, as mentioned above, we used the same value
of ρ_i^L for both. Nevertheless, this equation serves for any number of tissue types the
modeller wishes to include.

The resistance per unit length of each extracellular cable is then:

$$r_{L,k} = \frac{\rho_k^{Lu,L}}{A_{E,k}}, \qquad (5.2)$$

where $A_{E,k}$ is the aforementioned extracellular cross-sectional area of the polygon. If $A_{P,k}$ is the total area of the polygon and D_k is the diameter of fiber k, $A_{E,k}$ is given by:

$$A_{E,k} = A_{P,k} - \pi D_k^2 \tag{5.3}$$

If the polygon does not contain a fiber but a NAELC,

$$A_{E,k} = A_{P,k} \tag{5.4}$$
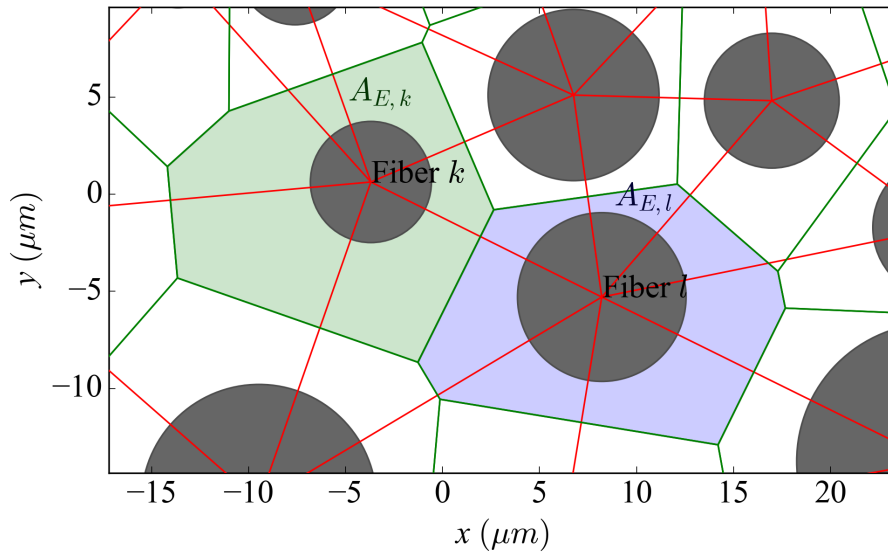
Figure 5.3: Cross-sectional view of a random fascicle including the tessellation (green lines) and the triangulation (red). Additional information is used to display the details of the connection between two randomly chosen nearest-neighbouring fibers k and l. The coloured areas represent the extracellular area assigned to the calculation of the longitudinal extracellular resistance of each fiber (green for fiber k and blue for fiber l).

Transverse resistances of the RN Sides shared by adjacent polygons in the power diagram represent electrical contacts between the polygons (which is equivalent to surface contacts between polygonal prisms because the polygons are extruded along the z-axis) and determine which cables or fibers are coupled by transverse resistors. The weighted Delaunay triangulation dual to the power diagram [180] (red lines in Figs 5.2 and 5.3) indicates these connections. The resistance of such a contact depends directly on the distance $d_{C,(k,l)}$ between the centers of the two circles and inversely on the product of its segment's length $s_{k,l}$ (green segment joining the

two coloured polygons in Fig. 5.3) times its length along the z-axis $c_{k,l}^n$. The value
of the n-th extracellular transverse resistor between two fibers follows Eq. 4.8, with
the addition that the transverse resistivity is in this case also a lumped value:

$$R_{T,(k,l)}^n = \rho_{k,l}^{Lu,T} \frac{d_{C,(k,l)}}{c_{k,l}^n \cdot s_{k,l}} \tag{5.5}$$

The transverse component of the lumped resistivity $\rho_{k,l}^{Lu,T}$ is computed in the
following way:

$$\rho_{k,l}^{Lu,T} = \sum_i b_{k,l}^i \cdot \rho_i^T, \tag{5.6}$$

where $b_{k,l}^i$ is the distance crossed by the resistor within the tissue of type i, scaled
over $d_{C,(k,l)}$.

For merely geometrical arrangements, the perineurium is modelled as an in-
finitely thin layer, so it does not affect the calculations of r_L. Yet its nominal
thickness was not ignored for the calculations of the resistances of transverse re-
sistors crossing it, since its thickness is known to affect the results of stimulation
[132]. Its thickness was added in the calculation of the corresponding $R_{T,(k,l)}^n$ in the
following way:

$$R_{T,(k,l)}^n = \frac{1}{c_{k,l}^n \cdot s_{k,l}} \left(\rho_{k,l}^{Lu,T} \left(d_{C,(k,l)} - n_P \Delta_P \right) + \rho_P^T n_P \Delta_P \right), \tag{5.7}$$

where n_P is the number of perineurial membranes crossed by a resistor (1 between
an axon and a NAELC, 2 between two axons in different fascicles, 0 otherwise).

NAELC are always discretised in regular intervals, using the shortest internodal
length in the nerve for $c_{k,l}^n$. Transverse resistors connecting a NAELC and a fiber
are located on the nodes of Ranvier of the fiber.

5.2.4   Nerve's External Environment and Electrodes

The nerve was centered along the axis of a larger cylindrical container (z-axis) filled
with a saline bath. The surface of this larger cylinder was connected to ground

(zero potential), as done before by [7]. For modelling purposes, this can be used as a sufficient representation of the animal's body surrounding the nerve, assuming that in a real experiment, the ground would presumably be found on a distant location, right outside the animal's body or in the Central Nervous System.

This model framework allows the user to define cuff electrodes for stimulation and recording. We used cuff electrode models based on [188]. These electrodes are 4.25 mm long and contain four rings separated by 750 μm each. Each ring contains four pads, placed at 0°, 90°, 180° and 270° with respect to the x-axis. More details about the geometry and materials of these electrodes can be found in [188]. In this work, the cuff model was simplified by leaving only one ring in the center, and by adapting the inner diameter to the nerve model diameter.

The methods used to simulate stimulation are explained in more detail in Chapter 4.

5.3 Results

5.3.1 Field generated by the electrode

In this subsection, we represent the extracellular potential field, v_E, generated by the pulses exerted by one active pad on a cuff electrode on a nerve model. For this and the following subsection, we used a 1 cm long nerve (model named Nerve 1 in Methods) surrounded on part of its length by a stimulating cuff electrode that provided one square stimulating pulse. The cuff model was centered at the middle of the nerve's length. The 0° pad (blue diamond on Fig 5.4) injected a square pulse with a duration of 200 μs and an intensity of -3 μA. The fiber diameters were randomly chosen following a distribution based on [186], although the diameters were bounded between 3 and 20 μm. No fibers thinner than 3 μm were taken into account, since low diameter fibers have short internodal lengths and would increase the RN resolution, along with the simulation's computational cost. Considering that the fields obtained here are used in the stimulation studies in the next subsection, it is important to remark that, in order to save computational resources, the RN was connected only in the region under the cuffs. This was considered as a safe assumption since the fields far from the stimulation point were too small to play a relevant role during stimulation. The rest of the nerve's length was left in order to avoid the effects of sealed-end boundary conditions of the axons.

A cross-sectional view of the absolute value of the field v_E over the nerve can be seen in Fig 5.4, and three samples of its longitudinal profile (z-axis) can be seen in Fig 5.5. The field, which is negative across the entire domain, has a minimum value

of -2413.62 mV at the location of the active pad, but its absolute value is lower than
1000 mV over the rest of the domain. The field can be seen to decrease with the
distance from the active pad both in Fig 5.4 and in Fig 5.5. At the ends of the cuff,
the field is effectively zero (Fig 5.5). The field shown in Fig 5.4 presents deviations
from a smooth relationship with distance on the x-y plane, at points where $|v_E|$ is
lower than it should be expected for such a smooth relationship. This is due to
the conductive axoplasm of the axons, which lowers the impedance to ground on
their locations. This effect of the presence of the axons is not visible in simulations
where the presence of these is merely accounted for by an anisotropic endoneurium's
resistivity tensor.

5.3.2   Effects of ephaptic coupling on axon recruitment and selectivity

In order to study the effects of EC on axon recruitment and selectivity during
stimulation, we tested the differences in stimulation results from simulations with
and without EC. For this, we used the model Nerve 1 under the same conditions
as the previous subsection. Two sets of simulations were run for this study: one
including EC (labeled as SEC; results in Fig 5.6 for a pulse of -2 μA) and one
not including it (SNOEC). SEC simulations were run by modelling the nerve as
a RN. SNOEC simulations were prepared in the following way: The axon models
are the same as in SEC. However, there is no RN interconnecting the axons, and
therefore, no explicit modelling of any extracellular tissue or device. In order to
model stimulation, the extracellular fields along all the axons in SEC were captured
at the time step following the start of the stimulating pulse, and then used in SNOEC
as the extracellular stimulating field on the axons.

In order to quantify the effects of stimulation, we measured the axon recruitment
in response to the stimulating pulses. The presence of APs on each fiber was detected
when the transmembrane potential of the fiber (v_m) reached 15 mV. This AP
detection method was used throughout this study. We ran pairs of simulations
{SEC, SNOEC} for current pulse amplitudes ranging from -0.2 to -4 μA, with
steps of -0.2 μA.

The method used for the stimulating fields in SNOEC ensures the axons are
stimulated with the same field coming from the electrodes in SNOEC and SEC.
However, results vary substantially between both cases . The response of the axons
to the stimulating fields in sEC is faster than in SNOEC (Fig. 5.7, left panel, which
shows the results for a pulse of -2 μA). Also, the recruitment in SEC is, for all
fascicles and pulse amplitudes, higher than in SNOEC (Fig. 5.8). Recruitment
ratios are only equal between SEC and SNOEC in trivial cases: when recruitment
is zero and when it is saturated (i.e., the maximum number of axons in a fascicle
has been recruited) in both simulations. This is due to the endogenously generated
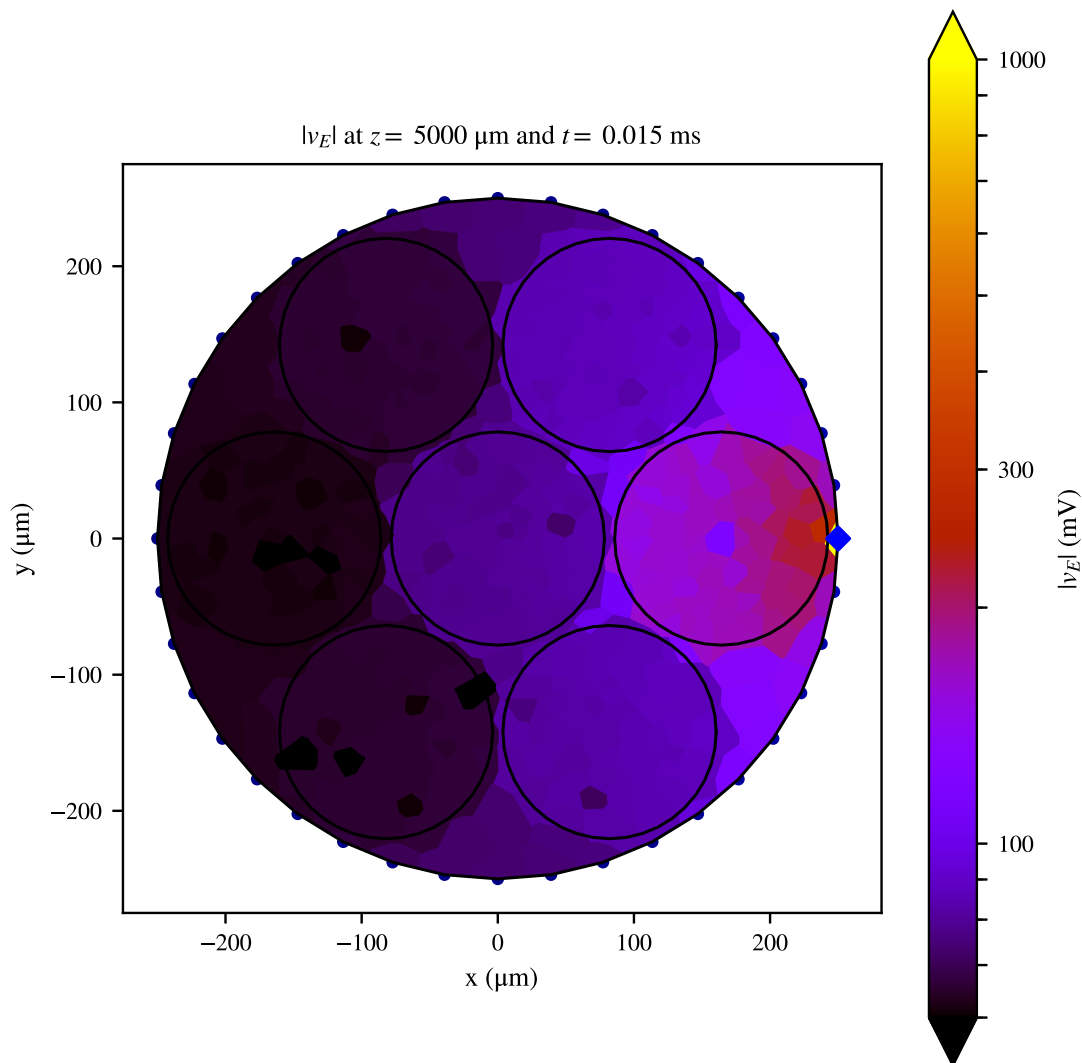
Figure 5.4: Cross-sectional slice of the extracellular field generated by the electrodes over the model Nerve 1 at the middle of its length ($z = 5000$ μm), where the stimulation pad (blue diamond) is situated, and at the time step following the onset of the stimulating pulse. The RN assumes the field is constant over the surface of each tessellation polygon. The contours of the nerve and the fascicles are indicated with a black solid line for better identification. Axons are not shown in this figure. Although the maximum value of $|v_E|$, situated at the active site, is 2413.62 mV, the colorbar was cut at 1000 mV in order to facilitate the visualisation of the spatial details of the field.

field (or ephaptic field), which adds up to the artificial field from the electrodes and generates an increased depth of the total stimulating field over all axons (see Fig 5.7, middle and bottom right panels, where the ephaptic field and membrane voltage are represented for a random axon under a stimulating pulse with amplitude
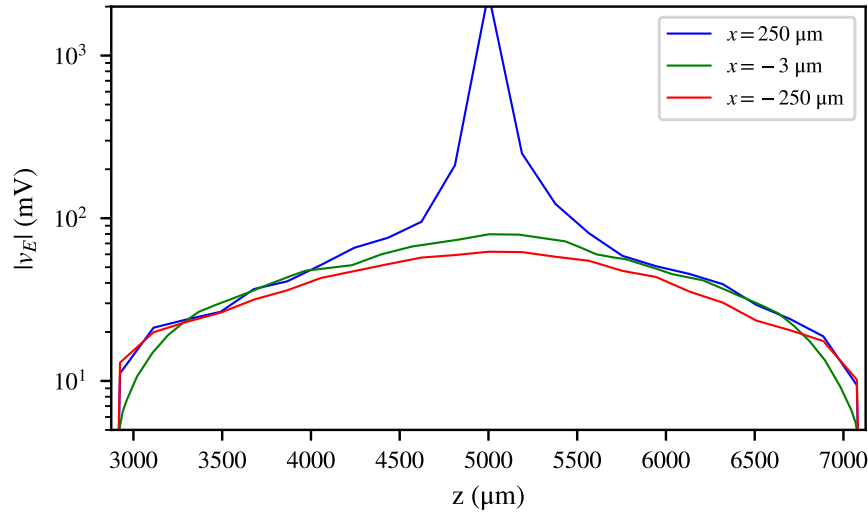
Figure 5.5: Longitudinal profile (z-axis) of the extracellular field (absolute value,
log scale) generated by the electrodes over the model Nerve 1, along the length of
the cuff electrode, at three different points on the x-y plane: the position of the
active pad ($x = 250$ μm, blue), the position of the central-most axon in the nerve
($x = -3$ μm, green), and the farthest point from the active pad ($x = -250$ μm,
red). All three points are located at $y = 0$ μm.

-2 μA). The ephaptic field activates axons by pushing them over their thresholds,
where the electrode fields are not enough. In the simulation with a stimulating pulse
amplitude of -2 μA, this ephaptic field is deeper than -50 mV on average (right
bottom panel), although it reaches depths in the range between -60 and -80 mV
for some axons. There are no axons for which this field is positive throughout the
duration of the stimulating pulse. It does, however, become positive after the pulse,
likely due to the refractory periods of the axons.

This model contains 658 axons, most of which are firing APs at similar times
in SEC for strong enough stimulating pulses. From a MF model perspective, this
means that the individual contribution to the ephaptic field from each axon might be
in the order of, at least, 10 μV. In cases where an electrode is set to selectively target
a group of axons, the collective influence of these on the ephaptic field may be lower,
and therefore, the effects on axon recruitment may be lower as well. Nevertheless,
we can tell that the magnitude of the effect of EC on the axons response is big
enough to be taken into account unless working with much smaller groups.

The position of the active pad with respect to Fascicle 1 was assumed to be the
optimal for maximising the selectivity for this fascicle. We studied the variation of
the selectivity for Fascicle 1 with the presence of EC. We used the inter-fascicular
selectivity provided by [179], and calculated its value for the whole range of stimu-
lating pulse amplitudes. Results (Fig 5.9) indicate that EC, in the case of Fascicle
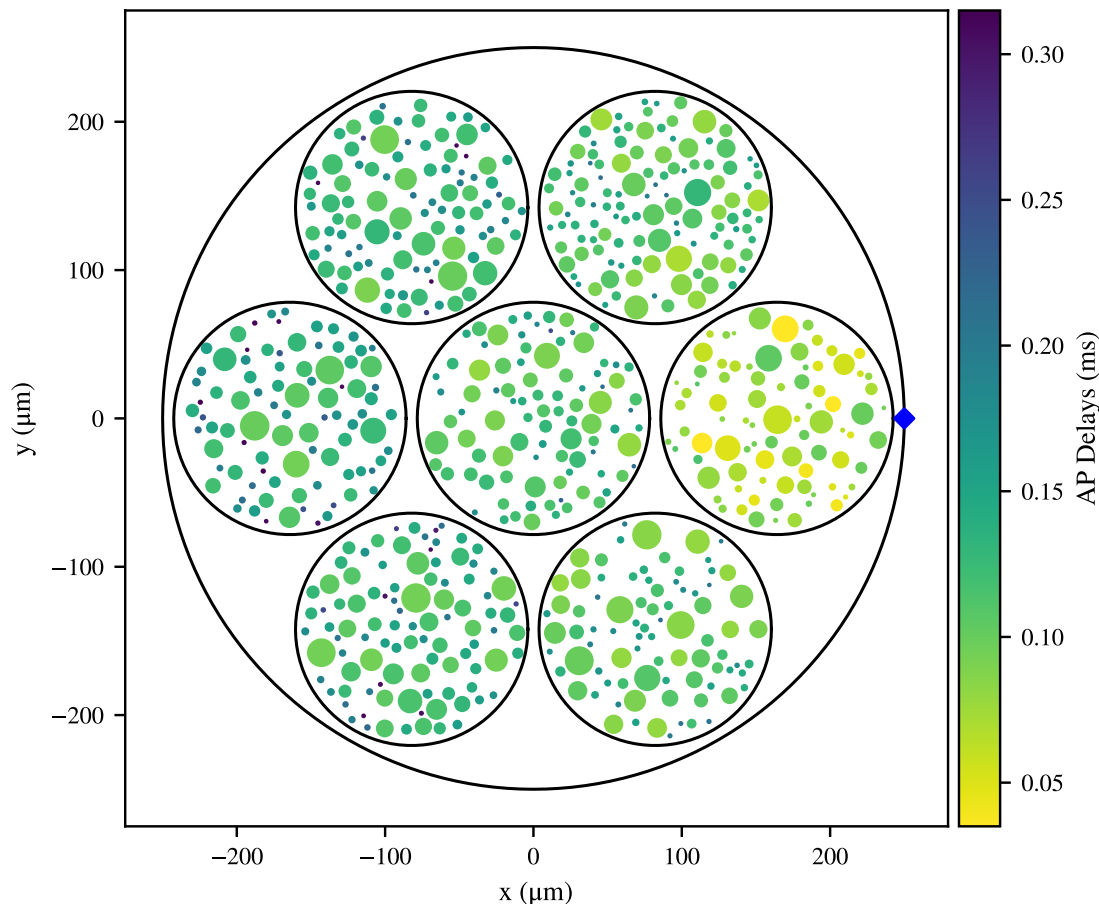
Figure 5.6: Activation map of the Nerve 1 model which contains 7 fascicles. The stimulation pad position is marked with a blue diamond. Colours represent the time (delay) between the start of the stimulating pulse and when the transmembrane potential of each fiber (v_m) reaches 15 mV (value chosen for the detection of an AP).

1, has the effect of both narrowing the range of pulse amplitudes for which the selectivity is optimal and shifting the peak of the selectivity by approximately 1 μA. Also, the maximum selectivity that can be reached is lower than in SNOEC. This can be understood thanks to the increase in axon recruitment in all other fascicles for pulse amplitudes from -0.6 μA and stronger. Recruitment in Fascicle 1 is always higher than in the other fascicles thanks to its proximity to the active pad, and it reaches its maximum recruitment sooner. Therefore, selectivity for Fascicle 1, while using only the current active pad, cannot be negative. The possible effects of EC on the selectivity of other fascicles, however, may be different, since their optimal selectivity configurations vary.

One last observation that can be made on the activation map (Fig. 5.6) is that the AP delays display a degree of independence from fiber diameter. This is especially obvious for Fascicle 1, and slightly visible for its surrounding fascicles; on fascicles distant from the active pad, AP delays seem to depend more closely on fiber
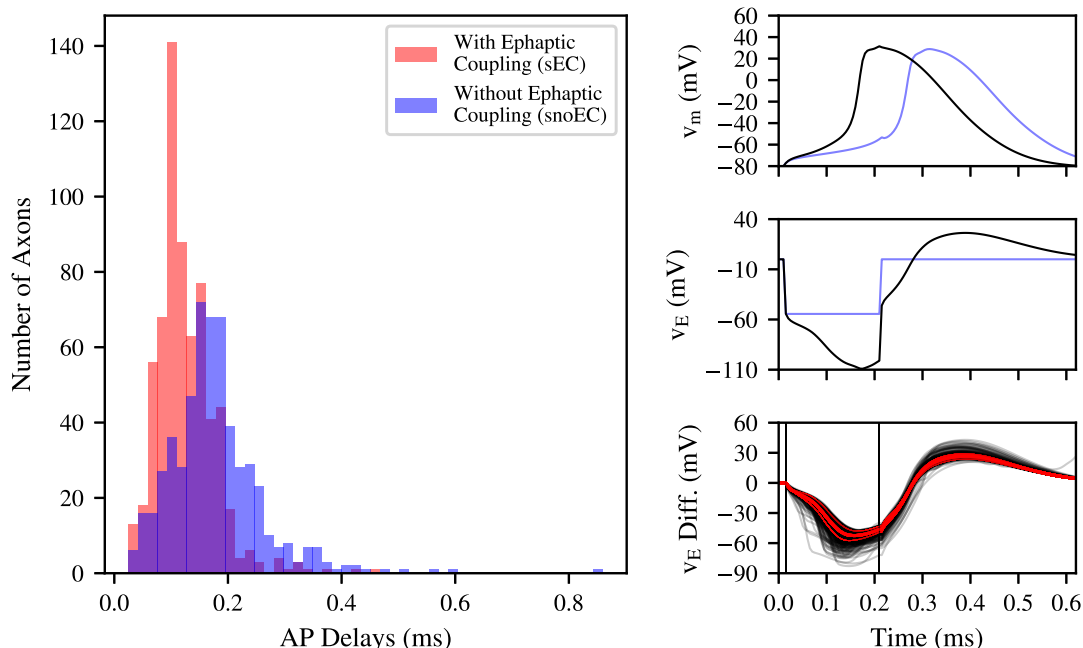
Figure 5.7: Left: Histogram representing the delays of the APs in the simulations (first
AP on each axon for all the axons) with EC (sEC, blue) and without EC (snoEC, light
red). Right: For one particular axon, randomly chosen as an example, middle panel
shows the time evolution of the extracellular potential (v_E) on the node of Ranvier
lying closer to the electrode's active pad for both simulations (blue for SNOEC, black
for SEC), and top panel shows the time evolution of the transmembrane potential (v_m,
same location and legend). Note in this panel how the EC produces an AP earlier than
in SNOEC. Bottom panel: Time evolution of the endogenous fields ($v_E^{SEC} - v_E^{SNOEC}$)
for all the axons (thin black lines) on the nodes lying closer to the active pad. Red lines
indicate the mean of these fields (averaged for each time step, middle thick line) with
their standard deviation (thin lines). The two black vertical lines indicate the start and
finish of the pulse.

diameter, with smaller fibers firing later. This apparent dissociation between fiber
diameter and AP delay is due to i) the misalignment between the nodes of Ranvier
of the fibers and the active pad, as seen in Chapter 4, and ii) the effects of EC: all
fibers are under a slightly different ephaptic field, and also respond differently to it
due to their diameters.

5.3.3   Effects of Ephaptic Coupling on Propagation

We intended to study the effects that EC may have on propagation of APs. For this,
we used the same approach: we ran a pair of simulations, SEC and SNOEC, on the
same model, using the same stimulation protocol, and their results were compared.
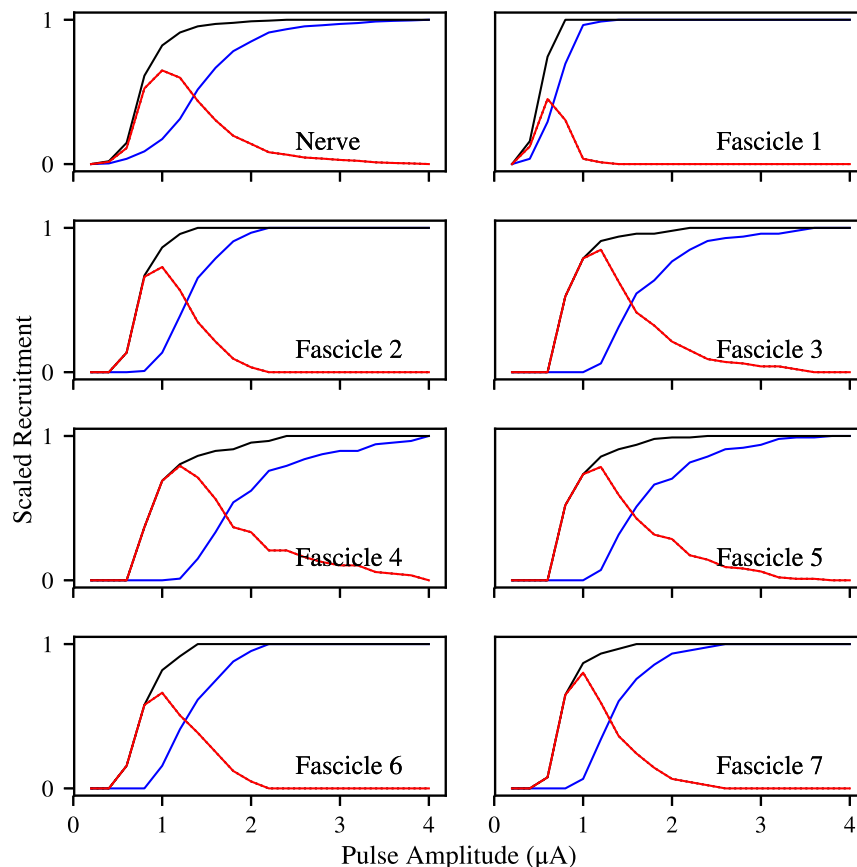
Figure 5.8: Scaled recruitment curves for all the fascicles and the whole nerve. Black lines correspond to SEC and blue lines correspond to SNOEC simulations. Red lines show the difference between the two. The horizontal axis indicates the pulse amplitudes exerted on the electrode's active pad. Pulses are always negative in the simulations, but they have been represented as absolute values in this figure for clarity.

Propagation with EC needs to be studied along a longer model than Nerve 1, and for a longer period of time. Increasing the length of Nerve 1 highly increases the computational demands of simulations, so we instead used a thinner mono-fascicular nerve model: Bundle 1 (see Methods), which is 6 cm long and has a diameter of 100 μm. No perineurial tissue was taken into account. In order to increase the effects of EC, the epineurial walls of the bundle were given the same resistivity as the cuffs, thus providing a virtual quasi-isolation from the surrounding saline bath. The bundle's ends were not covered by this isolating surface, so the tissues were in contact with the paths to ground on those two surfaces.

Bundle 1 contains 39 axons whose fiber diameters follow a continuous and uniform distribution, in the range from 9 μm to 10.9 μm, and in steps of 0.05 μm. This range was chosen so that the conduction velocities (CVs) did not vary drasti-
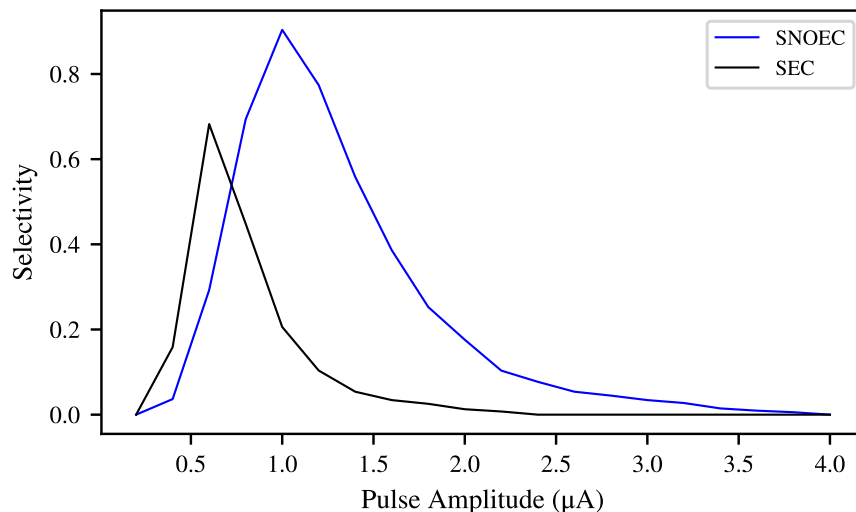
Figure 5.9: Selectivity for Fascicle 1 for the various pulse amplitudes in use.

cally and thus to facilitate the possibility of signal locking between fibers of similar diameters.

An intracellular current injection was given to all axons on their first node of Ranvier, consisting of one square pulse of -10 nA at $t = 0.01$ ms with a duration of 10 μs.
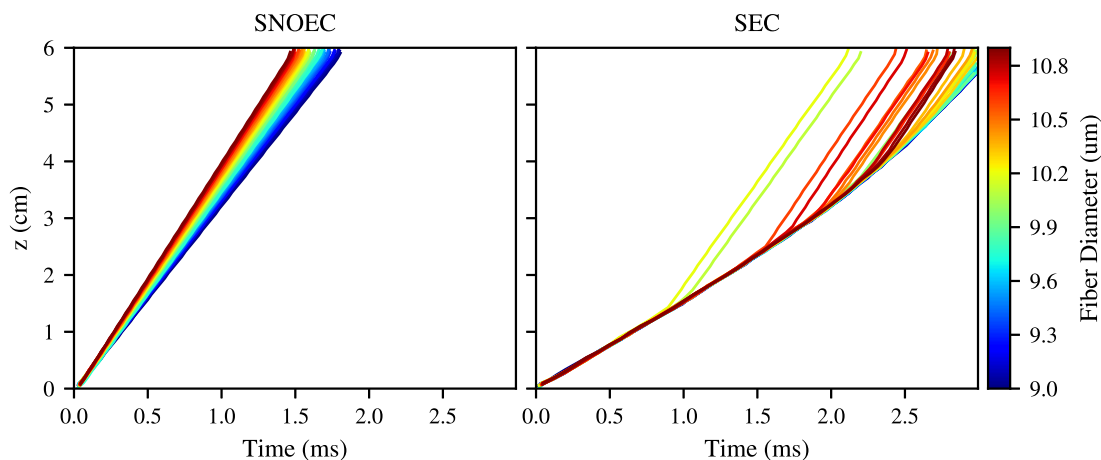
Figure 5.10: Trajectories of the axons on the z-t space for SNOEC and SEC. Each trajectory is coloured according to its corresponding fiber's diameter. These results correspond to Bundle 1.

Results (Fig 5.10) show the presence of an effective lock of the APs. However, it is also apparent that this lock is unstable. A certain grouping of trajectories is visible during the first 0.5 to 1 ms of the simulation. This grouping turns into an

effective lock during the first 1 ms in SEC. From around this point onward, APs
tend to detach from the main group along time and increase their CVs. The first
APs in detaching do not belong to the higher diameter fibers, but rather, to mid-
to-high diameter fibers. These are then followed by higher diameter fibers. As a
first hypothesis to explain this observation, this could be due to the loss of a bond
between the higher and lower diameter fibers when the mid-to-high diameter fibers
depart. However, the causes of this generalised detachment of trajectories from the
main AP lock can be numerous and complex. The weakness—or instability—of the
EC between fibers of different diameters could be explained by the differences in the
CVs they tend to have in the absence of EC, which would act against locking their
APs. The observation that these detachments occur after a certain distance along
the z-axins suggests the presence of factors that trigger the separation of APs when
certain conditions are met. One of this is, potentially, the variation along the z-axis
of the alignment between nodes of Ranvier of different axons, which would modify
the strength of their EC.
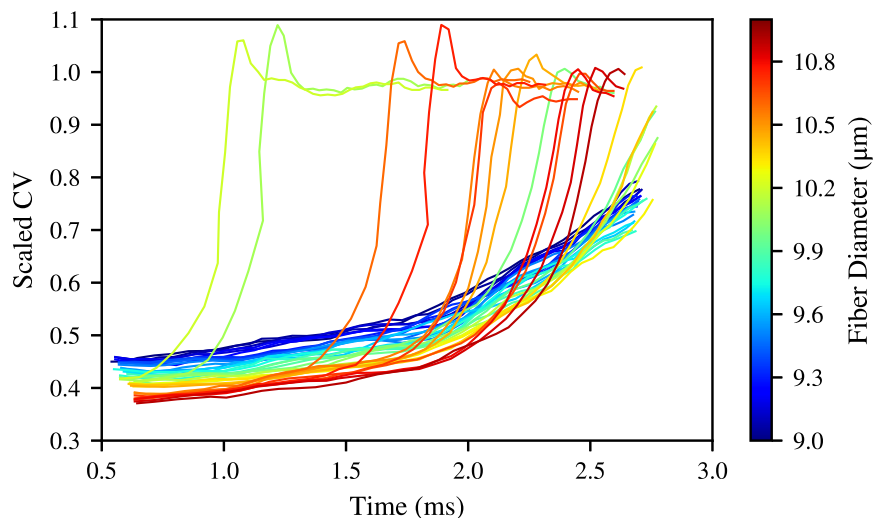
Figure 5.11: CVs of the fibers in the simulation SEC, scaled over their respective values
in SNOEC, which are stationary. CVs are obtained from a linear regression on the (t,
z) points of the trajectories, using a window of 11 nodes or Ranvier, so the curves do
not span the whole simulation. Error margins are not shown in order to aid a clearer
visualisation. These data correspond to Bundle 1.

The CVs of the fibers can be directly related with the presence of their APs in
or outside the AP lock. APs that separate from the group quickly reach the CVs
they have in the absence of EC (Fig 5.11, left). At the beginning of the simulation,
when all the APs form a locked group, they all have CVs of less than half of the
values they have in SNOEC. These CVs in the lock, however, gradually increase
along time as APs separate from the lock.

The same simulation sets were run for Bundle 2. Bundle 2 follows a natural
diameter distribution (starting from 3 μm), and the bundle diameter is larger than

in Bundle 1 in order to facilitate the presence of more axons, and hence, a smoother
diameter variability within the model. Results (not shown) indicate much weaker
or nearly nonexistent AP lockings. This is in contrast with the apparent, although
unstable and temporary, locking seen for Bundle 1. This is probably due to the wide
range of different diameters in Bundle 2. However, the general slowdown of the CVs
for higher levels of EC is present, especially for higher diameter fibers. From these
results, it is apparent that the strength of the effects of EC on the propagation of APs
is highly dependent on the diameter variability between the fibers in a bundle. This
implies that the effects of EC on propagation might be weak, and even irrelevant, in
proximal sections of nerves, where fiber diameters are homogeneously distributed,
but they could be stronger, and forming effective lockings, in more distal regions,
where fibers may be clustered by size.

5.3.4   Dependence of the Ephaptic Interactions with Distance

We ran two simulations in which we stimulated one random axon in each with
an internal current injection and observed the response of the other (unstimulated,
meaning they were not artificially stimulated) axons transmembrane potentials. We
compared these responses with the distance from the artificially unstimulated axons
to the artificially stimulated axon.

In this study, we used two models in order to study different scenarios, which
differ in the presence of fascicles separated by perineurium:

- Bundle 3 is a 3 cm long, 250 μm diameter, mono-fascicular nerve filled with
  20 μm diameter fibers. This model has a larger diameter than Bundle 1
  because we wanted to obtain a characterisation of the strength of EC across
  a wider cross-sectional distance. As in the case of Bundle 1 and Bundle 2, no
  perineurium is considered. Also, in this and the model below, the epineurial
  walls of the models were strongly isolated from the saline bath.

- Nerve 2 uses the same epineurial and perineurial profile as Nerve 1—it has
  the same contours for the nerve and the fascicles cross-section—but it is filled
  exclusively with 20 μm diameter fibers, as Bundle 3, and is also 3 cm long.

Results for Bundle 3 are shown in Fig 5.12(a), and results for Nerve 2 are shown
in Fig 5.12(b). The responses of the unstimulated axons in Bundle 3 follow a clear
decreasing trend with the distance from the stimulated axon. The irregularities can
be attributed to the limitations of the RN at modelling three-dimensional space and,
to a lesser extent, to inter-axonal ephaptic interactions between unstimulated axons.
Nevertheless, the total change of the responses along 150 μm of distance does not
vary much above 8 μV. This suggests the acceptability of the application of a MF
assumption in cases like this model, since variations on v_m of this order of magnitude
would not imply big differences in the results from MF and distance-based EC
simulations. It is important to bear in mind, however, that this order of magnitude
in the unstimulated axons responses is due to the activity of one stimulated axon
only. The combined effect of more axons carrying APs would increase it.

The responses in Nerve 2 are larger, of the order of 0.2 mV inside the fascicle
where the stimulated axon is, and approximately between 0.08 and 0.12 μV for the
other fascicles. This is in rough agreement with the order of magnitude estimated
in the second subsection of the Results if we have in mind that the nerve's length
affects this magnitude (a longer length increases the resistance to the saline bath or
ground). Axons belonging to different fascicles are easy to identify in Fig 5.12(b),
since the isolation provided by the perineurium makes the response of all axons inside
each fascicle similar between them but notably different to the responses in other
fascicles. The order of magnitude of these results could mean that the responses
would be in the order of several mV should there be more stimulated axons, as
seen in Fig 5.7. However, the intrafascicular variations are, at least, one order of
magnitude lower. This would support a local MF choice for each fascicle. However,
this choice would be incompatible with modelling inter-fascicle ephaptic interactions
or fields from extracellular electrodes.

These observations, especially when considering the activity of many axons tak-
ing place in simulations, support the importance of choosing a distance-based model.

5.4   Discussion

The model framework developed in this study permits simulating the stimulation
and propagation from a peripheral nerve trunk in a single run. The model introduces
a new method to build nearest-neighbour electrical interactions between fibers which
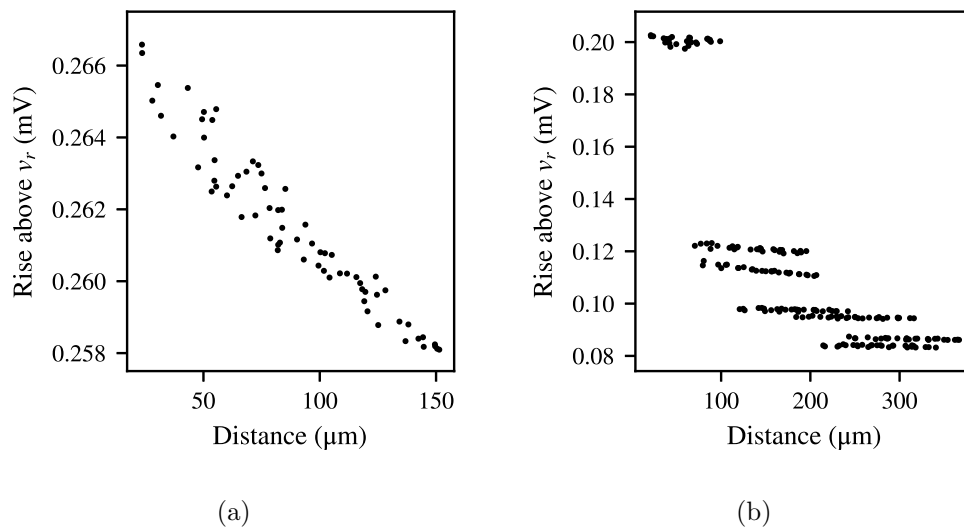
Figure 5.12: Maximum variation of v_m above v_r (resting potential, -80 mV) at the third node of Ranvier for all the unstimulated axons, represented against the distance to the stimulated axon. (a) Bundle 3; (b) Nerve 2, which contains seven fascicles separated by a perineurium, same as Nerve 1.

builds up a whole electrical network for the nerve. This network simulates the fields coming from electrodes and from the fibers, thus enabling the integrated simulation of EC.

This model has the advantage of being able to simulate the interactions between fibers and electrodes as well as with all other fibers in a nerve, where the nerve may have any reasonable shape, contain any number of fascicles separated by perineurial membranes and randomly located fibers of various diameters. However, running this with a reasonable level of computational efficiency has only been possible, so far, by accepting a series of assumptions and limitations:

- Axons are cylindrical and use a 1D cable equation. The effects of the transverse components of polarisation around the membranes are not regarded. Although these effects have been found to play no major role in myelinated axons when studying stimulation [117], no study has been done on their influence on ephaptic interactions of two very nearby cells. Only [72] provide simulation results which could provide clues on this, yet it is not their main focus.

- Axons are straight. However, tortuosity is known to affect recordings [110]. Also, it could affect EC in a way that might be highly dependent on whether a MF or a distance-based approach is used.

- Electrical currents through space are only modelled along the z-axis and on the x-y plane. A FEM scheme could simulate these currents more accurately.

- No capacitive properties have been regarded for any extracellular tissues since
  we used the QS approximation.

- The contact surface impedance of the electrodes was not modelled. Although
  this parameter represents an influencing factor on the resulting fields from
  stimulation, and, eventually, on the axons response to stimulation, the elec-
  trodes in this work are regarded as current point sources, and the stimulation is
  current-controlled, which reduces the need for modelling this parameter [147].

- Unmyelinated axons are not regarded in this model. Although of low relevance
  for our purposes, a more complete model should take them into account.

- Fibers thinner than 3 μm in diameter were not included in this work. This has
  been done in order to save computational time, since low diameter fibers have
  short internodal lengths, and therefore, increase the RN's resolution. However,
  this could affect results since fibers below this size are present in nerves, and
  could still affect EC.

- The largest nerve model we have used in this work has a diameter of 500
  μm, and contains fascicles with a diameter of 156.67 μm. These numbers are
  smaller than the known physiological ranges for human limb peripheral nerves
  where stimulation is typically studied [184, 185]. Also, the number of axons
  is lower, not only as a result of this, but also because fiber packing ratios are
  generally lower than physiological values. The computation time of the RN is
  highly sensitive to increasing the number of axons in the model. Hence, using
  physiologically more plausible numbers of axons would have been unattainable.

Further improvements on some of the limitations of this model can be carried
out in further work. These range from increasing the variety of axon models in use,
to including capacitive properties of tissues and electrode impedance, and adding
tortuosity. The latter could be achieved by dividing the nerve's length in layers,
each layer having its particular arrangement of fiber positions according to their
tortuosity and hence, having its particular power diagram.

Computational cost is generally a drawback for simulations with this model. Cal-
culations over a RN are expensive and this limits the size and resolution that the
model can have in order to get reasonable simulation time investments. Parallelisa-
tion of the RN could not be done, to the best of our efforts, without compromising
numerical stability. This also compromises the results of simulations with EC, since
small changes in the RN resolution or arrangement have large effects on EC.

Laguerre tessellations are used for building nearest-neighbour connections be-
tween fibers. This method is used for the study of granular structures, like poly-
crystals and foams [189–191], whose field of application is strikingly different from
the applications of this work. Yet, it proves to be a convenient method for modelling

these connections, since it provides a general tool which serves any possible packing of cylindrical fibers. Prior to this work, no similar approach has been found for this purpose. Point or line-source approximations [183] can be used for this. However, even their adaptations to anisotropic media neglect the complexities the nerve may have outside each individual fiber, which can turn into an inaccurate modelling when these complexities are important. Also, using the equations from [183] in our case of mutual EC between many fibers may lead to numerical instability, as seen in [177]. Furthermore, no study has been found so far using any distance-based approach for a similar type of nerve model.

This has allowed us to simulate stimulation and propagation in a somewhat realistic nerve model. From the numerical simulations presented here, we have found that EC drives an increased axon recruitment (compared to simulations that neglect EC) during stimulation with a cuff electrode. This increase in recruitment has a maximum of 64.9% for the whole nerve, and it is above 60% for all fascicles, except for Fascicle 1 (Fascicle 2: 72.9%; Fascicle 3: 84.8%; Fascicle 4: 79.3%; Fascicle 5: 78.6%; Fascicle 6: 66.3%; and Fascicle 7: 80.2%). Fascicle 1 has a maximum recruitment increase of 45.1%. For all the former fascicles, this maximum seems to be centered around a stimulating pulse of -1 μA, and around -0.6 μA for Fascicle 1. These high peak levels in recruitment increase are mostly resolved from the fact that, for pulses near the peak, EC fires APs in a large number of axons that lie under their thresholds in simulations without EC. Recruitment difference decreases for stronger (i.e., more negative) pulses, even when stimulation has not reached its maximum in SEC, because axons start activating in SNOEC. We have observed how axons interact between them during stimulation, and although the strength of the individual influence from one axon is generally weak, their collective interactions are determinant to whether axons lying close to their thresholds fire an AP or not. We used a configuration where axons of different diameters are uniformly spread across the nerve's cross-section. This is representative of proximal sections of nerves. However, more distal sections present clustering of fiber types and diameters. This is known to affect the spread of activation thresholds within a fascicle [192], so further studies would be necessary to assess the validity of these findings in such configurations. The possibility of AP firing due to EC during propagation has not been studied in this work. In the study of the dependence of EC with distance, the observed rise in v_m of axons was due to the activity of only one neighbouring axon. It is inferred, from the orders of magnitude under consideration, and from the observed ephaptic fields in the stimulation study, that the simultaneous activity of many more axons could drive unstimulated axons to fire APs. Although studying this possibility is outside the scope of this present work, it is proposed as further work.

By following these considerations, EC should be taken into account in simulations of axon recruitment with electrodes, but if it is to be neglected in favour of lower computational costs, it should at least be held in mind that neglecting it may lead to certain inaccuracies in the results. Ideally, such a study lacking EC could

consider these effects by applying a modifying function to recruitment numbers after
a simulation.

We have observed how, in this work, certain already existing findings [64–66]
about the effects of EC on few fibers during propagation—CV reduction and AP
locking—also apply for bundles with more numerous and heterogeneous fibers. How-
ever, these effects are strongly conditioned by similarity between fibers and com-
promised by heterogeneity to the point of losing their validity when assumptions of
homogeneous fibers are not used. The results of this work also have assessed the
validity of choosing a MF model: although physically not accurate and unsuitable
for studies involving extracellular electrodes, it can be justified for others, especially
for small mono-fascicular nerves or locally within fascicles.

5.5   Conclusion

A detailed computer model of a peripheral nerve trunk has been developed, which
involves the implicit coupling of intra- and extracellular electrical activity in a single
simulation. It conveniently uses NEURON with a Python framework that handles
all the geometrical methods and wraps the whole model. Specific experimental
data for validation would be desirable. However, the model succeeds in behaving
within physiologically expected ranges. We hope that this new method provided here
brings researchers to use it further in order to study more complex cases of ephaptic
interactions, and that the results from this study serve to add more knowledge on
the effects of EC in bundles of fibers with different sizes, eventually to determine
the extent to which modelling EC for studying sensory feedback is necessary.

Chapter 6

Overall Discussion

This work provides a modelling approach for peripheral nerves and their interfaces with electrodes for artificial stimulation and recording. The aim is to facilitate the creation of realistic and functional models of the PNS for optimising designs of stimulating neural interfaces for sensory feedback restoration. In this work, there is a particular interest in modelling ephaptic coupling (EC), one aspect of the electrical activity of neurons, but specifically of myelinated axons, which is generally disregarded but has potential to play a functional role, and for which experimental evidence of its presence in the PNS exists [67]. Therefore, its inclusion in models should be reconsidered.

EC has been studied in various ways in previous literature. Typically, EC is modelled using a low number of cells [11, 65, 72] or is normally studied for cells of other parts of the nervous system [70]. For bundles of fibers, restrictive assumptions such as the MF model or very organised axon packings are used [65, 66, 68]. In this work, we have focused our efforts in defining the electrical interactions between any two neighbouring and parallel myelinated axons, regardless of their size and position, and have extended this interaction model to any possible packing of parallel axons.

A model has been developed that allows the definition of the anatomy of a nerve trunk or fiber bundle and its accompanying elements—electrodes and container—in order to run simulations of its activity. The model includes a Resistor Network (RN) which is built based on a weighted Voronoi tessellation of the elements in the bundle, including both nerve fibers and tissue elements (referred to as NAELC when they are regarded as longitudinal resistive elements along the z-axis; see Chapters 4 and 5). This RN defines the electrical connections through extracellular tissue between fibers and tissue elements (NAELC), creating a volume-conductor representation of the whole bundle over which all relevant electrical fields (generated by electrodes and by endogenous neural activity) are computed. The RN creates an EMI-type model of the whole nerve trunk or bundle model, in which all the extracellular and

intracellular fields, as well as the neuronal transmembrane currents, are solved at every time step of a simulation. The RN has been validated on theoretical grounds, comparing its results in simple simulations to analytical results and outputs from FEM simulations (see Chapter 4).

The flexibility of the model parameter inputs and the RN configuration allows defining nerve trunks with virtually any physiologically plausible anatomical shape, tissue presence, and cylindrical fiber packings, including any location and diameter configurations, as long as no fibers overlap in space with other fibers or tissues. Also, the framework facilitates choice of ohmic electrical properties of the tissues and physiological properties of the fibers. All these features permit the simulation of many different scenarios of interest.

The framework has been used in this work to elucidate answers to the main scientific questions of this thesis through numerical simulations. First, the effects of EC on myelinated axon bundles was studied. Prior to the use of the provided framework, a simpler model of EC using a distance-dependent model of the extracellular fields was used in order to quantify the effects of unidirectional ephaptic stimulation from the activity of one axon on the CV of a second axon, and to study how such distance-based model affects the CVs of three axons that mutually interact with each other. Findings from these simple cases were compared to existing knowledge on the effects of EC on AP propagation. Second, these mutual effects were studied using the RN for both a low number of axons, whose results are discussed for coincidences, discrepancies and novelties compared to the results using a simpler model, and for bundles containing a large number of axons, both mono- and multi-fascicular and including different known tissues in the nerve. Third, the effects of EC were assessed during an artificial stimulation scenario of a nerve trunk model under a cuff electrode. Finally, the RN is used to study the spatial variations of the strength of ephaptic interactions, and results are discussed against the possibility of using a MF model. This chapter provides a discussion on the main findings, their relationship with the thesis expected contributions and scientific questions, and the limitations of this work.

6.1   Findings and Implications of this Research

This research has elucidated the relevance of EC in the cases of artificial stimulation and AP propagation in fiber bundles and nerve trunk models. It has been revealed that EC is not only distance-dependent across a bundle's cross-section, but also that it can affect the recruitment numbers from artificial stimulation with cuff electrodes. Below is a discussion of the most important results.

6.1.1   Effects of Ephaptic Coupling on Propagation

Preliminary Quantification of the Ephaptic Influence of One Fiber over the Conduction Velocity of a Neighbour and Mutual Ephaptic Interactions

Chapter 3 presents a preliminary study, using an EC model based on [69] and not yet using the RN, which aims to quantify the unidirectional effects on CV that one myelinated axon can have on an identical and parallel neighbour, and to observe the effects of mutual EC between three parallel and identical myelinated axons on their CVs and, therefore, on the tendency towards AP synchronisation.

Results for the unidirectional ephaptic stimulation of one myelinated axon (source) onto another (target) quantify how the relative timing (which could be linearly related to separation along the z-axis) and transverse (perpendicular to the z-axis) distance between the axons affect the amount to which the presence of an AP on the source axon deflects the CV of an AP on the target. Results indicate that:

1. The relative timing between the two APs modifies the CV in the target axon when these are near, generally increasing it when the AP on the source is slightly ahead and decreasing it when this is behind. This represents a *de facto* attraction mechanism on the target AP towards the source that drives synchronised propagation. An additional CV decreasing region was detected when the source AP was about 2 to 6 ms ahead from the target, indicating that in such a case, there is a repulsive influence, so that the target AP is prevented from approaching the source. This is likely due to the refractory period of the source AP and its role might be, in bundles of many axons, to allocate APs with similar timings into different groups, all separated among each other by timings of the order of at least 1 ms.

2. The ephaptic influence decays with distance, as it is expected from the equation that governs the extracellular field (Eq. 2.1).

Results for the mutual EC between three axons show how, at least for the chosen parameters, the APs of the three axons modify their CVs through ephaptic interactions in such a way that their AP trajectories, represented on the z-t plane (where the z-axis is parallel to the axons; note that this is the x-axis in Chapter 3, although this choice is arbitrary), show a clear attraction among them. Consequently, the APs of the three axons tend to lock in order to travel synchronously. Also, the final compound CV of the three axons when synchronisation is close to occuring is lower than the CV that the axons have before synchronisation. These two observations are both in close agreement with the findings from previous studies on EC on parallel fibers, whether myelinated [64, 66] or unmyelinated [65].

These results are informative about the effects of EC on a few fibers and indicate that using Eq. 2.1 to model distance-dependent EC is possible. However, consideration of these results needs to be done whilst bearing in mind certain constraints and limitations that are intrinsic to the model in use. Eq. 2.1 for the calculation of the extracellular potential is obtained and used in fiber bundles under a number of assumptions which do not strictly hold for real nerves:

- **The extracellular medium is homogeneous.** The extracellular medium is not homogeneous due to the presence of other fibers and different tissues. This means that the same value for the electrical conductivity does not hold over the whole space, and discontinuities exist. This has no major implication for the simple case shown here, but it can make this model unsuitable when many axons are present between any other two, or for inter-fascicular EC. A more representative model of the extracellular medium would be needed, especially for the latter case.

- **The extracellular medium has isotropic conductivity.** The extracellular medium's electrical conductivity is not necessarily, and generally is not, isotropic. Anisotropies exist in extracellular media surrounding nerve fibers due to the non-homogeneous configuration of tissues around space and the presence and orientation of the axons in a bundle [132, 178]. There exist, however, other versions of Eq. 2.1 that account for the anisotropy of the medium [193], which are used for studying stimulation with electrodes. Taking this anisotropy into account for studies of EC could provide more accurate results as to the modelling of the endogenous extracellular field along axons.

- **The electrical ground is infinitely far away.** The allocation of a ground reference in a biological system is more complex than assuming it is at an infinitely far location and independent of the angle. Grounds or current return paths exist along the nerves toward the CNS, also across other surrounding non-neural tissues or bath preparations (saline, oil, etc.), and when specific electrode configurations for this purpose exist. The specific paths to ground in each case of study greatly influence how endogenous extracellular currents flow through them, and in turn, the nature of ephaptic interactions between axons. The current flow solely along the nerve is indeed arguably the most relevant current flow direction for EC studies in fiber bundles, so a radial current flow to a distant ground partially ignores the role of these longitudinal currents.

- **Axon compartments are represented as current point sources.** Neuron compartments are actually membrane patches which are surface sources of distributed current. The assumption of current point source has an implication on the values of the endogenous extracellular potential near a compartment, where Eq. 2.1 may yield unrealistically high values at close locations. Models of tightly packed axons, especially when these are not considered cylindrical

but with shapes more adapted to the packings, could use a study assessing of the consequences of this assumption, since it is known that transverse modes of stimulation exist [116, 117].

- **The presence of other axons does not modify the endogenous extracellular field generated by one axon.** The extracellular field generated by one axon is computed using its membrane currents and applied as accumulative stimulation forcing along other axons. Axons are bulky and anisotropic physical elements that effectively modify the electrical impedance between two points in the medium, especially when these axons are located somewhere between these two points. However, Eq. 2.1 does not regard the details of the presence of other axons and provides only one isotropic value for the whole extracellular space. While this value may of course be informed by measurements made in nerves where all these complexities are present [178], the specific arrangement of the axons in the medium can modify this value between two axons. It is indeed one finding of Chapter 4 that the presence of more axons in a bundle reduces the strength of ephaptic effects by increasing the effective conductivity of the bundle.

There are also a number of approximations and simplifications that have been chosen in our study:

- **There is a very low number of axons.** A low number of axons greatly simplifies the study, allowing ephaptic effects to be visualised in a simple way. However, studies with a larger number of axons are needed in order to assess these effects on more physiological numbers. This study is carried out in Chapter 5.

- **Axons are all identical, parallel, and their nodes of Ranvier are aligned.** Homogeneity in the properties of the axons also simplifies the degrees of freedom that can influence ephaptic effects. As it is seen in Chapter 5, axons with different properties, especially different diameters, interact differently to identical axons.

- **The chosen conductivity that yields visible ephaptic effects is small and not physiological.** The chosen value in Chapter 3 for which we have obtained our most relevant results is $\sigma = 10^{-3} S/m$, which is unrealistically low (so the medium is unrealistically resistive). A more physiologically plausible value, $\sigma_T = 0.085 S/m$, which represents a more conductive medium, still shows ephaptic effects, but these are much smaller and difficult to study since they are similar in size to the error margins. Studies with more informed values are needed. Chapter 5 partially addresses this issue, where anisotropic conductivity values obtained from the literature are used.

These assumptions and simplifications imply a calculation of an extracellular field that may very likely be different to the real one in realistic bundles. In fact, the use of this approach for a higher number of fibers lead us to numerical instabilities in the simulations. Despite all these considerations, these results are representative of the basic consequences of EC on AP propagation on fibers, and offer a basis which can be relied upon for a preliminary understanding of EC.

A qualitative study of the effects of EC in a low number of fibers has been carried out here, which has facilitated relevant observations involving the effects of EC on CV and synchronisation. However, models with a more complex representation of the system and the extracellular space are needed in order to study ephaptic interactions between a higher number of heterogeneous fibers in a realistic bundle. Chapters 4 and 5 provides a new approach that addresses most of these points.

Interaction among Few Axons Using the Resistor Network

The RN was used in Chapter 4 to run simulations of bundles of low numbers of parallel and identical myelinated axons. The strength of EC was controlled with the ratio between extracellular and axoplasmic resistances in the bundles. Results show that APs from the axons do tend to form AP lockings, where APs travel synchronously with a reduced CV. This is in agreement with Chapter 3 and previous knowledge [65, 66]. As expected, the strength of EC, or the strength of this synchronisation process, increases with an increasing value of the resistances ratio. When this ratio is near 0.1, meaning that the longitudinal extracellular resistance is low compared to the axoplasmic total resistance, the bundle's longitudinal currents flow mostly along the extracellular space and the ephaptic interactions are weak. Instead, when these resistances are equal (ratio equal to 1) or the extracellular resistance is higher than the axoplasmic (ratio equal to 10 or above), the ephaptic interactions are clear and stronger as the ratio increases.

Despite this, while using the RN in these simulations we made the observation that the strength of the ephaptic influence that one axon can exert upon others is reduced with the number of axons in a bundle. This is due to the higher presence of low-resistance axoplasmic paths to ground (if the grounds are assumed to be near the ends of the bundle). Therefore, for bundles with a relatively large number of axons, the strength of ephaptic interactions is dependent on the number of axons that are simultaneously active, which would increase the ephaptic current. Although this observation has been made in this work, it is actually in agreement with the discussions on the ratio of stimulated vs. unstimulated axons in [65, 66].

EC is thought to be negligible in fiber bundles due to the assumption of a large extracellular space, which reduces extracellular resistance [63]. However, this assumption is not realistic in mammalian peripheral nerves, where fiber packings can

be tight, as also happens in other parts of the nervous system [65]. Therefore, when accounting for the effects of extracellular space, EC should be considered. On the other hand, it is the presence of many axons in a bundle what reduces the strength of the ephaptic influence of one axon on others. This is a factor worth account for when considering the inclusion of EC in nerve models. When a low number of axons are meant to be active and propagating APs, compared to the total number of axons in the nerve, ephaptic interactions may be small enough to be ignored. This is not so, however, when almost half of them are to be active.

Interaction between Axons of Different Diameters

Simulations were run in Chapter 5 for two small bundles containing fibers of different diameters. In all simulations, all the fibers were stimulated nearly simultaneously using intracellular current injections on their first node of Ranvier, at the left end of the bundle, and propagation of the APs from all the fibers was observed.

One bundle contained fibers with diameters ranging from 9 μm to 10.9 μm following a continuous distribution. Results from this bundle show a certain interaction between fibers of similar diameters, where groups of fibers of the smaller diameters (from approximately 9 μm to 10 μm) tend to travel in AP lockings. Higher diameter fibers, however, do not strongly interact with lower diameter fibers, and furthermore interactions amongst them are weaker. In general, AP lockings have been found to be unstable, especially as diameter differences among fibers increase. This apparent grouping of AP lockings according to diameter could have a computational explanation for information treatment within nerves, since fibers of different diameters are meant to carry different types of information.

The second bundle contained fibers randomly chosen following a natural distribution based on [186]. For computational efficiency purposes, fiber diameters were bound between 3 μm to 20 μm. This is a wider range than the one used in the previous bundle. Propagation results in this bundle, as opposed to the former, do not present any AP locking between fibers under the influence of EC.

The latter is an impactful result that is in clear contrast with the behaviour expected according to previous knowledge on EC between identical fibers ([65, 66]; see also Chapter 3). These references all use fibers of equal diameters in their studies, which greatly simplifies the interpretation of the results. We have found no numerical simulation studies on the effects of EC on propagation on bundles containing fibers of different diameters, with the exception of [169]. In [169], however, only two coupled FitzHugh-Nagumo fibers were used. The work of [194], although it was not meant to study EC, used a somewhat complex bi-directional model of 50 unmyelinated fibers, divided in two types: HH and C fibers, with a set diameter for each —they did, however, account for the variability of CVs by randomising the intracellular

resistivities. To our knowledge, this is the first study of EC using bundles of more than two physiologically realistic myelinated fibers of different diameters, and it has been found that previous knowledge on identical fibers is not applicable in this case. For fibers of different diameters, synchronisation of pulses was found to be unstable in Chapter 5. Instability of synchronised pulses was also found in [169], where they suggested its relationship to the differences in fiber diameter. In the case of a bundle with a natural fiber diameter distribution, results in Chapter 5 suggest that EC appears to have no effect on CV or AP position modulation. The implications of this finding on how nerves process information during propagation are unknown, although it suggests that it is limited, at most, to synchronising the APs of fibers of very similar diameters. While the results for studies with equal diameter fibers may induce to conclude that EC does effectively syncrhonise APs, and therefore reduce the dispersion in nerves[1], scenarios with a broad range of fiber diameter variability are more common in natural nerves, and the results in the present work do not suggest that EC can effectively reduce dispersion.

These results suggest that the necessity of including EC on simulations of propagation along bundles with natural fiber diameter distributions is not confirmed. However, further assessment of this using alternative models and parameters is desirable in order to provide a more solid statement on this aspect.

6.1.2   Effects of Ephaptic Coupling on Axon Activation from Artificial Electrode Stimulation

In Chapter 5, simulations using the RN have been used to study how EC affects the recruitment of axons during stimulation. For this, using a self-consistent model such as the RN allows for computing fields from all sources (electrodes and axons) at every time step in a scheme that facilitates numerical stability. These simulations are run over a model of a nerve trunk with 7 circular fascicles that contain fibers of different diameters. The nerve trunk is embedded in a cylindrical container with a saline bath, and it is stimulated by a cuff electrode.

The first important difference between a self-consistent simulation with EC and a hybrid field-neuron simulation without EC is that the EC simulation presents a higher recruitment. A further exploration of the extracellular fields on the fibers during the evolution of the EC simulation shows that, during the stimulating pulse, the extracellular potential progressively gains strength and therefore drives the activation of more fibers. After the stimulation pulse finishes, this field does not drop to zero, but generally shows a decay along time. This means that it keeps stimulating fibers after the stimulating pulse has finished. These variations in the extracellular

---

[1]dispersion in a Compound Action Potential (CAP) is defined as the reduction in the CAP's amplitude due to the variability in CVs; see [194, 195]

field cannot be explained only by the stimulating pulse of the electrode, which consists of a square pulse. It can only be explained by the activity of the axons in the bundle, which generate an endogenous extracellular field. This field adds linearly to the field generated by the electrodes and increases the effective strength of the stimulation.

The maximum difference in fiber recruitment between the EC and non-EC simulations in Chapter 5 was found to be a 64.9% of the total number of fibers in the nerve trunk model, where, as opposed to Chapter 3, physiologically plausible values for tissue electrical parameters were used [132,178]. This finding shows that EC can have a measurable effect on recruitment numbers during artificial stimulation with electrodes. Also, EC was found to shift and narrow the range of optimal stimulating pulse amplitudes for maximising selectivity on a given fascicle, thus limiting the precision of the electrode under study. Nevertheless, it needs to be studied whether ephaptic effects on selectivity would be so strong when a small number of axons is targeted with a high-precision electrode, such as a TIME or Utah array. In view of this finding, non-EC hybrid field-neuron models could be revisited for a potential inclusion of EC, and assessments of the effects of EC on selectivity could be undertaken.

6.1.3   Dependence of Ephaptic Coupling on Inter-Axonal Distance

The dependence of the effect of EC on CV on the separation distance between axons was already quantified in Chapter 3 for the distance-dependent EC model given by [69] (Fig. 3.2(b)). This effect is decreasing with distance, as it is expected from Eq. 2.1. In Chapter 5, this dependence was studied for a bundle using the RN. The dependence of the strength of EC—measured there as the maximum absolute change of v_m in axons that are not artificially stimulated due to the ephaptic influence of one axon that is and which propagates an AP—is quantified against the separation distance between axons. Results are conclusive in showing that EC does have a dependence on distance, both in a single bundle and in a nerve with several fascicles, and shows that a MF assumption is always a simplification which comes with inaccuracies. The small ranges of change of v_m, however, indicate that for cases where a small number of axons are activated, or where the transverse component of the extracellular conductivity is very high compared to the longitudinal component, a MF approximation can be enough to represent the extracellular space in a bundle. Simultaneous activity of many axons, however, may lead to stronger ephaptic interactions and a larger range of change of v_m. If for only one activated axon inside a fascicle (Fig. 5.12(a)), this range is of the order of 1 to 10 μV, simultaneous activity of 100 axons in a specific region could widen this range up to the order of 1 mV if endogenous extracellular potentials from the axons have the right phase difference to constructively sum up, range for which the choice of a MF model could be ques-

tioned. Also, the chosen bundle is 250 μm thick and the distances to the stimulated axon are not much greater than 150 μm. This corresponds to a relatively small bundle. For larger bundles with longer inter-axonal distances, the range of change in v_m could be increased.

The perineurium provides a degree of electrical isolation between the different fascicles (Fig. 5.12(b)). We can observe that, although for fibers in the same fascicle, the variations of the maximum absolute change of v_m with the distance are very small, the mean value of the maximum absolute change in v_m differs for different fascicles. Hence, a local MF approximation for each individual fascicle may be justified, but of course, only when fields from stimulating external electrodes are not present.

The MF model is a convenient simplification that greatly reduces the computational costs of simulations of AP conduction in bundles of ephaptically coupled fibers, and results of such simulations can be very informative about the effects of EC on propagation [65, 66, 68]. Despite the choice of a MF model being justified in certain scenarios, it is not suitable for two particular situations of interest:

1. The MF model is not compatible with simulations involving stimulating extracellular electrodes due to the nature of its core assumption. The potential field resulting from stimulation exerted by extracellular electrodes does have variations across the cross-section of the nerve which are well above the order of 1 mV and can be of the order of 100 mV [109, 152]. These variations are key to determining regions of axonal activation and excitability changes across the cross-section of the nerve, information which is very relevant for selectivity studies. Hence, reducing these fields to a mean field, constant over the nerve's cross-section, eliminates all their relevant spatial details —except those dependent on the axis parallel to the fibers.

2. As seen in the results in Chapter 5 for the 500 μm diameter multifascicular nerve model (Fig. 5.12(b)), the range of change of v_m due to the activity of a single axon is around 120 μV, which means that simultaneous activity from 100 axons could potentially increase this value to near 12 mV. Furthermore, it is visible that the strength of EC is somewhat discretised between fascicles. Hence, although a local MF model for each fascicle could work, a MF model applied over the whole nerve's cross-section cannot accurately represent the extracellular field. The inaccuracies could be even greater for larger diameter nerve models with more fascicles.

Dependence of EC in inter-axonal distance is therefore not strictly necessary to be accounted for in all scenarios, but it provides a more accurate representation of EC for multifascicular nerve models, and is necessary for simulations involving extracellular stimulating electrodes.

Spatial Range of Ephaptic Coupling

We have found in our simulations that the activity from one fiber always influences the membrane potential of all other fibers if EC is included in the simulations. In no case has the activity from one fiber been observed having a zero or nearly null effect on the v_m of another fiber within a nerve or fascicle model. When estimating which is the spatial range of EC, choosing a threshold value of v_m is needed. The criterion for such choice could possibly be where the deflection of v_m on distant fibers became statistically insignificant compared to other fibers, or it could be the choice of a threshold value of the order of 1 μV. In the simulation in Fig. 5.12(b), which is the simulation presenting the lowest ephaptic influence of the two in subsection 5.3.4, the minimum found deflection of v_m was near 80 μV and the total variation of this variable was similar. Therefore, we cannot state that the range or spatial range of EC is smaller than 400 μm for this model.

It is possible that the spatial range of EC would be smaller than the radius of a much thicker nerve. In that case, we would be able to observe that the activity of one fiber does not significantly affect the membrane potential of another distant fiber. However, we have not tested this case in this work, and this is left as an open question. The ratio between longitudinal and transverse components of the extracellular conductivity also plays a role in this spatial range. If we think about how these two components drive current flow over the extracellular space, the spatial range of EC should follow a negative trend with respect to this ratio, i.e., a low longitudinal conductivity compared to the transverse conductivity would favour a large spatial reach of EC—note that the MF model is the special case when the transverse conductivity is infinite, which is the extreme of this case—and vice versa: a high longitudinal conductivity compared to the transverse conductivity would allow ephaptic currents to flow largely along the nerve, and the endogenous extracellular field generated by an axon would decay quickly with the radial distance from it.

6.2   Scientific Contributions of this Research

6.2.1   Scientific Questions: Assessing the Effects of Ephaptic Coupling in Mammalian Peripheral Nerves

I. Distance Dependence of Electrical Interactions.

This contribution can be found in Chapter 5 and publication [15].

The findings on the dependence on inter-axonal distance of EC indicate that a

MF model is not suitable for all scenarios of interest, especially for scenarios involving artificial stimulation with extracellular electrodes, and that spatial variations of ephaptic effects are present across the cross-section of bundles. We believe this is the first study in providing a reference with which to assess the accuracy of MF models and the exclusion of EC from peripheral nerve models altogether, since it studies such interactions with a level of detail that, whilst it is possible to simulate in theory by using existing methods that allow for it [71, 72], has not been found during our literature review for our system of interest.

II. Quantification of the Effects of Ephaptic Coupling on Propagation

This contribution can be found in Chapters 3, 4 and 5 and in publications [13,15,177].

Propagation in groups of small numbers of fibers has, as expected, been found to be affected by EC when the physical parameters of the system facilitate this. The known effects of EC on propagation have been observed in our simulations. These are AP attraction among fibers, synchronised propagation in AP lockings, and CV reduction. However, most of these effects lose their presence in larger bundles with fibers of different diameters, which is the case of natural bundles in nerves. Only CV reduction has been observed in a bundle which had a natural distribution of fiber diameters, but no AP lockings or even attraction of AP trajectories was observed. Activation of inactive fibers due to the ephaptic stimulation from propagating APs in neighbouring fibers was not observed either, although models of damaged fibers were not used, nor a study with the purpose of observing this was run.

This study uses a higher level of detail in the models compared to previous works [66,68], and this has allowed this study to be the first, to our knowledge, that simulates EC in bundles of fibers with varying diameters. Therefore, these findings are not yet enough to completely rule out the influence of EC in propagation in realistic nerves, but it is a first indication that its relevance is still to be found.

III. Quantification of the Effects of Ephaptic Coupling on Stimulation

This contribution can be found in Chapter 5 and publication [15].

EC has been found to increase recruitment numbers in simulations of stimulation of a nerve with a cuff electrode by as much as 64.9% of the total axonal population. Also, we have observed that EC decreases axon response times to stimulating fields, making axons fire more synchronously from the start. Furthermore, the optimal pulse amplitude ranges for maximum inter-fascicular selectivity are shifted and narrowed by EC. These are interesting results that contribute to our knowledge about

the role of EC in the PNS. The first of these two findings is especially relevant for functional electrical stimulation of the PNS, since it suggests that EC can influence the selectivity of electrodes.

6.2.2 Technological Contribution: Open-Source Framework to Model Nerves and Electrode-Nerve Interfaces

The framework developed here to define anatomical and physiological properties of models has allowed us to run the simulations presented in this work in Chapters 4 and 5.

This software[2], which has been developed in Python, is notably helpful for the user at modelling realistic nerve trunks since it lets them define any cross-sectional anatomical profile including fascicles, fiber locations and diameters, and extrude it along the desired length. It also allows for easily defining the ohmic properties of tissues, and for configuring the presence and properties of stimulating and recording electrodes. Finally, the user can run simulations under the defined parameters using this software.

This software is meant to be open-source and released to the public in the near future. Available models of peripheral nerves are scarce. It is therefore a considerable contribution to the community to release a model framework like this. There are rarely other available models of peripheral nerves, with the clear exception of [110], and especially if anatomical richness and customisation options are needed.

Utility of the Framework for Stimulation Studies Using Other Electrode Geometries

As mentioned above, the framework allows the users to define and configure the presence and properties of stimulating and recording electrodes. In this work, we have developed models of cuff electrodes both for stimulation and recording. These are defined in templates which can be easily edited and permit specification of the multiple parameters needed for the function of the simulated electrodes: size, shape, location, electrical properties, rings, active pads, stimulation protocols, variables to record, etc. Once the electrodes and their intended roles (i.e., recording or stimulation, including all the necessary parameters for stimulation) are defined in the templates, the framework automatically incorporates them to the model, adapting them to the nerve's geometrical properties and embedding them in the whole nerve-electrodes-bath system. When the simulation is run, their programmed stimulation

---

[2]The software will be available on the following repository: https://github.com/mcapllonch/SenseBackSim.git
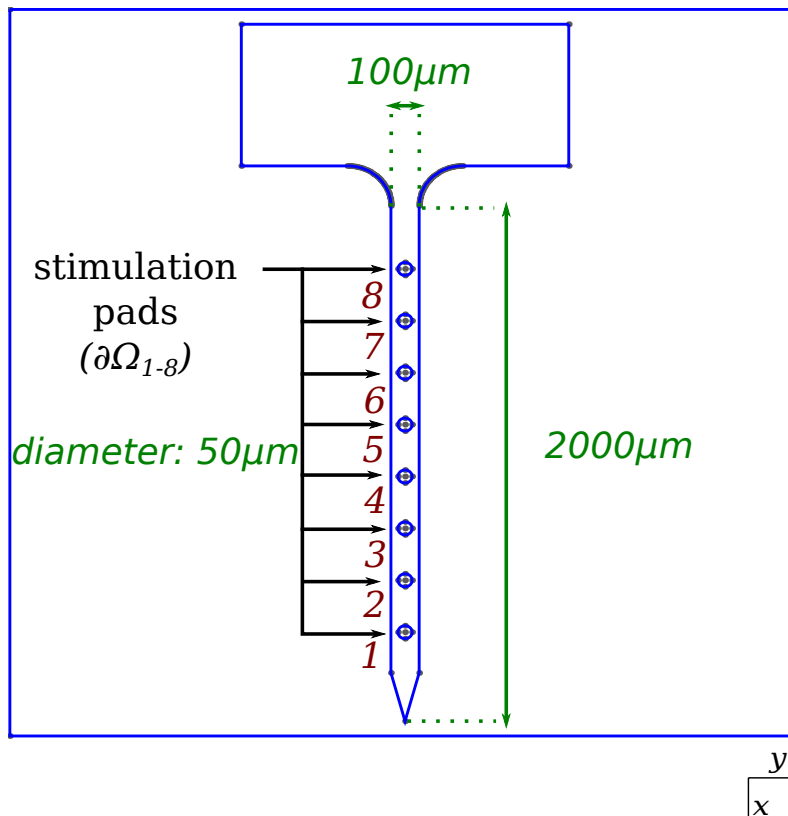
Figure 6.1: TIME electrode design for the SenseBack project [1]. This image represents the contours of the design and includes some details regarding its geometry and active sites. This design was implemented in a FE mesh in [5] for use with the FEniCS FEM solver [4]. Taken with permission from [5].

or recordings are executed. Templates for intracellular and extracellular current stimulation have also been created, as well as templates defining electrical ground points or regions. Along with the release of the code to the public, we intend to incorporate templates for TIME, LIFE, and Utah electrode arrays. Further work should show the results of simulations using these templates.

Our intention is to allow this software to be easily used for the electrode designs of choice of future users, since it is aimed to provide a versatile nerve modelling framework to the community. This has the chance of contributing to the scientific community with a tool that can be used for optimisation studies of electrode designs. The electrode-nerve interface models that have so far been presented in the field, whether they use cuff electrodes [7,124,132,196]—including FINE [8,58,133]—TIME [40] Utah electrode arrays [197], or even micro-electrode arrays (MEA) [147, 198, 199], share the fact that they are closed source software, mostly because the FEM solvers in use are commercial, such as ANSYS (Ansys Corporation, Canonsburg, PA; used by [7, 124, 148, 196]), Maxwell 3D (property of ANSYS; used by [8, 58, 132, 133]) and COMSOL (COMSOL Multiphysics®; used by [40, 147, 197–199]). Making tools of this kind available to the community as open source software will

facilitate more studies in this field. We have not only worked with our RN, which is developed in NEURON and Python, but also with the FEniCS Project software [4], which is an open-source framework for FEM simulations. To date, preliminary implementations of TIMEs have been made in this project using FEM [5] (Fig. 6.1), although these studies have not been included as part of this thesis. A few tools for simulating recordings from neural activity are luckily available [110, 134]. Of these, only [110] uses FEM, while [134] is limited to using the known analytical model for the extracellular potential of [69]. Still, the complexity of nerve bundles for electrode recording simulations needs to be extended further, and our software intends to fulfil that goal.

Implementation of geometries like TIMEs, LIFEs or Utah electrodes are currently undergoing. As opposed to cuff electrodes, intracellular and extracellular current point injections, these electrode designs are invasive, so they contain material components that penetrate the nerves. Modelling these electrodes can be done, in the first instance, using the point or surface current sources that correspond to the electrodes' active pads inside the physiological extracellular medium. But of course, accounting for the presence, shape, and electrical properties of their structural components, may provide higher accuracy. Although this is not implemented yet, these components would be accounted for, in principle, by assuming they are made of insulating materials, removing the connections in the RN which are supposed to cross them. An explicit representation of their presence and shapes is possible, although that would come along with a considerable rise in computational cost for the simulations. Displacement and bending of axons in the nerve due to the presence of these elements is not considered for the near future, but it is a desirable task for further work to model and then implement these physical movements in the models, so that their effects can be studied.

6.3   Limitations of this Research

6.3.1   Validation

The model framework developed in this work comes with a series of limitations that need to be taken into account when using it. The main limitation is related to the shortcomings in the validation that we could provide for the results of its simulations. We briefly explain here the nature, reasons and importance of these shortcomings, as well as the reasons why this model framework is still valid for use in neurophysiology computational studies despite these limitations.

Lack of Comparisons to FEM Results of Nerve Models

While the resistor network method in use has been validated to a certain point using FEM simulations of a simple electrical problem in an ohmic medium, we do not provide comparisons of solutions of the fields solved by the RN over detailed nerve models to solutions using FEM simulations, which is the most commonly accepted technique. The reason for this is that FEM are not used in our work due to implementation time constraints. FEM are trusted for having a strong mathematical background that makes them, thus far, the most reliable tool for solving the fields over a nerve or a tissue after electrical stimulation from electrodes. Our model is of course not intended to compete with FEM, but it is offered as an alternative tool when modelling ephaptic interactions is required. As our model is EMI-type [114] (meaning that it contains extracellular space, membranes, and intracellular spaces to be solved together), it offers a self-contained and self-consistent scheme for the simulations that includes EC, whilst trying to model EC with FEM would need a two-step scheme that would need to couple the computation of the neural activity (intracellular spaces and membranes) to FEM simulations to compute the fields over the extracellular domain. When considering that reaching consistency between the neural and the FEM simulations would require an iterative convergence algorithm, that could be considerably expensive in terms of computational resources.

Despite the lack of comparisons to FEM simulations of nerve models, we did provide comparisons to FEM simulations of a simple problem on an ohmic medium and to an analytical solution to a cubic geometry. The results from these comparisons indicate that the RN is well suited for solving the electrical potential of ohmic materials. This is of course expected from the fact that the RN is fully implemented in NEURON (while using a Python wrapper) through the *LinearMechanism* tool, which is known to work without errors or serious numerical inaccuracies [200].

Lack of Specifically Designed Experimental Validation

The models developed here have not undergone a validation process with experimental studies specifically designed for the purpose. This is, the models do not have the support of any study involving an *in vivo* experimental setup designed to match a specific scenario as simulated by the models, including nerve anatomical properties, and stimulation and recording materials and protocols.

While this type of validation would be highly desirable, it has not been possible to undertake it during this project. Nevertheless, we are still able to provide grounded reasons to consider the validity of our models and of the results presented in this work:

1. **Axon models** used in this work are exclusively taken, without modification except for the anatomical regressions also made in [110], from existing models that have been experimentally validated by their designers (see [101, 108] for the MRG model, and [113] for the sensory fibers), and by many other works after them (see [152] for references about validation of the MRG model after its development in [108]).

2. The values of the **electrical and geometrical properties of the tissues** used in the models presented here (endoneurium, epineurium and perineurium) have been obtained from the literature, from sources with a strong experimental basis [132, 178].

These two choices ensure that the fiber bundles of this work are simulated according to experimental data from previous works. Thus, they help to prevent the deviations of the nerve models from natural neural behaviours to grow more than what can be a direct consequence of 1) the intrinsic inaccuracies of the models and parameters taken from the literature, 2) our conservative choice of considering the endoneurium as isotropic in Chapter 5, and 3) our choices at combining such parameters in a full nerve model. In this regard, it should be noted that the chosen parameters come from experimental data obtained from different animals. For instance, the resistivities used for endoneurium and epineurium are valid for cats [178], and the membrane dynamics and geometrical properties of the MRG model are built from experimental measurements on humans, cats and rats [108] —in consequence, so is, to an extent, the sensory fiber model from [113]—. Therefore, although parameters for mammals may be similar, more species-specific parameter choices should be pursued in order to properly and precisely model specific animal physiology. Also, to this date this is not entirely possible since these combined animal models are among the most up-to-date. This would be the case if using this model framework for human sensory feedback restoration, where more human-specific parameters should be searched as thoroughly as possible.

Our model framework is not at the level of a fully experimentally validated model. However, what has been explained in this latter discussion, together with the confidence we lay on the RN for the reasons expressed above, leaves us to propose that our models and methods are computational tools with great potential for use in further studies, and with a well grounded level of reliability.

One last observation that needs to be made is that this framework allows the implementation of models that can be validated by any other users. With regards to the models that have been used in this particular work, it is left as further work to fill the gaps in their validation with FEM simulations and experimental data.

6.3.2 Difficulty of Interpreting the Results for Peripheral Nerve Models

Finally, the complexity of our model is larger than previous studies on EC for axons, and its results yield a level of complexity that is usually difficult to interpret correctly. This is especially the case for the results on propagation in bundles with fibers of different diameters in Chapter 5. A relevant observation could be made from those results. Namely, that the synchronisation mechanisms that were expected from known results on bundles of identical fibers were not observed in bundles with fibers of different diameters, and those mechanisms were weaker, virtually inexistent, for the bundle in which fiber diameters follow a natural distribution. However, these mechanisms were observed to occur to a certain extent in the bundle of fibers with similar diameters, although they were also observed to be unstable. In these cases, however, the behaviour of the fibers as a collective bundle was complex, as the underlying reasons for the separation of AP trajectories along the simulation could be guessed but not demonstrated.

Chapter 7

Conclusions and Future Directions

7.1 Conclusions

This project was undertaken in order to study the effects of ephaptic coupling on stimulation of myelinated fibers in nerve trunks and action potential propagation, with the ultimate aim in mind of assessing its role for sensory feedback restoration. For this, a software tool was developed for building anatomically and electrically detailed models of peripheral nerves. Simulations using this model have been used to answer the scientific questions that were raised in this study. The main contributions and findings of the results of this project can be summarised as follows:

- **Effects of ephaptic coupling on propagation.** Results from our simulations show that the known effects of ephaptic coupling between parallel fibers on the propagation of action potentials become difficult to identify and interpret in large bundles of myelinated fibers of varying diameters. On the one hand, fibers with very different diameters (more than 1 μm) have weaker interactions than fibers of similar diameters. On the other hand, the presence of a large number of fibers in a bundle generally diminishes the strength with which these interact ephaptically, unless the activity of many fibers is synchronous. In any case, for bundles with realistic extracellular electrical conductivity and fibers of different diameters, the effects of ephaptic coupling are present but are too weak to result in the known action potential lockings. One aspect that remains visible in all simulations including ephaptic coupling, however, is the reduction in conduction velocity resulting from close-phase propagation of action potentials in parallel axons, independently of the cause of the phase proximity.

- **Effects of ephaptic coupling on artificial stimulation.** Unlike the effects of that it has on action potential propagation in large bundles, ephaptic

coupling shows a considerable influence on axon recruitment in nerve trunk models stimulated by cuff electrodes. During pulses of depolarising stimulation, an ephaptic field is created in the nerve due to the activity of all axons, which adds to the field created by the electrodes and further depolarises all the axons. This field can be of the order of 10 μV, and its direct effect is a quicker depolarisation of all axon membranes, which 1) makes all axons reach their thresholds and fire action potentials quicker, and 2) elicits action potentials in axons for which the field from the electrodes alone would not reach their thresholds. The net effect of this is not only more synchrony in action potential elicitation, but also higher recruitment numbers. It was found in our models that this increase can be higher than 64.9% of all the axons in a bundle. This finding raises a call of attention to this phenomenon, always neglected in artificial stimulation studies.

- **Spatial dependence of ephaptic coupling.** On the spatial variation of ephaptic coupling with inter-axonal distances, it has been found that while spatial variations always exist, these can be ignored in some ideal cases and a mean-field model may be used. However, they cannot be ignored in cases where artificial stimulation with extracellular electrodes is studied and in complex bundles with perineurial membranes separating different fascicles.

- **Open source software for nerve modelling.** A software tool has been developed that allows the design of a nerve trunk model with any arbitrary cross-sectional anatomy, distribution of tissues and fiber packing. The software is capable of simulating the activity of the nerve in a self-consistent EMI model under the influence of stimulating electrodes and the presence of recording electrodes. Given its self-consistent nature, the model simulates the ephaptic interactions among all fibers within a nerve, which allows us to quantify the effects of ephaptic coupling in various aspects of the fibers activity. Not only can the software simulate the activity of the nerve in a self-consistent model, but it also contains a hybrid field-neuron approach, where fields from stimulating electrodes can be simulated in advance and later used in purely neural simulations, where ephaptic interactions are disregarded. To date, we have found no open source software similar to ours that allows users to design anatomically detailed nerve models and include large-scale ephaptic coupling. With this software, we aim to provide a useful modelling tool for the scientific community.

Despite the advances that have been made in this research, these results and the model itself leave room for further investigation. The model can still be substantially improved in further work by properly including a FEM simulation system and other electrode designs. Also, the results presented in this thesis can be further explored and quantified against other relevant variables. Although some of these points for further work were mentioned in Chapter 6, we summarise them below.

7.2   Future Directions

7.2.1   Necessary Improvements on the Model

- **Validation of the electrode fields with FEM simulations.** Although the resistor network has been validated against expected results for simple problems with a FEM simulation and an analytical solution in Chapter 4, the fields generated by the electrodes over realistic nerve bundles simulated with the resistor network should be compared to results from FEM simulations on equivalent nerve models. It must be noted that in the case of using the resistor network with full axon models embedded in it instead of a homogeneous isotropic tissue, which is the application this model is designed for, we expect the results from the two techniques to differ because in the resistor network, axons are modelled explicitly and the effects of their models contribute to the field, whereas in a FEM simulation, their presence is accounted merely by the anisotropy of the endoneurium's conductivity tensor. Nevertheless, results from both schemes should be compared for consistency, since that would provide a stronger source of validation than what has been provided in this study. Simulations where the endoneurium is modelled as merely an anisotropic tissue in the resistor network should yield results with a close match to FEM simulations.

- **Validation of the model using corresponding experimental designs.** We have used models of fibers that were thoroughly validated with experimental data along the last years by their designers and other works. We have also used parameters for the anatomical and electrical properties of the tissues that were also obtained from experiments performed by their respective studies. This, together with the preliminary validation we performed of the resistor network in Chapter 4, lets us trust the validity of our model to an acceptable degree. However, we have not been able to provide a validation study involving a simulation and an experiment with equivalent scenarios and parameters. For a complete validation of the model, it is necessary to run a study in which, ideally, a nerve is stimulated *in vivo* with electrodes at one end, and electrode recordings are performed at a distal end. Then, results need to be compared to a simulation that imitates the experimental conditions.

7.2.2   Desirable Improvements on the Model

- **Reduction of the computational costs.** A resistor network is an expensive method to simulate electrical activity in a nerve with hundreds of fibers. The largest simulations run in Chapter 5 took more than 24h to compute, and they were optimised in order to avoid larger computation times by limiting the ephaptic coupling zones to the regions under the cuff electrodes, or by

greatly limiting the cross-sectional sizes of the bundles in simulations where ephaptic coupling was present all along the bundles. The costs in computation time of the resistor network dramatically increase for a large and detailed nerve trunk model as the network's longitudinal resolution (i.e., the number of transverse resistors per unit length) increases, thus limiting the practical length that can be given to a nerve trunk model if ephaptic interactions along its full length are intended. Therefore, a more efficient method needs to be further investigated. Also, parallel computing of simulations using this resistor network has not been achieved yet, and this is proposed for future work. A thorough study of the computational costs, measured as total simulation time, should be carried out in the future in order to study their dependence on nerve length, resolution along the z-axis, and number of cables and transverse resistors. For this, a sensitivity analysis should be carried out on all of these parameters. Results are expected to shed light on the most compromising model choices for computational efficiency.

- **Simulations with other electrode geometries.** Future work can implement designs of electrode geometries other than cuff electrodes in the model framework and simulate stimulation with them. Specifically, we are aiming to implement designs of TIMEs, LIFEs and Utah arrays. The presented software is aimed to be used by researchers when studying stimulation with different electrode designs, so more clarity on how to do this needs to be provided.

- **Tortuosity.** Tortuosity of axons within a nerve is known to affect the results from stimulation and electrode recordings. Also, invasive electrode designs such as TIMEs, LIFEs and Utah arrays provoke axon bending. It would be desirable to extend the model to allow the inclusion of such axon bending and study their effects. Furthermore, tortuosity likely has implications on ephaptic interactions, since it means that the assumption of parallel axons no longer holds.

7.2.3 Suggested Extensions on the Research Results

- **Further quantifying the effects of ephaptic coupling on propagation in realistic bundles.** Results in this thesis regarding the effects of ephaptic coupling on large bundles of fibers with varying diameters provide some initial insights, but do not fully explain the observed behaviours of axons. It is suggested as further work to perform more studies on this matter. Ideally, such studies could involve more controlled parameter ranges in order to minimise the degrees of freedom influencing the results. It is suggested to use more constrained axon diameter ranges and lower numbers of axons in the bundles.

- **Simulation of sensory information encoding.** In order to close the gap between the detailed modelling approach presented here and studies on sensory

feedback restoration, we propose the use of this model to simulate, with and without ephaptic coupling, the action potential patterns, both spatial and in time, generated in the axons by artificial stimulation. Relating results of these simulations to experiments reporting user-reported sensory percepts from actual artificial stimulation would allow elucidating the neural codes associated with such percepts, a knowledge that is nowadays not mature yet.

Bibliography

[1] SenseBack. (2014) Enabling technologies for sensory feedback in next-generation assistive devices. ep/m025977/1. [Online]. Available: `http://www.senseback.com`

[2] M. L. Hines and N. T. Carnevale, "The NEURON simulation environment," *Neural computation*, vol. 9, no. 6, pp. 1179–1209, 1997.

[3] C. Geuzaine and J.-F. Remacle, "Gmsh: a three-dimensional finite element mesh generator with built-in pre-and post-processing facilities," in *Proceedings of the Second Workshop on Grid Generation for Numerical Computations, Tetrahedron II*, 2007.

[4] A. Logg, K.-A. Mardal, and G. Wells, *Automated solution of differential equations by the finite element method: The FEniCS book.* Springer Science & Business Media, 2012, vol. 84.

[5] F. Kolbl, M. C. Juan, and F. Sepulveda, "Impact of the angle of implantation of transverse intrafascicular multichannel electrodes on axon activation," in *2016 IEEE Biomedical Circuits and Systems Conference (BioCAS)*. IEEE, 2016, pp. 484–487.

[6] S. Raspopovic, M. Capogrosso, J. Badia, X. Navarro, and S. Micera, "Experimental validation of a hybrid computational model for selective stimulation using transverse intrafascicular multichannel electrodes," *IEEE Transactions on Neural Systems and Rehabilitation Engineering*, vol. 20, no. 3, pp. 395–404, 2012.

[7] A. Q. Choi, J. K. Cavanaugh, and D. M. Durand, "Selectivity of multiple-contact nerve cuff electrodes: a simulation analysis," *IEEE Transactions on Biomedical Engineering*, vol. 48, no. 2, pp. 165–172, 2001.

[8] M. A. Schiefer, R. J. Triolo, and D. J. Tyler, "A model of selective activation of the femoral nerve with a flat interface nerve electrode for a lower extremity neuroprosthesis," *IEEE transactions on neural systems and rehabilitation engineering*, vol. 16, no. 2, pp. 195–204, 2008.

[9] B. Katz and O. H. Schmitt, "Electric interaction between two adjacent nerve fibres," *The Journal of physiology*, vol. 97, no. 4, p. 471, 1940.

[10] M. Brill, S. Waxman, J. Moore, and R. Joyner, "Conduction velocity and spike configuration in myelinated fibres: computed dependence on internode distance." *Journal of Neurology, Neurosurgery & Psychiatry*, vol. 40, no. 8, pp. 769–774, 1977.

[11] R. C. Barr and R. Plonsey, "Electrophysiological interaction through the interstitial space between adjacent unmyelinated parallel fibers." *Biophysical journal*, vol. 61, no. 5, p. 1164, 1992.

[12] M. C. Juan, F. Kölbl, and F. Sepulveda, "Optimisation of the spatial discretisation of myelinated axon models," in *2016 8th Computer Science and Electronic Engineering (CEEC)*.   IEEE, 2016, pp. 216–221.

[13] M. Capllonch-Juan, F. Kölbl, and F. Sepulveda, "Unidirectional ephaptic stimulation between two myelinated axons," in *Engineering in Medicine and Biology Society (EMBC), 2017 39th Annual International Conference of the IEEE*.   IEEE, 2017, pp. 230–233.

[14] M. Capllonch-Juan and F. Sepulveda, "Evaluation of a resistor network for solving electrical problems on ohmic media," in *2019 11th Computer Science and Electronic Engineering (CEEC)*, Sep. 2019, pp. 35–40.

[15] M. Capllonch-Juan and F. Sepulveda, "Modelling the effects of ephaptic coupling on selectivity and response patterns during artificial stimulation of peripheral nerves," Unpublished manuscript; submitted to PLOS Computational Biology on 5/6/2019.

[16] W. V. McCallister, S. R. Cober, A. Norman, and T. E. Trumble, "Using intact nerve to bridge peripheral nerve defects: an alternative to the use of nerve grafts," *The Journal of hand surgery*, vol. 26, no. 2, pp. 315–325, 2001.

[17] J. E. Shea, J. W. Garlick, M. E. Salama, S. D. Mendenhall, L. A. Moran, and J. P. Agarwal, "Side-to-side nerve bridges reduce muscle atrophy after peripheral nerve injury in a rodent model," *journal of surgical research*, vol. 187, no. 1, pp. 350–358, 2014.

[18] B. Battiston, S. Geuna, M. Ferrero, and P. Tos, "Nerve repair by means of tubulization: literature review and personal clinical experience comparing biological and synthetic conduits for sensory nerve repair," *Microsurgery*, vol. 25, no. 4, pp. 258–267, 2005.

[19] S. K. Lee and S. W. Wolfe, "Peripheral nerve injury and repair," *Journal of the American Academy of Orthopaedic Surgeons*, vol. 8, no. 4, pp. 243–252, 2000.

[20] S. Shahdoost, S. Frost, G. Van Acker, S. DeJong, C. Dunham, S. Barbay, R. Nudo, and P. Mohseni, "Towards a miniaturized brain-machine-spinal cord interface (bmsi) for restoration of function after spinal cord injury," in *2014 36th Annual International Conference of the IEEE Engineering in Medicine and Biology Society*. IEEE, 2014, pp. 486–489.

[21] Y. Nishimura, S. I. Perlmutter, and E. E. Fetz, "Restoration of upper limb movement via artificial corticospinal and musculospinal connections in a monkey with spinal cord injury," *Frontiers in neural circuits*, vol. 7, p. 57, 2013.

[22] A. Jackson, C. T. Moritz, J. Mavoori, T. H. Lucas, and E. E. Fetz, "The neurochip bci: towards a neural prosthesis for upper limb function," *IEEE Transactions on Neural Systems and Rehabilitation Engineering*, vol. 14, no. 2, pp. 187–190, 2006.

[23] M. Lachowska, A. Pastuszka, Z. Łukaszewicz-Moszyńska, L. Mikołajewska, and K. Niemczyk, "Cochlear implantation in autistic children with profound sensorineural hearing loss," *Brazilian Journal of Otorhinolaryngology*, 2016.

[24] B. S. Wilson, C. C. Finley, D. T. Lawson, R. D. Wolford, D. K. Eddington, and W. M. Rabinowitz, "Better speech recognition with cochlear implants," *Nature*, vol. 352, no. 6332, pp. 236–238, 1991.

[25] J. P. Roche and M. R. Hansen, "On the horizon: cochlear implant technology," *Otolaryngologic Clinics of North America*, vol. 48, no. 6, pp. 1097–1116, 2015.

[26] V. Colletti, M. Carner, V. Miorelli, M. Guida, L. Colletti, and F. Fiorino, "Auditory brainstem implant (abi): new frontiers in adults and children," *Otolaryngology-Head and Neck Surgery*, vol. 133, no. 1, pp. 126–138, 2005.

[27] E. Margalit, M. Maia, J. D. Weiland, R. J. Greenberg, G. Y. Fujii, G. Torres, D. V. Piyathaisere, T. M. O'Hearn, W. Liu, G. Lazzi *et al.*, "Retinal prosthesis for the blind," *Survey of ophthalmology*, vol. 47, no. 4, pp. 335–356, 2002.

[28] A. B. Schwartz, X. T. Cui, D. J. Weber, and D. W. Moran, "Brain-controlled interfaces: movement restoration with neural prosthetics," *Neuron*, vol. 52, no. 1, pp. 205–220, 2006.

[29] L. R. Hochberg, D. Bacher, B. Jarosiewicz, N. Y. Masse, J. D. Simeral, J. Vogel, S. Haddadin, J. Liu, S. S. Cash, P. van der Smagt *et al.*, "Reach and grasp by people with tetraplegia using a neurally controlled robotic arm," *Nature*, vol. 485, no. 7398, pp. 372–375, 2012.

[30] A. M. Green and J. F. Kalaska, "Learning to move machines with the mind," *Trends in neurosciences*, vol. 34, no. 2, pp. 61–75, 2011.

[31] M. Zecca, S. Micera, M. C. Carrozza, and P. Dario, "Control of multifunctional prosthetic hands by processing the electromyographic signal," *Critical Reviews™ in Biomedical Engineering*, vol. 30, no. 4-6, 2002.

[32] T. Pistohl, C. Cipriani, A. Jackson, and K. Nazarpour, "Abstract and proportional myoelectric control for multi-fingered hand prostheses," *Annals of biomedical engineering*, vol. 41, no. 12, pp. 2687–2698, 2013.

[33] D. J. Tyler, "Neural interfaces for somatosensory feedback: bringing life to a prosthesis," *Current opinion in neurology*, vol. 28, no. 6, p. 574, 2015.

[34] T. Pistohl, D. Joshi, G. Ganesh, A. Jackson, and K. Nazarpour, "Artificial proprioceptive feedback for myoelectric control," *IEEE Transactions on Neural Systems and Rehabilitation Engineering*, vol. 23, no. 3, pp. 498–507, 2015.

[35] G. S. Dhillon, S. M. Lawrence, D. T. Hutchinson, and K. W. Horch, "Residual function in peripheral nerve stumps of amputees: implications for neural control of artificial limbs," *The Journal of hand surgery*, vol. 29, no. 4, pp. 605–615, 2004.

[36] G. Di Pino, A. Benvenuto, M. Tombini, G. Cavallo, L. Denaro, V. Denaro, F. Ferreri, L. Rossini, S. Micera, E. Guglielmelli *et al.*, "Overview of the implant of intraneural multielectrodes in human for controlling a 5-fingered hand prosthesis, delivering sensorial feedback and producing rehabilitative neuroplasticity," in *2012 4th IEEE RAS & EMBS International Conference on Biomedical Robotics and Biomechatronics (BioRob)*.   IEEE, 2012, pp. 1831–1836.

[37] D. W. Tan, M. A. Schiefer, M. W. Keith, J. R. Anderson, J. Tyler, and D. J. Tyler, "A neural interface provides long-term stable natural touch perception," *Science translational medicine*, vol. 6, no. 257, pp. 257ra138–257ra138, 2014.

[38] S. Raspopovic, M. Capogrosso, F. M. Petrini, M. Bonizzato, J. Rigosa, G. Di Pino, J. Carpaneto, M. Controzzi, T. Boretius, E. Fernandez *et al.*, "Restoring natural sensory feedback in real-time bidirectional hand prostheses," *Science translational medicine*, vol. 6, no. 222, pp. 222ra19–222ra19, 2014.

[39] M. Ortiz-Catalan, B. Håkansson, and R. Brånemark, "An osseointegrated human-machine gateway for long-term sensory feedback and motor control of artificial limbs," *Science translational medicine*, vol. 6, no. 257, pp. 257re6–257re6, 2014.

[40] S. Raspopovic, M. Capogrosso, and S. Micera, "A computational model for the stimulation of rat sciatic nerve using a transverse intrafascicular multichannel electrode," *Ieee Transactions On Neural Systems And Rehabilitation Engineering*, vol. 19, no. 4, pp. 333–344, 2011.

[41] P. D. Marasco, K. Kim, J. E. Colgate, M. A. Peshkin, and T. A. Kuiken, "Robotic touch shifts perception of embodiment to a prosthesis in targeted reinnervation amputees," *Brain*, vol. 134, no. 3, pp. 747–758, 2011.

[42] J. J. B. Jack, D. Noble, and R. W. Tsien, *Electric current flow in excitable cells.* Clarendon Press Oxford, 1975.

[43] F. Rattay, "The basic mechanism for the electrical stimulation of the nervous system," *Neuroscience*, vol. 89, no. 2, pp. 335–346, 1999.

[44] W. Rushton, "A theory of the effects of fibre size in medullated nerve," *The Journal of physiology*, vol. 115, no. 1, p. 101, 1951.

[45] L. Goldman and J. S. Albus, "Computation of impulse conduction in myelinated fibers; theoretical basis of the velocity-diameter relation," *Biophysical journal*, vol. 8, no. 5, p. 596, 1968.

[46] R. Fitzhugh, "Computation of impulse initiation and saltatory conduction in a myelinated nerve fiber," *Biophysical journal*, vol. 2, no. 1, p. 11, 1962.

[47] N. Hutchinson, Z. Koles, and R. Smith, "Conduction velocity in myelinated nerve fibres of xenopus laevis," *The Journal of physiology*, vol. 208, no. 2, p. 279, 1970.

[48] R. Pumphrey and J. Young, "The rates of conduction of nerve fibres of various diameters in cephalopods," *Journal of Experimental Biology*, vol. 15, no. 4, pp. 453–466, 1938.

[49] J. Hursh, "Conduction velocity and diameter of nerve fibers," *American Journal of Physiology–Legacy Content*, vol. 127, no. 1, pp. 131–139, 1939.

[50] I. Tasaki, K. Ishii, and H. Ito, "On the relation between the conduction-rate, the fiber-diameter and the internodal distance of the medullated nerve fiber," *Jpn J Med Sci III, Biophysics*, vol. 9, no. 1, pp. 189–99, 1943.

[51] B. Frankenhaeuser and A. Huxley, "The action potential in the myelinated nerve fibre of xenopus laevis as computed on the basis of voltage clamp data," *The Journal of Physiology*, vol. 171, no. 2, p. 302, 1964.

[52] G. Reid, A. Scholz, H. Bostock, and W. Vogel, "Human axons contain at least five types of voltage-dependent potassium channel," *The Journal of Physiology*, vol. 518, no. 3, pp. 681–696, 1999.

[53] J. Clark and R. Plonsey, "A mathematical evaluation of the core conductor model," *Biophysical journal*, vol. 6, no. 1, p. 95, 1966.

[54] V. Schnabel and J. J. Struijk, "Evaluation of the cable model for electrical stimulation of unmyelinated nerve fibers," *IEEE Transactions on biomedical Engineering*, vol. 48, no. 9, pp. 1027–1033, 2001.

[55] P. H. Veltink, J. Van Alste, and H. B. Boom, "Simulation of intrafascicular and extraneural nerve stimulation," *IEEE transactions on biomedical engineering*, vol. 35, no. 1, pp. 69–75, 1988.

[56] S. Raspopovic, F. M. Petrini, M. Zelechowski, and G. Valle, "Framework for the development of neuroprostheses: From basic understanding by sciatic and median nerves models to bionic legs and hands," *Proceedings of the IEEE*.

[57] J. E. Arle, K. W. Carlson, and L. Mei, "Investigation of mechanisms of vagus nerve stimulation for seizure using finite element modeling," *Epilepsy Research*, vol. 126, pp. 109–118, 2016.

[58] M. A. Schiefer, D. J. Tyler, and R. J. Triolo, "Probabilistic modeling of selective stimulation of the human sciatic nerve with a flat interface nerve electrode," *Journal of computational neuroscience*, vol. 33, no. 1, pp. 179–190, 2012.

[59] F. Rattay, "Analysis of models for external stimulation of axons," *IEEE transactions on biomedical engineering*, no. 10, pp. 974–977, 1986.

[60] O. Izad, "Computationally efficient method in predicting axonal excitation," Ph.D. dissertation, Case Western Reserve University, 2009.

[61] A. Arvanitaki, "Effects evoked in an axon by the activity of a contiguous one," *Journal of neurophysiology*, vol. 5, no. 2, pp. 89–108, 1942.

[62] V. Markin, "Electrical interaction of parallel non-myelinated nerve fibres. 1. change in excitability of adjacent fibre," *BIOPHYSICS-USSR*, vol. 15, no. 1, p. 122, 1970.

[63] J. Segundo, "What can neurons do to serve as integrating devices," *Journal of Theoretical Neurobiology*, vol. 5, no. 1, pp. 1–59, 1986.

[64] S. Binczak, J. Eilbeck, and A. C. Scott, "Ephaptic coupling of myelinated nerve fibers," *Physica D: Nonlinear Phenomena*, vol. 148, no. 1, pp. 159–174, 2001.

[65] H. Bokil, N. Laaris, K. Blinder, M. Ennis, and A. Keller, "Ephaptic interactions in the mammalian olfactory system," *J Neurosci*, vol. 21, pp. 1–5, 2001.

[66] S. Reutskiy, E. Rossoni, and B. Tirozzi, "Conduction in bundles of demyelinated nerve fibers: computer simulation," *Biological cybernetics*, vol. 89, no. 6, pp. 439–448, 2003.

[67] F. Bolzoni and E. Jankowska, "Ephaptic interactions between myelinated nerve fibres of rodent peripheral nerves," *European Journal of Neuroscience*, 2019.

[68] J. H. Goldwyn and J. Rinzel, "Neuronal coupling by endogenous electric fields: cable theory and applications to coincidence detector neurons in the auditory brain stem," *Journal of neurophysiology*, vol. 115, no. 4, pp. 2033–2051, 2016.

[69] G. R. Holt, "A critical reexamination of some assumptions and implications of cable theory in neurobiology," Ph.D. dissertation, California Institute of Technology, 1997.

[70] R. G. Stacey, L. Hilbert, and T. Quail, "Computational study of synchrony in fields and microclusters of ephaptically coupled neurons," *Journal of neurophysiology*, vol. 113, no. 9, pp. 3229–3241, 2015.

[71] A. Agudelo-Toro and A. Neef, "Computationally efficient simulation of electrical activity at cell membranes interacting with self-generated and externally imposed electric fields," *Journal of neural engineering*, vol. 10, no. 2, p. 026019, 2013.

[72] K. Xylouris and G. Wittum, "A three-dimensional mathematical model for the signal propagation on a neuron's membrane," *Frontiers in computational neuroscience*, vol. 9, 2015.

[73] S. Appukuttan, K. L. Brain, and R. Manchanda, "Modeling extracellular fields for a three-dimensional network of cells using neuron," *Journal of neuroscience methods*, vol. 290, pp. 27–38, 2017.

[74] A. Weerasuriya, R. A. Spangler, S. I. Rapoport, and R. Taylor, "Ac impedance of the perineurium of the frog sciatic nerve," *Biophysical journal*, vol. 46, no. 2, pp. 167–174, 1984.

[75] C. A. Bossetti, M. J. Birdno, and W. M. Grill, "Analysis of the quasi-static approximation for calculating potentials generated by neural stimulation," *Journal of neural engineering*, vol. 5, no. 1, p. 44, 2007.

[76] S. Joucla and B. Yvert, "Modeling extracellular electrical neural stimulation: from basic understanding to mea-based applications," *Journal of Physiology-Paris*, vol. 106, no. 3-4, pp. 146–158, 2012.

[77] R. Scott, R. Brittain, R. Caldwell, A. Cameron, and V. Dunfield, "Sensory-feedback system compatible with myoelectric control," *Medical and Biological Engineering and Computing*, vol. 18, no. 1, pp. 65–69, 1980.

[78] K. A. Kaczmarek, J. G. Webster, P. Bach-y Rita, and W. J. Tompkins, "Electrotactile and vibrotactile displays for sensory substitution systems," *IEEE Transactions on Biomedical Engineering*, vol. 38, no. 1, pp. 1–16, 1991.

[79] Y. Visell, "Tactile sensory substitution: Models for enaction in hci," *Interacting with Computers*, vol. 21, no. 1-2, pp. 38–53, 2008.

[80] S. G. Meek, S. C. Jacobsen, and P. P. Goulding, "Extended physiologic taction: design and evaluation of a proportional force feedback system," *J Rehabil Res Dev*, vol. 26, no. 3, pp. 53–62, 1989.

[81] G. Lundborg, B. Rosén, and S. Lindberg, "Hearing as substitution for sensation: a new principle for artificial sensibility," *The Journal of hand surgery*, vol. 24, no. 2, pp. 219–224, 1999.

[82] J. Gonzalez, H. Soma, M. Sekine, and W. Yu, "Psycho-physiological assessment of a prosthetic hand sensory feedback system based on an auditory display: a preliminary study," *Journal of neuroengineering and rehabilitation*, vol. 9, no. 1, p. 33, 2012.

[83] P. D. Marasco, A. E. Schultz, and T. A. Kuiken, "Sensory capacity of reinnervated skin after redirection of amputated upper limb nerves to the chest," *Brain*, vol. 132, no. 6, pp. 1441–1448, 2009.

[84] C. Antfolk, M. D'alonzo, B. Rosen, G. Lundborg, F. Sebelius, and C. Cipriani, "Sensory feedback in upper limb prosthetics," *Expert review of medical devices*, vol. 10, no. 1, pp. 45–54, 2013.

[85] S. L. Carey, D. J. Lura, and M. J. Highsmith, "Differences in myoelectric and body-powered upper-limb prostheses: Systematic literature review." *Journal of Rehabilitation Research & Development*, vol. 52, no. 3, 2015.

[86] T. Pistohl, D. Joshi, G. Ganesh, A. Jackson, and K. Nazarpour, "Artificial proprioceptive feedback for myoelectric control," *IEEE Transactions on Neural Systems and Rehabilitation Engineering*, vol. 23, no. 3, pp. 498–507, 2014.

[87] D. W. Tan, M. A. Schiefer, M. W. Keith, J. R. Anderson, and D. J. Tyler, "Stability and selectivity of a chronic, multi-contact cuff electrode for sensory stimulation in human amputees," *Journal of neural engineering*, vol. 12, no. 2, p. 026002, 2015.

[88] F. W. Clippinger, "A sensory feedback system for an upper-limb amputation prosthesis," *Bulletin of Pusthetics Research Fall 1974*, pp. 247–258, 1974.

[89] X. Navarro, T. B. Krueger, N. Lago, S. Micera, T. Stieglitz, and P. Dario, "A critical review of interfaces with the peripheral nervous system for the control of neuroprostheses and hybrid bionic systems," *Journal of the Peripheral Nervous System*, vol. 10, no. 3, pp. 229–258, 2005.

[90] S. Micera, J. Carpaneto, and S. Raspopovic, "Control of hand prostheses using peripheral information," *IEEE reviews in biomedical engineering*, vol. 3, pp. 48–68, 2010.

[91] E. H. Rijnbeek, N. Eleveld, and W. Olthuis, "Update on peripheral nerve electrodes for closed-loop neuroprosthetics," *Frontiers in neuroscience*, vol. 12, 2018.

[92] D. J. Tyler and D. M. Durand, "Functionally selective peripheral nerve stimulation with a flat interface nerve electrode," *IEEE Transactions on Neural Systems and Rehabilitation Engineering*, vol. 10, no. 4, pp. 294–303, 2002.

[93] G. S. Dhillon and K. W. Horch, "Direct neural sensory feedback and control of a prosthetic arm," *IEEE transactions on neural systems and rehabilitation engineering*, vol. 13, no. 4, pp. 468–472, 2005.

[94] T. Boretius, J. Badia, A. Pascual-Font, M. Schuettler, X. Navarro, K. Yoshida, and T. Stieglitz, "A transverse intrafascicular multichannel electrode (time) to interface with the peripheral nerve," *Biosensors and Bioelectronics*, vol. 26, no. 1, pp. 62–69, 2010.

[95] A. Branner and R. A. Normann, "A multielectrode array for intrafascicular recording and stimulation in sciatic nerve of cats," *Brain research bulletin*, vol. 51, no. 4, pp. 293–306, 2000.

[96] A. Branner, R. B. Stein, and R. A. Normann, "Selective stimulation of cat sciatic nerve using an array of varying-length microelectrodes," *Journal of neurophysiology*, vol. 85, no. 4, pp. 1585–1594, 2001.

[97] R. R. Riso, "Strategies for providing upper extremity amputees with tactile and hand position feedback–moving closer to the bionic arm," *Technology and Health Care*, vol. 7, no. 6, pp. 401–409, 1999.

[98] H. Von Helmholz, "Messungen über den zeitlichen verlauf der zuckung animalischer muskeln und die fortpflanzungsgeschwindigkeit der reizung in den nerven," *Archiv für Anatomie, Physiologie und wissenschaftliche Medicin*, vol. 17, pp. 176–364, 1850.

[99] C. Matteucci, "Sur le pouvoir electro-moteur secondaire des nerfs, et son application a l'electro-physiologie," *Compt. Rend*, vol. 56, p. 760, 1863.

[100] W. Rall, "Core conductor theory and cable properties of neurons," *Comprehensive physiology*, pp. 39–97, 1977.

[101] A. L. Hodgkin and A. F. Huxley, "A quantitative description of membrane current and its application to conduction and excitation in nerve," *The Journal of physiology*, vol. 117, no. 4, p. 500, 1952.

[102] T. Brismar, "Potential clamp analysis of membrane currents in rat myelinated nerve fibres." *The Journal of physiology*, vol. 298, p. 171, 1980.

[103] M. Baker, H. Bostock, P. Grafe, and P. Martius, "Function and distribution of three types of rectifying channel in rat spinal root myelinated axons." *The Journal of Physiology*, vol. 383, p. 45, 1987.

[104] J. Röper and J. R. Schwarz, "Heterogeneous distribution of fast and slow potassium channels in myelinated rat nerve fibres." *The Journal of Physiology*, vol. 416, p. 93, 1989.

[105] J. R. Schwarz and G. Eikhof, "Na currents and action potentials in rat myelinated nerve fibres at 20 and 37 c," *Pflügers Archiv*, vol. 409, no. 6, pp. 569–577, 1987.

[106] D. R. McNeal, "Analysis of a model for excitation of myelinated nerve," *IEEE Transactions on Biomedical Engineering*, no. 4, pp. 329–337, 1976.

[107] E. F. Barrett and J. N. Barrett, "Intracellular recording from vertebrate myelinated axons: mechanism of the depolarizing afterpotential," *The Journal of physiology*, vol. 323, no. 1, pp. 117–144, 1982.

[108] C. C. McIntyre, A. G. Richardson, and W. M. Grill, "Modeling the excitability of mammalian nerve fibers: influence of afterpotentials on the recovery cycle," *Journal of neurophysiology*, vol. 87, no. 2, pp. 995–1006, 2002.

[109] N. A. Pelot, B. J. Thio, and W. M. Grill, "Modeling current sources for neural stimulation in comsol," *Frontiers in Computational Neuroscience*, vol. 12, p. 40, 2018.

[110] C. H. Lubba, Y. Le Guen, S. Jarvis, N. S. Jones, S. C. Cork, A. Eftekhar, and S. R. Schultz, "Pypns: Multiscale simulation of a peripheral nerve in python," *Neuroinformatics*, vol. 17, no. 1, pp. 63–81, 2019.

[111] J. R. Schwarz, G. Reid, and H. Bostock, "Action potentials and membrane currents in the human node of ranvier," *Pflügers Archiv*, vol. 430, no. 2, pp. 283–292, 1995.

[112] W. Wesselink, J. Holsheimer, and H. Boom, "A model of the electrical behaviour of myelinated sensory nerve fibres based on human data," *Medical & biological engineering & computing*, vol. 37, no. 2, pp. 228–235, 1999.

[113] J. L. Gaines, K. E. Finn, J. P. Slopsema, L. A. Heyboer, and K. H. Polasek, "A model of motor and sensory axon activation in the median nerve using surface electrical stimulation," *Journal of computational neuroscience*, vol. 45, no. 1, pp. 29–43, 2018.

[114] A. Tveito, K. H. Jæger, G. T. Lines, Ł. Paszkowski, J. Sundnes, A. G. Edwards, T. Māki-Marttunen, G. Halnes, and G. T. Einevoll, "An evaluation of the accuracy of classical models for computing the membrane potential and extracellular potential for neurons," *Frontiers in computational neuroscience*, vol. 11, p. 27, 2017.

[115] H. Meffin, B. Tahayori, D. B. Grayden, and A. N. Burkitt, "Modeling extracellular electrical stimulation: I. derivation and interpretation of neurite equations," *Journal of neural engineering*, vol. 9, no. 6, p. 065005, 2012.

[116] B. Tahayori, H. Meffin, S. Dokos, A. N. Burkitt, and D. B. Grayden, "Modeling extracellular electrical stimulation: Ii. computational validation and numerical results," *Journal of neural engineering*, vol. 9, no. 6, p. 065006, 2012.

[117] B. Wang, A. S. Aberra, W. M. Grill, and A. V. Peterchev, "Modified cable equation incorporating transverse polarization of neuronal membranes for accurate coupling of electric fields," *Journal of neural engineering*, vol. 15, no. 2, p. 026003, 2018.

[118] K. W. Altman and R. Plonsey, "A two-part model for determining the electro-magnetic and physiologic behavior of cuff electrode nerve stimulators," *IEEE transactions on biomedical engineering*, no. 3, pp. 285–293, 1986.

[119] D. Stegeman, J. De Weerd, and E. Eijkman, "A volume conductor study of compound action potentials of nerves in situ: the forward problem," *Biological cybernetics*, vol. 33, no. 2, pp. 97–111, 1979.

[120] P. H. Veltink, B. K. Van Veen, J. J. Struijk, J. Holsheimer, and H. B. Boom, "A modeling study of nerve fascicle stimulation," *IEEE transactions on biomedical engineering*, vol. 36, no. 7, pp. 683–692, 1989.

[121] J. D. Sweeney, D. A. Ksienski, and J. T. Mortimer, "A nerve cuff technique for selective excitation of peripheral nerve trunk regions," *IEEE Transactions on Biomedical Engineering*, vol. 37, no. 7, pp. 706–715, 1990.

[122] P. Koole, J. Holsheimer, J. J. Struijk, and A. J. Verloop, "Recruitment characteristics of nerve fascicles stimulated by a multigroove electrode," *IEEE transactions on rehabilitation engineering*, vol. 5, no. 1, pp. 40–50, 1997.

[123] B. Coburn and W. K. Sin, "A theoretical study of epidural electrical stimulation of the spinal cord part i: finite element analysis of stimulus fields," *IEEE transactions on biomedical engineering*, no. 11, pp. 971–977, 1985.

[124] J. K. Cavanaugh, J.-C. Lin, and D. M. Durand, "Finite element analysis of electrical nerve stimulation," in *Proceedings of 18th Annual International Conference of the IEEE Engineering in Medicine and Biology Society*, vol. 1. IEEE, 1996, pp. 355–356.

[125] M. Dali, O. Rossel, D. Andreu, L. Laporte, A. Hernández, J. Laforet, E. Marijon, A. Hagège, M. Clerc, C. Henry *et al.*, "Model based optimal multipolar stimulation without a priori knowledge of nerve structure: application to vagus nerve stimulation," *Journal of neural engineering*, vol. 15, no. 4, p. 046018, 2018.

[126] K. Zhu, L. Li, X. Wei, and X. Sui, "A 3d computational model of transcutaneous electrical nerve stimulation for estimating aβ tactile nerve fiber excitability," *Frontiers in neuroscience*, vol. 11, p. 250, 2017.

[127] L. J. Cauller and B. W. Connors, "Functions of very distal dendrites: experimental and computational studies of layer i synapses on neocortical pyramidal cells," in *Single neuron computation.* Elsevier, 1992, pp. 199–229.

[128] P. A. Rhodes and C. M. Gray, "Simulations of intrinsically bursting neocortical pyramidal neurons," *Neural Computation*, vol. 6, no. 6, pp. 1086–1110, 1994.

[129] Z. F. Mainen and T. J. Sejnowski, "Influence of dendritic structure on firing pattern in model neocortical neurons," *Nature*, vol. 382, no. 6589, p. 363, 1996.

[130] M. Hines, "A program for simulation of nerve equations with branching geometries," *International journal of bio-medical computing*, vol. 24, no. 1, pp. 55–68, 1989.

[131] A. Destexhe, Z. F. Mainen, and T. J. Sejnowski, "Kinetic models of synaptic transmission," *Methods in neuronal modeling*, vol. 2, pp. 1–25, 1998.

[132] Y. Grinberg, M. Schiefer, D. Tyler, and K. Gustafson, "Fascicular perineurium thickness, size, and position affect model predictions of neural excitation." *IEEE transactions on neural systems and rehabilitation engineering: a publication of the IEEE Engineering in Medicine and Biology Society*, vol. 16, no. 6, pp. 572–581, 2008.

[133] N. Brill and D. Tyler, "Optimizing nerve cuff stimulation of targeted regions through use of genetic algorithms," in *2011 Annual International Conference of the IEEE Engineering in Medicine and Biology Society*. IEEE, 2011, pp. 5811–5814.

[134] H. Lindén, E. Hagen, S. Leski, E. S. Norheim, K. H. Pettersen, and G. T. Einevoll, "Lfpy: a tool for biophysical simulation of extracellular potentials generated by detailed model neurons," *Frontiers in neuroinformatics*, vol. 7, p. 41, 2014.

[135] J. M. Bower, D. Beeman, and M. Hucka, "The genesis simulation system," 2003.

[136] M. L. Hines and N. T. Carnevale, "Translating network models to parallel hardware in NEURON," *Journal of neuroscience methods*, vol. 169, no. 2, p. 425, 2008.

[137] M. Hines, A. P. Davison, and E. Muller, "NEURON and Python," *Frontiers in neuroinformatics*, vol. 3, p. 1, 2009.

[138] J. A. García-Grajales, G. Rucabado, A. García-Dopico, J.-M. Peña, and A. Jérusalem, "Neurite, a finite difference large scale parallel program for the simulation of electrical signal propagation in neurites under mechanical loading," *PloS one*, vol. 10, no. 2, p. e0116532, 2015.

[139] M. Diesmann and M.-O. Gewaltig, "Nest: An environment for neural systems simulations," *Forschung und wisschenschaftliches Rechnen, Beiträge zum Heinz-Billing-Preis*, vol. 58, pp. 43–70, 2001.

[140] D. F. Goodman and R. Brette, "Brian simulator," *Scholarpedia*, vol. 8, no. 1, p. 10883, 2013.

[141] E. L. Graczyk, M. A. Schiefer, H. P. Saal, B. P. Delhaye, S. J. Bensmaia, and D. J. Tyler, "The neural basis of perceived intensity in natural and artificial touch," *Science Translational Medicine*, vol. 8, no. 362, pp. 362ra142–362ra142, 2016.

[142] D. R. Merrill, M. Bikson, and J. G. Jefferys, "Electrical stimulation of excitable tissue: design of efficacious and safe protocols," *Journal of neuroscience methods*, vol. 141, no. 2, pp. 171–198, 2005.

[143] R. Plonsey and D. B. Heppner, "Considerations of quasi-stationarity in electrophysiological systems," *The Bulletin of mathematical biophysics*, vol. 29, no. 4, pp. 657–664, 1967.

[144] R. Plonsey and D. Fleming, "Bioelectric phenomena. 1969."

[145] K. Altman and R. Plonsey, "Development of a model for point source electrical fibre bundle stimulation," *Medical and Biological Engineering and Computing*, vol. 26, no. 5, pp. 466–475, 1988.

[146] J. J. Struijk, J. Holsheimer, G. G. van der Heide, and H. B. Boom, "Recruitment of dorsal column fibers in spinal cord stimulation: influence of collateral branching," *IEEE Transactions on Biomedical Engineering*, vol. 39, no. 9, pp. 903–912, 1992.

[147] S. Joucla and B. Yvert, "Improved focalization of electrical microstimulation using microelectrode arrays: a modeling study," *PloS one*, vol. 4, no. 3, p. e4828, 2009.

[148] C. C. McIntyre and W. M. Grill, "Extracellular stimulation of central neurons: influence of stimulus waveform and frequency on neuronal output," *Journal of neurophysiology*, vol. 88, no. 4, pp. 1592–1604, 2002.

[149] I. V. Tarotin, "Model of impedance changes in nerve fibres," Ph.D. dissertation, UCL (University College London), 2019.

[150] I. Tarotin, K. Aristovich, and D. Holder, "Model of impedance changes in unmyelinated nerve fibers," *IEEE Transactions on Biomedical Engineering*, vol. 66, no. 2, pp. 471–484, 2018.

[151] I. Tarotin, K. Aristovich, and D. Holder, "Simulation of impedance changes with a FEM model of a myelinated nerve fibre," *Journal of neural engineering*, vol. 16, no. 5, p. 056026, 2019.

[152] E. Peterson, O. Izad, and D. J. Tyler, "Predicting myelinated axon activation using spatial characteristics of the extracellular field," *Journal of neural engineering*, vol. 8, no. 4, p. 046030, 2011.

[153] E. N. Warman, W. M. Grill, and D. Durand, "Modeling the effects of electric fields on nerve fibers: determination of excitation thresholds," *IEEE Transactions on Biomedical Engineering*, vol. 39, no. 12, pp. 1244–1254, 1992.

[154] C. T. Choi, W.-D. Lai, and Y.-B. Chen, "Optimization of cochlear implant electrode array using genetic algorithms and computational neuroscience models," *IEEE transactions on magnetics*, vol. 40, no. 2, pp. 639–642, 2004.

[155] C. R. Butson and C. C. McIntyre, "Role of electrode design on the volume of tissue activated during deep brain stimulation," *Journal of neural engineering*, vol. 3, no. 1, p. 1, 2005.

[156] C. T. Choi and S.-S. Lee, "A new flat interface nerve electrode design scheme based on finite element method, genetic algorithm and computational neuroscience method," *IEEE transactions on magnetics*, vol. 42, no. 4, pp. 1119–1122, 2006.

[157] C. A. Anastassiou and C. Koch, "Ephaptic coupling to endogenous electric field activity: why bother?" *Current opinion in neurobiology*, vol. 31, pp. 95–103, 2015.

[158] K.-S. Han, C. Guo, C. H. Chen, L. Witter, T. Osorno, and W. G. Regehr, "Ephaptic coupling promotes synchronous firing of cerebellar purkinje cells," *Neuron*, vol. 100, no. 3, pp. 564–578, 2018.

[159] L. Voronin, M. Volgushev, M. Sokolov, A. Kasyanov, M. Chistiakova, and K. Reymann, "Evidence for an ephaptic feedback in cortical synapses: postsynaptic hyperpolarization alters the number of response failures and quantal content," *Neuroscience*, vol. 92, no. 2, pp. 399–405, 1999.

[160] F. E. Dudek, T. Yasumura, and J. E. Rash, "'non-synaptic'mechanisms in seizures and epileptogenesis," *Cell biology international*, vol. 22, no. 11-12, pp. 793–805, 1998.

[161] S. Wang, L. J. Leon, and F. A. Roberge, "Interactions between adjacent fibers in a cardiac muscle bundle," *Annals of biomedical engineering*, vol. 24, no. 6, pp. 662–674, 1996.

[162] Y. Mori, G. I. Fishman, and C. S. Peskin, "Ephaptic conduction in a cardiac strand model with 3d electrodiffusion," *Proceedings of the National Academy of Sciences*, vol. 105, no. 17, pp. 6463–6468, 2008.

[163] S. F. Roberts, "Non-uniform interstitial loading in cardiac microstructure during impulse propagation," Ph.D. dissertation, Duke University, 2009.

[164] V. Markin, "Electrical interaction of parallel non-myelinated nerve fibres. 2. collective conduction of impulses," *BIOPHYSICS-USSR*, vol. 15, no. 4, p. 713, 1970.

[165] A. C. Scott, *Nonlinear science.* Oxford University Press, Oxford, 1999, vol. 4.

[166] J. Kocsis, J. Ruiz, and K. Cummins, "Modulation of axonal excitability mediated by surround electric activity: an intra-axonal study," *Experimental brain research*, vol. 47, no. 1, pp. 151–153, 1982.

[167] S. Cardanobile, D. Mugnolo, and R. Nittka, "Well-posedness and symmetries of strongly coupled network equations," *Journal of Physics A: Mathematical and Theoretical*, vol. 41, no. 5, p. 055102, 2008.

[168] M. D. Bateman and E. S. Van Vleck, "Traveling wave solutions to a coupled system of spatially discrete nagumo equations," *SIAM Journal on Applied Mathematics*, vol. 66, no. 3, pp. 945–976, 2006.

[169] H. Suetani, T. Yanagita, and K. Aihara, "Pulse dynamics in coupled excitable fibers: Soliton-like collision, recombination, and overtaking," *arXiv preprint nlin/0610071*, 2006.

[170] I. Maïna, C. Tabi, H. E. Fouda, A. Mohamadou, and T. Kofane, "Discrete impulses in ephaptically coupled nerve fibers," *Chaos: An Interdisciplinary Journal of Nonlinear Science*, vol. 25, no. 4, p. 043118, 2015.

[171] H. Das and P. Sahu, "Coupled nerve: A technique to increase the nerve conduction velocity in demyelinating polyneuropathic patients," *Procedia Engineering*, vol. 64, pp. 275–282, 2013.

[172] K. H. Pettersen, H. Lindén, A. M. Dale, and G. T. Einevoll, "Extracellular spikes and csd," *Handbook of Neural Activity Measurement*, vol. 1, pp. 92–135, 2012.

[173] A. R. Shifman and J. E. Lewis, "Elfenn: A generalized platform for modeling ephaptic coupling in spiking neuron models," *Frontiers in Neuroinformatics*, vol. 13, p. 35, 2019.

[174] N. A. Malik, "Frequency-dependent response of neurons to oscillating electric fields," Ph.D. dissertation, University of Warwick, 2011.

[175] L. Leon and F. Roberge, "Structural complexity effects on transverse propagation in a two-dimensional model of myocardium," *IEEE Transactions on Biomedical Engineering*, vol. 38, no. 10, pp. 997–1009, 1991.

[176] D. A. Hooks, K. A. Tomlinson, S. G. Marsden, I. J. LeGrice, B. H. Smaill, A. J. Pullan, and P. J. Hunter, "Cardiac microstructure: implications for electrical propagation and defibrillation in the heart," *Circulation research*, vol. 91, no. 4, pp. 331–338, 2002.

[177] M. Capllonch-Juan and F. Sepulveda, "Conduction velocity effects due to ephaptic interactions between myelinated axons," in *EMBEC & NBC 2017*. Springer, 2017, pp. 659–662.

[178] J. B. Ranck and S. L. BeMent, "The specific impedance of the dorsal columns of cat: an anisotropic medium," *Experimental neurology*, vol. 11, no. 4, pp. 451–463, 1965.

[179] S. Raspopovic, M. Capogrosso, and S. Micera, "A computational model for the stimulation of rat sciatic nerve using a transverse intrafascicular multichannel electrode," *IEEE Transactions on Neural Systems and Rehabilitation Engineering*, vol. 19, no. 4, pp. 333–344, Aug 2011.

[180] L. Burtseva and F. Werner, *Modeling of Spherical Particle Packing Structures Using Mathematical Tessellation.* Univ., Fak. für Mathematik, 2015.

[181] A. T. Y. I. L. Wemple, "Mixed-signal switching noise analysis using voronoi-tessellated substrate macromodels," in *32nd Design Automation Conference.* IEEE, 1995, pp. 439–444.

[182] X. Franceries, B. Doyon, N. Chauveau, B. Rigaud, P. Celsis, and J. Morucci, "Solution of poisson's equation in a volume conductor using resistor mesh models: application to event related potential imaging," *Journal of applied physics*, vol. 93, no. 6, pp. 3578–3588, 2003.

[183] G. R. Holt and C. Koch, "Electrical interactions via the extracellular potential near cell bodies," *Journal of computational neuroscience*, vol. 6, no. 2, pp. 169–184, 1999.

[184] K. J. Gustafson, G. C. Pinault, J. J. Neville, I. Syed, J. A. Davis Jr, J. Jean-Claude, and R. J. Triolo, "Fascicular anatomy of human femoral nerve: implications for neural prostheses using nerve cuff electrodes," *Journal of rehabilitation research and development*, vol. 46, no. 7, p. 973, 2009.

[185] N. A. Brill and D. J. Tyler, "Quantification of human upper extremity nerves and fascicular anatomy," *Muscle & nerve*, vol. 56, no. 3, pp. 463–471, 2017.

[186] Y. Assaf, T. Blumenfeld-Katzir, Y. Yovel, and P. J. Basser, "Axcaliber: a method for measuring axon diameter distribution from diffusion mri," *Magnetic resonance in medicine*, vol. 59, no. 6, pp. 1347–1354, 2008.

[187] T. Duval, S. Lévy, N. Stikov, J. Campbell, A. Mezer, T. Witzel, B. Keil, V. Smith, L. L. Wald, E. Klawiter *et al.*, "g-ratio weighted imaging of the human spinal cord in vivo," *Neuroimage*, vol. 145, pp. 11–23, 2017.

[188] E. Brunton, C. W. Blau, and K. Nazarpour, "Multichannel cuff electrodes for peripheral nerve stimulation and recording," in *Systems, Man, and Cybernetics (SMC), 2016 IEEE International Conference on.* IEEE, 2016, pp. 003 223–003 227.

[189] A. Lyckegaard, E. M. Lauridsen, W. Ludwig, R. W. Fonda, and H. F. Poulsen, "On the use of laguerre tessellations for representations of 3d grain structures," *Advanced Engineering Materials*, vol. 13, no. 3, pp. 165–170, 2011.

[190] C. Lautensack, "Fitting three-dimensional laguerre tessellations to foam structures," *Journal of Applied Statistics*, vol. 35, no. 9, pp. 985–995, 2008.

[191] C. Redenbach, I. Shklyar, and H. Andrä, "Laguerre tessellations for elastic stiffness simulations of closed foams with strongly varying cell sizes," *International Journal of Engineering Science*, vol. 50, no. 1, pp. 70–78, 2012.

[192] T. Frieswijk, J. Smit, W. Rutten, and H. Boom, "Force-current relationships in intraneural stimulation: Role of extraneural medium and motor fibre clustering," *Medical and Biological Engineering and Computing*, vol. 36, no. 4, pp. 422–430, 1998.

[193] W. M. Grill, "Modeling the effects of electric fields on nerve fibers: influence of tissue electrical properties," *IEEE Transactions on Biomedical Engineering*, vol. 46, no. 8, pp. 918–928, 1999.

[194] I. Tarotin, K. Aristovich, and D. Holder, "Effect of dispersion in nerve on compound action potential and impedance change: a modelling study," *Physiological measurement*, vol. 40, no. 3, p. 034001, 2019.

[195] W. J. Freeman, "Spatial divergence and temporal dispersion in primary olfactory nerve of cat." *Journal of neurophysiology*, vol. 35, no. 6, pp. 733–744, 1972.

[196] S. Helmers, J. Begnaud, A. Cowley, H. Corwin, J. Edwards, D. Holder, H. Kostov, P. Larsson, P. Levisohn, M. De Menezes *et al.*, "Application of a computational model of vagus nerve stimulation," *Acta Neurologica Scandinavica*, vol. 126, no. 5, pp. 336–343, 2012.

[197] S. Kim, P. Tathireddy, R. A. Normann, and F. Solzbacher, "Thermal impact of an active 3-d microelectrode array implanted in the brain," *IEEE Transactions on Neural Systems and Rehabilitation Engineering*, vol. 15, no. 4, pp. 493–501, 2007.

[198] C. Moulin, A. Glière, D. Barbier, S. Joucla, B. Yvert, P. Mailley, and R. Guillemaud, "A new 3-d finite-element model based on thin-film approximation for microelectrode array recording of extracellular action potential," *IEEE Transactions on Biomedical Engineering*, vol. 55, no. 2, pp. 683–692, 2008.

[199] S. Joucla, L. Rousseau, and B. Yvert, "Focalizing electrical neural stimulation with penetrating microelectrode arrays: a modeling study," *Journal of neuroscience methods*, vol. 209, no. 1, pp. 250–254, 2012.

[200] N. T. Carnevale and M. L. Hines, *The NEURON book.* Cambridge University Press, 2006.